*NOAA Atlas NESDIS* 92

# WORLD OCEAN ATLAS 2023
# Volume 4: Dissolved Inorganic Nutrients (Phosphate, Nitrate, and Silicate)

Silver Spring, MD
February 2024

**U.S. DEPARTMENT OF COMMERCE**
**National Oceanic and Atmospheric Administration**
National Environmental Satellite, Data, and Information Service
National Centers for Environmental Information

## NOAA National Centers for Environmental Information

Additional copies of this publication, as well as information about NCEI data holdings and services, are available upon request directly from NCEI.


NOAA/NESDIS
National Centers for Environmental Information
SSMC3, 4th floor
1315 East-West Highway
Silver Spring, MD 20910-3282
U.S.A.

Phone:: +1 (828) 271-4800
E-mail: ncei.info@noaa.gov
WEB: https://www.ncei.noaa.gov/


For updates on the data, documentation, and additional information about the WOA23 please refer to:
https://www.ncei.noaa.gov/products/ocean-climate-laboratory

This document should be cited as:


Garcia H.E., C. Bouchard, S.L. Cross, C.R. Paver, T.P. Boyer, J.R. Reagan, R.A. Locarnini, A.V. Mishonov, O.K. Baranova, D. Seidov, Z. Wang, and D. Dukhovskoy (2024). World Ocean Atlas 2023, Volume 4: Dissolved Inorganic Nutrients (Phosphate, Nitrate, Silicate). A. Mishonov Technical Editor. *NOAA Atlas NESDIS 92*, 79pp. https://doi.org/10.25923/39qw-7j08


This document is available online at https://www.ncei.noaa.gov/products/world-ocean-atlas

*NOAA Atlas NESDIS* **92**

# *WORLD OCEAN ATLAS 2023*
# *Volume 4: Dissolved Inorganic Nutrients (Phosphate, Nitrate, and Silicate)*

Hernan E. Garcia, Courtney Bouchard, Scott L. Cross,
Christopher R. Paver, Timothy P. Boyer, James R. Reagan,
Ricardo A. Locarnini, Alexey V. Mishonov, Olga K. Baranova,
Dan Seidov, Zhankun Wang, and Dmitry Dukhovskoy

Technical Editor: Alexey Mishonov

National Centers for Environmental Information (NCEI)

Silver Spring, Maryland
February 2024



**U.S. DEPARTMENT OF COMMERCE**
Gina M. Raimondo, U.S. Secretary of Commerce

**National Oceanic and Atmospheric Administration**
Richard W. Spinrad, Ph.D., Under Secretary of Commerce for Oceans and Atmosphere and NOAA Administrator

**National Environmental Satellite, Data, and Information Service**
Stephen Volz, Assistant Administrator

# To Sydney (Syd) Levitus

Syd exemplifies the craft of careful, systematic inquiry of the large-scale distributions and low-frequency variability from seasonal-to-decadal time scales of ocean properties. He was one of the first to recognize the importance and benefits of creating objectively analyzed climatological fields of measured ocean variables including temperature, salinity, oxygen, nutrients, and derived fields such as mixed layer depth. Upon publishing *Climatological Atlas of the World Ocean* in 1982, he distributed this work without restriction, an act not common at the time. This seminal atlas moved the oceanographic diagnostic research from using hand-drawn maps to using objectively analyzed fields of ocean variables.

With his NODC Ocean Climate Laboratory (OCL) colleagues, and unprecedented cooperation from the U.S. and international ocean scientific and data management communities, he created the *World Ocean Database (WOD)*; the world's largest collection of ocean profile data that are available internationally without restriction. The *World Ocean Atlas (WOA)* series represents the gridded objective analyses of the WOD and these fields have also been made available without restriction.

The WOD and WOA series are used so frequently that they have become known generically as the "Levitus Climatology". These databases and products enable systematic studies of ocean variability in its climatological context that were not previously possible. His foresight in creating WOD and WOA has been demonstrated by their widespread use over the years. Syd has made major contributions to the scientific and ocean data management communities. He has also increased public understanding of the role of the oceans in climate. He retired in 2013 after 39 years of distinguished civil service. He distilled the notion of the synergy between rigorous data management and science; there are no shortcuts.

All of us at the Ocean Climate Laboratory group would like to dedicate this atlas to Syd, his legacy, vision, and generous mentorship.

The OCL team members

## Table of Contents

## List of Acronyms

| Acronym | Expanded Term |
|---|---|
| APB | Autonomous Pinniped Bathythermograph |
| BAMS | Bulletin of the American Meteorological Society |
| BCG-Argo | BioGeoChemical Argo PFL, an extension of the Argo core program |
| CFA | Continuous Flow Analyzer |
| CSV | Comma-Separated Value |
| CTD | Conductivity Temperature Depth |
| DBT | Drifting Bathythermograph |
| DNA | Deoxyribonucleic Acid |
| DOC | Department of Commerce |
| DOE | Department of Energy |
| DRB | Drifting Buoy dataset in WOD |
| EEI | Earth Energy Imbalance |
| ENSO | El Niño-Southern Oscillation, |
| ERL | Earth Research Laboratory |
| EOV | Essential Ocean Variable |
| ETOPO2 | Earth Topography 2 arc minute |
| EVR | Extended Vertical Resolution |
| FAIR | Findable, Accessible, Interoperable, and Reusable |
| GIS | Geographic Information System |
| GLD | Glider dataset in WOD |
| GMT | Greenwich Mean Time, or Generic Mapping Tools |
| GLODAP | Global Ocean Data Analysis Project |
| GODAR | Global Ocean Data Archaeology and Rescue |
| GOBAI-$O_2$ | Gridded Ocean Biogeochemistry from Artificial Intelligence for $O_2$ |
| GTSPP | Global Temperature-Salinity Profile Program |
| IAPSO | International Association for the Physical Sciences of the Oceans |
| IOC | Intergovernmental Oceanographic Commission of UNESCO |
| IODE | International Oceanographic Data Exchange of IOC |
| IRI | International Research Institute for Climate and Society |
| JAMSTEC | Japan Agency for Marine-Earth Science and Technology |
| JPOTS | Joint Panel on Oceanographic Tables and Standards |
| LDEO | Lamont-Doherty Earth Observatory |
| MAST | Marine Science and Technology |
| MBT | Mechanical Bathythermograph |
| MEDAR | Mediterranean Data Archeology and Rescue |
| MRB | Moored Buoy |
| NAO | North Atlantic Oscillation |
| NASA | National Aeronautics and Space Administration |
| NATO | North Atlantic Treaty Organization |
| NCEI | National Centers for Environmental Information |
| NESDIS | National Environmental Satellite, Data, and Information Service |
| NOAA | National Oceanic and Atmospheric Administration |
| OSD | Ocean Station Data dataset in WOD |

| Acronym | Expanded Term |
|---|---|
| NODC | National Ocean Data Center |
| O2S | Dissolved oxygen saturation solubility (%) |
| OCL | Ocean Climate Laboratory |
| ODV | Ocean Data View (Schlitzer, R., 2023) |
| PFL | Profiling Float dataset in WOD |
| PIRATA | Prediction and Research Moored Array in the Tropical Atlantic |
| PDO | Pacific Decadal Oscillation |
| PSS | Practical Salinity Scale |
| QC | Quality Control |
| QCF | Quality Control Flags |
| RAMA | Research Moored Array for African-Asian-Australian Monsoon Analysis and Prediction |
| RDML | Rear Admiral |
| SOCCOM | Southern Ocean Carbon and Climate Observations and Modeling |
| RNA | Ribonucleic Acid |
| SST | Sea Surface Temperature |
| SME | Subject Matter Expert |
| SUR | Surface |
| TAO/TRITON | Tropical Atmosphere Ocean moored buoy array |
| TSK | Tsurumi-Seiki Company |
| UN | United Nations |
| UNESCO | United Nations Educational, Scientific and Cultural Organization |
| UOR | Undulating Oceanographic Recorder |
| USA | United States of America |
| USN | United States Navy |
| WDC | World Data Center |
| WDS | World Data System |
| WDS Oceanography | World Data Service for Oceanography of WDS |
| WOA | World Ocean Atlas |
| WOA18 | World Ocean Atlas version 2018 |
| WOA23 | World Ocean Atlas version 2023 (WOA23F and WOA23N)) |
| WOA23F | World Ocean Atlas version 2023 (1965-2022) |
| WOA23N | World Ocean Atlas version 2023 Climate Normal (1971-2000) |
| WOCE | World Ocean Circulation Experiment |
| WOD | World Ocean Database |
| WOD18 | World Ocean Database version 2018 used for WOA18 |
| WOD23 | World Ocean Database version 2023 used for WOA23 |
| XBT | Expendable Bathythermograph |
| XCTD | Expendable Conductivity Temperature Depth |

# Preface

The World Ocean Atlas 2023 (WOA23) is the latest in a line of research quality oceanographic analyses of subsurface (profile) measured Essential Ocean Variables (EOV) at standard depths extending back to the groundbreaking *Climatological Atlas of the World Ocean* (Levitus, 1982). The WOA line of products has been published semi-regularly since 1994, with versions in 1998, 2001, 2005, 2009, 2013, 2018, and now 2023. Previous iterations of the WOA have proven to be of great utility to the oceanographic, climate research, geophysical, and operational environmental forecasting communities. The oceanographic variable analyses are used as boundary and/or initial conditions in numerical ocean circulation models and atmosphere-ocean models, for verification of numerical simulations of the ocean, as a form of "sea truth" for satellite measurements such as altimetric observations of sea surface height, for computation of nutrient fluxes by Ekman transport, and for planning oceanographic expeditions among others.

WOA23 includes objective analyses on a one-degree grid for all quality-controlled variables at annual, seasonal, and monthly (temperature, salinity, dissolved inorganic nutrients, and oxygen). WOA23 also includes data analyses on a quarter-degree grid for temperature and salinity only. Since WOA18, the ocean variable analyses are produced on 102 standard depth levels from the surface to 5,500 m (previously 33 levels within the same depth limits). WOA23 provides one-degree climate normal for temperature. salinity, and dissolved oxygen. Ocean data and analyses of data at higher temporal and spatial resolution than previously available are needed to document ocean variability, isopycnal analysis, uncertainty, including improving diagnostics, understanding, and modeling of the physics of the ocean.

In the acknowledgment section of this publication, we have expressed our view that creation of global ocean profile and plankton databases and data analyses are only possible through the sharing of data and cooperation of data centers, scientists, data managers, and scientific administrators throughout the U.S. and international scientific community including the International Oceanographic Data and Information Exchange (IODE) of the Intergovernmental Oceanographic Commission (IOC) of UNESCO.

Ocean Climate Laboratory Team
NOAA NESDIS National Centers for Environmental Information
Silver Spring, MD
February 2024

# Acknowledgments

This work was made possible by a grant from the NOAA Climate and Global Change Program, which enabled the establishment of a research group at the National Centers for Environmental Information (NCEI). The purpose of this group is to prepare research quality oceanographic databases, as well as to compute objective analyses of, and diagnostic studies based on, these databases. Support is now from base funds and from the NOAA Climate Program Office.

The data on which this atlas is based are in *World Ocean Database 2023* and are distributed on-line by NCEI. Many data were acquired as a result of the IOC/IODE *Global Oceanographic Data Archaeology and Rescue* (GODAR) project, the IOC/IODE *World Ocean Database* project (WOD), and the World Data Service for Oceanography (WDS-Oceanography) of the World Data System (WDS) hosted at NCEI.

The WOD is a composite of publicly available shared ocean profile data, both historical and recent. The data in WOD data are updated quarterly and are Findable, Accessible, Interoperable, and Reusable (FAIR, Wilkinson *et al.*, 2016). We acknowledge the scientists, technicians, and programmers who have collected and processed data, those individuals who have submitted and shared data to national, regional, and global data centers as well as the data managers and staff at the various data centers. We are working on a more substantive and formalized way to acknowledge all those who have collected and contributed to oceanographic measurements used to calculate the fields in the WOA including Persistent Unique Identifiers (*i.e.*, Digital Object Identifiers, DOI). All of the originator's data included in WOD are archived at NCEI and includes all metadata provided by the data provider including assigned DOIs. Until we have a more comprehensive system in place within the WOD metadata, we direct the reader's attention to lists of primary investigators, institutions, and projects, which contributed data (codes can be used to locate data in the World Ocean Database). We also thank our colleagues at the NCEI. Their efforts have made this and similar works possible. We are grateful the review comments of Dr. Jia-Zhong Zhang and anonymous reviewers whose comments greatly improved the WOA23 for nutrients

We dedicate this work to Carla Coleman who always contributed with a smile and was taken from us too soon.

# WORLD OCEAN ATLAS 2023
# Volume 4: Dissolved Inorganic Nutrients
## (phosphate, nitrate, and silicate)

# Chapter 1: Introduction and Data Analysis Procedures

**Hernan E. Garcia**

## ABSTRACT

This World Ocean Atlas 2023 (WOA23) document describes the data quality control (QC), processing, and objective analysis (OA) used to estimate global ocean climatological mean content of quality-controlled *in situ* dissolved inorganic nutrients (phosphate, nitrate, and silicate) collected between January 1, 1965 and December 31, 2022. Global mean ocean content for each nutrient variable are calculated for composite time periods (annual, seasonal, monthly, seasonal and monthly difference fields from the annual mean field, standard deviation, number of observations) at 102 standard depths (0-5500 m depth) on a one-degree latitude-longitude spatial grid resolution. WOA23 is based on quality-controlled nutrient measurements from NOAA's World Ocean Database 2023 (WOD23). The global mean content inventories for phosphate, nitrate, and silicate are 3.1, 42.2, and 122.4 Pmol, respectively. The uncertainty estimates of the objectively analyzed content fields are about 0.00 ± 0.01 μmol·kg$^{-1}$ for phosphate, 0.04 ± 0.16 μmol/kg for nitrate, and 0.07 ± 0.20 μmol·kg$^{-1}$ for silicate. The WOA23 OA nutrient content fields are in close agreement with those in the WOA18 as well as in GLODAPv2.2016b. This atlas is divided into four chapters. In chapter 1, we describe QC and OA data analysis process. Chapters 2 (phosphate), 3 (nitrate and nitrate + nitrite), and 4 (silicate) provide additional information and description of the large-scale features and global content distribution of these essential ocean variables. WOA23 is available online in different interoperable digital formats.

## 1.1. INTRODUCTION

Dissolved inorganic macronutrients (phosphate, nitrate, nitrate + nitrite, and silicate) in the global ocean are non-conservative Essential Ocean Variables (EOV). Their spatial and temporal distribution and content in the world ocean is affected both by biogeochemical sink and source processes (*i.e.,* marine biological production, respiration, redox, geochemistry) and physical-forcing dynamics (*i.e.,* water mass renewal, ventilation, advection, mixing). By "dissolved inorganic nutrients" in this atlas, we mean *in situ* chemically reactive dissolved inorganic nitrate, nitrate + nitrite, phosphate, and silicate content (in units of micro-mole per kilogram of seawater, μmol·kg$^{-1}$). We use the term nutrient "content" to denote amount of nutrient solute per unit mass of seawater (*i.e.*, Jiang *et al.* 2022). The nutrient data used in this atlas were collected from January 01, 1965 to December 31, 2022 and measured using manual or continuous flow analyzer (CFA) photometric methods.

We note that when reported by the data provider, we use nitrate values. In cases

where nitrate + nitrite (N+N) is reported instead and nitrate or nitrite are not, we use the nitrate + nitrite (N+N) values to represent nitrate. Nitrite is an intermediate in oxidative and reductive processes such as nitrification and denitrification and it is also used by phytoplankton. Dissolved nitrite content in the ocean is nominally low (< 0.5 $\mu mol \cdot kg^{-1}$) with significant exceptions. Relatively high nitrite content values of up to about 10 $\mu mol \cdot kg^{-1}$ can be observed in oxygen-deficient zones such as in eastern boundary upwelling regions, Oxygen Minimum Zones (OMZ), suboxic trenches, and fjords. For example, in the eastern Pacific, WOCE line P21 at about 20°S shows nitrate values as high as about 44 $\mu mol \cdot kg^{-1}$ at or near 800-1000 m depth, and nitrite values as high as 10 $\mu mol \cdot kg^{-1}$ in the upper 400 m depth or 23% of the N+N content. We use N+N only when nitrate is not reported to help increase the number of available observations.

This atlas is part of the *World Ocean Atlas 2023* (WOA23; Reagan *et al.*, 2023, Reagan et al. 2024a) series. The WOA23 series includes analysis for dissolved inorganic nutrients (this atlas), temperature (Locarnini *et al.*, 2024), salinity (Reagan *et al.*, 2024), and dissolved oxygen, apparent oxygen utilization (AOU), and percent oxygen saturation (Garcia *et al.*, 2024a).

This atlas presents annual, seasonal, and monthly composite climatologies and related statistical fields for quality controlled dissolved inorganic nutrients. Climatologies in this atlas are defined as mean oceanographic fields at selected standard depth levels based on the objective analysis of historical and recent oceanographic profiles and selected surface-only data. A profile is defined as a set of measurements of seawater samples collected at discrete depths taken as an instrument such as a rosette sampler (also known as a CTD-rosette or carousel) drops or rises vertically in the water column.

This atlas includes an objective analysis of all scientifically quality-controlled historical nutrient measurements available in the *World Ocean Database 2023* collected after 1965 (WOD23; Mishonov *et al.,* 2024; Garcia *et al.*, 2024b). We present data analysis procedures and horizontal maps showing annual, seasonal, and monthly climatologies and related statistical fields at selected standard depth levels between the surface and the ocean bottom to a maximum depth of 5500 m. The complete set of maps, statistical and objectively analyzed data fields, and documentation are all available on-line at the National Centers for Environmental Information (NCEI).

All of the nutrient climatologies use all available quality control data collected in the 1965-2022 time period. We note that most of the nutrient measurements in WOD23 used in this atlas were collected on or after 1965. Earlier nutrient data collected prior to 1965 present are generally of lower research quality. The annual climatology was calculated using all data regardless of the month in which the observation was made. Seasonal climatologies were calculated using only data from the defined season (regardless of year). The seasons are defined as follows. Winter is defined as the months of January, February, and March. Spring is defined as April, May, and June. Summer is defined as July, August, and September. Fall is defined as October, November, and December. Monthly climatologies were calculated using data only from the given month regardless of the day of the month in which the observation was made.

The dissolved inorganic nutrient data used in this atlas are available in uniform format and units in the World Ocean Database 2023 (WOD23). All of the original datasets in WOD23 are discoverable and accessible at NCEI exactly as shared by the data provider

(*i.e.*, scientists, programs, projects, data centers). Large volumes of oceanographic data have been acquired as a result of the fulfillment of several U.S. and international science and data management projects including:

a) the Intergovernmental Oceanographic Commission (IOC), International Oceanographic Data and Information Exchange (IODE) Global Oceanographic Data Archaeology and Rescue (GODAR) project (Levitus *et al.* 2005b);

b) the IOC IODE *World Ocean Database project* (WOD) managed at NOAA NCEI;

c) the IOC Global Temperature Salinity Profile project (GTSPP);

d) The Argo project (including BGC Argo)

e) Ship board and repeat hydrography including the World Ocean Circulation Experiment (WOCE), Climate and Ocean: Variability, Predictability and Change (CLIVAR), and the Global Ocean Ship-based Hydrographic Investigations Program (GO-SHIP data.

f) The NOAA NCEI-hosted World Data Service for Oceanography of the World Data System (WDS); formerly World Data Center for Oceanography, Silver Spring).

The WOD23 nutrient data used in the WOA23 have been analyzed in an internally consistent and objective manner on a one-degree latitude-longitude grid at 102 standard depth levels from the surface to a maximum depth of 5500 m. The procedures for "all-data" climatologies in the WOA23 are identical to those used in the *World Ocean Atlas 2018* (WOA18) series (Garcia *et al.*, 2019). Slightly different procedures were followed in earlier analyses (Levitus, 1982; *World Ocean Atlas 1994* series [WOA94, Levitus *et al.*, 1994; Levitus and Boyer, 1994 a, b]). The WOA18 and WOA23 use 102 standard depth levels.

The gridded objective data analyses shown in this atlas are constrained by the non-uniform data coverage and data quality. The nutrient data available in the World Ocean Database 2023 (WOD23; Mishonov *et al.* 2024) are non-uniform in space, time, and data quality. These limitations and characteristics are discussed below.

Since the publication of the WOA18, additional historical and recent nutrient data have become available. However, even with the additional data, we are still hampered in a number of ways by oceanographic data coverage and their science-based quality. The overall precision in the nutrient data have significantly improved over time since 1965, and particularly after 1972 with the Geochemical Ocean Sections Study (GEOSECS) research cruises (1972-1978). Because of the generally limited nutrient data coverage in time and space in some ocean areas and depths, we opted to examine the annual cycle by compositing all data regardless of the year of observation since 1965. Data may exist in an area for only one season, thus precluding any representative annual analysis. In some areas there may be a reasonable spatial distribution of quality-controlled data points on which to base an analysis, but there may be only a few (perhaps only one) data values in each one-degree latitude-longitude square.

This atlas is divided into four Chapters. Chapter 1 provides an overview of the QC and data analysis procedures. In Chapter 2: phosphate; Chapter 3: nitrate, and Chapter 4: silicate, we provide additional information about each nutrient variable.

In Chapter 1, we begin by describing the data sources and quality control (Section 1.2). Then we describe the general data processing procedures (Section 1.3), the results (Section 1.4), summary (Section 1.5), and future work

(Section 1.6). Global horizontal maps for each of the nutrients at each individual depth level for each time period are available on-line.

WOA23 is a time-composited objectively analyzed mean climatology of phosphate, nitrate, and silicate gridded fields using quality-controlled data spanning 57 years (January 1, 1965 to December 31, 2022). While the global mean uncertainty estimate of the gridded fields is near zero (described later in sections 1.4.4 and 1.4.5), WOA23 gridded mean values cannot be expected to simultaneously represent the long-term mean and variability. The WOA23 nutrient content values in any grid box and depth would not necessarily match the content and vertical gradients of any one individual nutrient profile or individual discrete values obtained at any given time, depth, and location.

WOA23 provides statistical fields of the quality-controlled observations used as well as their mean, standard deviation, and standard error. WOA23 also provides gridded fields of the difference between the statistical mean and the objectively analyzed content value. Analysis of the differences provide an estimate of the uncertainty error or precision of the objective analysis as shown in sections 1.4.4 and 1.4.5.

## 1.2. DATA SOURCES AND QUALITY

The WOA23 is based on the WOD23 which is set to be released by early 2024. WOD23 will contain all *in situ* ocean profiles assembled and processed by the Ocean Climate Laboratory (OCL) team at NCEI through December 31, 2022. This includes all Argo and BCG Argo measurements made by December 31, 2022, with quality control as of April 1, 2023. Additionally, WOD23 will contain updated quality control flags based on the quality improvements made during the construction of the WOA23. WOA23 will be completely reproducible from the data within the WOD23.

Data sources and quality control procedures are briefly described below. For further information on the data sources used in WOA23 refer to the *World Ocean Database 2023* (WOD23, Mishonov *et al.,* 2024). The quality control procedures used in preparation of these analyses are described by Garcia *et al.* (2024a,b).

### 1.2.1. Data sources

Historical and recent oceanographic nutrient data used in this atlas were obtained from the NCEI archives, WDS-Oceanography, GODAR, International Oceanographic Data and Information Exchange (IODE) of the Intergovernmental Oceanographic Commission (IOC), and worldwide ocean data research gathered as a result of IODE WOD project managed by NOAA. The majority of the nutrient data used in this atlas were typically obtained by means of photometric analysis of serial (discrete) samples using manual or Continuous Flow Analysis (CFA).

We refer to the discrete water sample dataset in WOD23 as Ocean Station Data (OSD). Typically, each profile in the OSD dataset consists of 1 to 36 discrete water sample measurements collected at various depths between the surface and the ocean bottom using Nansen, Niskin, and CTD-rosette samplers. Garcia *et al.* (2024 a,b) describes the quality control procedures used in preparation of the atlas analyses.

To understand the field procedures for taking individual oceanographic observations and constructing climatological fields, it is necessary to distinguish between "standard level data" and "observed level data". We refer to the actual "*in situ"* (Latin for in place) measured value of an oceanographic variable as an "observation" or a "measurement", and to the depth at which

such a measurement was made as the "observed level depth". We refer to such data as "observed level data". Before the development of oceanographic instrumentation that consistently measures at high frequencies along the vertical, oceanographers often attempted to make measurements at selected "standard levels" in the water column. Sverdrup *et al.* (1942) presented the suggestions of the International Association of Physical Oceanography (IAPSO) as to which depths oceanographic measurements should be made or interpolated for data analysis. Historically the World Ocean Atlas series used a modified version of the IAPSO standard depths. However, with the increased global coverage of high depth resolution instrumentation, such as profiling floats, gliders, and moorings, WOA has extended the standard depth levels from 33 to 102 starting in the *World Ocean Atlas 2018* (WOA18; Garcia *et al.*, 2019).

The WOA18 and WOA23 standard depth levels include the original 33 depth levels presented up to the WOA13, but have tripled the resolution in the upper 100 meters, more than doubled the depth resolution of the upper 1000 meters, and almost three and a half times the resolution for overall depth levels. For many purposes, including preparation of the present climatologies, observed level data are interpolated to standard depth levels if observations did not occur at the desired standard depths (see section 1.3.1 for details). The levels at which the nutrient climatologies were calculated and available fields are given in Table 1.1. Table 1.2 shows the depths of each standard depth level. Section 1.3.1 discusses the vertical interpolation procedures used in our work. Since not every quality-controlled nutrient measurement includes quality-controlled temperature and salinity data, it is difficult to conduct the analysis along constant density or isopycnal surfaces because this would result in a large decrease in nutrient data coverage and representativeness. For this reason, we have opted to conduct the analysis as a function of standard depth levels. Figure 3 shows the number of profiles per year available in WOD23 for phosphate (Figure 1.3a), nitrate (Figure 1.3b), and silicate (Figure 1.3c).

### 1.2.2. Data quality control

By data quality control, we mean that the nutrient measurements used to estimate the statistical mean fields as well as the resulting objectively analyzed fields are reproducible and of known science quality. Since the WOA product series use similar QC and data analysis, we also help ensure an internally consistent quality assurance process at all steps of the QC process as well between WOA versions.

Quality control of the nutrient data is a major task, the difficulty of which is directly related to sparse data coverage and metadata (for some areas) upon which to base statistical checks. Consequently, we applied certain empirical criteria (see sections 1.2.2.1 through 1.2.2.4), and as part of the last processing step, (Subject Matter Expert review) subjective judgment was used (see sections 1.2.2.5 and 1.2.2.6).

Individual data, and in some cases entire profiles or all profiles for individual research cruises or autonomous sensor-based measurements, have been flagged and not used because these data produced features that were subjectively judged to be non-representative or questionable. As part of our work, we have made available WOD23 which contains both observed profile measurements as well as profiles vertically interpolated to up to 102 depth levels (0-5500 m depth). The observed and depth interpolated include various Quality Control Flags (QCF) applied. The flags mark individual nutrient measurements, entire

profiles, or even research cruises which were not used in the next step of the procedure, either interpolation to standard depth levels for observed level data or calculation of statistical means in the case of standard depth level data. Section 1.4.5 discusses comparisons of WOA23 to other gridded data sets (Figure 1.4a-c, Tables 1.7 and 1.8). Table 1.9 shows an estimate of uncertainty in the objective analysis when compared to the statistical means.

Our evolving knowledge of the variability and circulation of the world ocean based on the instrumental record includes a greater appreciation and understanding of the ubiquity and impact of ocean eddies, rings, and lenses in some parts of the world ocean. This understanding extends to documented sub-seasonal, inter-annual, and longer scale variability of water mass properties associated with modal natural variability of the atmosphere such as the North Atlantic Oscillation (NAO), Pacific Decadal Oscillation (PDO), El Niño Southern Ocean Oscillation (ENSO). Climate variability is also affected by the release of man-made greenhouse gasses such as $CO_2$, $CH_4$, and other gasses that impact the formation of mode and deep water, ocean ventilation, circulation, ocean warming, deoxygenation, acidification, eutrophication, and other processes. Therefore, we have simply added quality control flags to the nutrient data, not eliminating them from the WOD23. In addition, some data values include the originator's quality flags (*i.e.*, World Ocean Circulation Experiment WOCE, CLIVAR, GO-SHIP). Thus, individual investigators and data users can make their own decision regarding the representativeness and quality of the data. Investigators studying the distribution of features such as eddies will be interested in those data that we may regard as unrepresentative or questionable for the purpose of the analyses shown in this atlas.

#### 1.2.2.1 Duplicate elimination

Because oceanographic measurements are received from many worldwide data sources, sometimes the same data set is received at NCEI/WDS-Oceanography more than once and/or with slightly different time and/or position and/or data and metadata values, data significant figures, and hence the data are not easily identified as "exact" duplicate stations. Therefore, to eliminate the repetitive data values our databases were checked for the presence of exact and near exact replicates using eight different criteria. The first checks involve identifying stations with exact position/date/time and data values; the next checks involve offsets in position/date/time. Profiles identified as duplicates in the checks with a large offset were individually verified to ensure they were indeed duplicate profiles. In summary, we eliminated all but one profile from each set of replicate profiles at the first step of our data processing.

#### 1.2.2.2 Data range and gradient checks

Range checking (*i.e.,* checking whether individual nutrient content values are within preset minimum and maximum values as a function of depth and ocean domain) was performed on all data values as a first quality control check to identify, flag and withhold from further use the relatively few values that were grossly outside expected oceanic nutrient content ranges (*i.e.*, unrealistic content values). Range checks were prepared for individual oceanic regions and depths. A check as to whether excessive vertical gradients occur in the data has been performed for each nutrient variable in WOD23 both in terms of positive and negative gradients. We flagged and did not use values that exceeded these gradients.

#### 1.2.2.3. Statistical checks

Statistical checks were performed as follows. All data for each nutrient variable

(irrespective of year), at each standard depth level, were averaged within five-degree latitude-longitude squares to produce a record of the number of observations, mean, and standard deviation in each square. Statistics were computed for the annual, seasonal, and monthly compositing periods. Below 50 m depth, if data were more than three standard deviations from the mean, the data were flagged and withheld from further use in objective analyses. Above 50 m depth, a five-standard-deviation criterion was used in five-degree squares that contained any land area. In selected five-degree squares that are close to land areas, a four-standard-deviation check was used. In all other squares a three-standard-deviation criterion was used for the 0-50 m depth layer. For standard depth levels situated directly above the ocean bottom, a four-standard-deviation criterion was used. We realize that the nutrient data in some regions show departures from being approximately normal. While we considered using statistical test less independent of the data distribution, we opted to use a simpler approach which is consistent across WOA23 products and previous WOA versions.

The reason for the relatively weaker standard deviation criterion in coastal and near-coastal regions is the exceptionally large variability in the coastal regions particularly those influenced by man-made excess nutrient and chemical inputs. Frequency distributions of some variables in some coastal regions are observed to be skewed or bimodal. Thus, to avoid flagging possibly "good" data in highly variable environments, the standard deviation criteria were broadened.

For each nutrient variable, the total number of measurements in each profile, as well as the total number of nutrient observations exceeding the standard deviation criterion, were recorded. If several nutrient observations in a profile were found to exceed the standard deviation criterion, then the entire profile was flagged. This check was imposed after tests indicated that surface data from particular casts (which upon inspection appeared to be questionable) were being flagged but deeper data were not. Other situations were found where erroneous nutrient data from the deeper portion of a cast were flagged, while near-surface data from the same cast were not flagged because of larger natural and climate variability in near surface layers. One reason for this was the decrease of the number of nutrient observations with depth and the resulting change in sample statistics. The standard-deviation check was applied twice to the data set for each compositing time period.

In summary, first the five-degree square statistics were computed, and the data flagging procedure described above was used to provide a preliminary data set. Next, new five-degree-square statistics were computed from this preliminary data set and used with the same statistical check to produce a new, "clean" data set. The reason for applying the statistical check twice was to flag (and withhold from further use), in the first round, any grossly erroneous or non-representative or low analysis-ready quality data from the data set that would increase the variances. The second check is then more effective in identifying smaller, but non-representative, observations.

#### 1.2.2.4. Subjective flagging of data

The nutrient data were averaged as a function of depth levels by one-degree squares for input to the objective analysis program. After initial objective analyses were computed, the input set of one-degree means could still contain questionable or unrepresentative data contributing to unrealistic distributions, yielding intense bull's-eyes or large spatial gradients in one or more one-degree squares. Examination of these "features" indicated

that some of them were due to profiles from particular oceanographic cruises. In such cases, data from an entire cruise were flagged and withheld from further use by setting a flag on each profile from the cruise. In other cases, individual profiles or measurements were found to cause these features and were flagged and not used in the analysis. This procedure is conducted several times to help identify questionable values.

#### 1.2.2.5. Representativeness of the data

Another quality control challenge is nutrient data representativeness. To mitigate the general paucity of data in some regions and time periods (*i.e.*, monthly, seasonal), we used data compositing of all quality controlled nutrient data to produce "climatological" fields for a given time period. In a given one-degree square, there may be data from a month or season of one particular year, while in the same or a nearby square there may be data from an entirely different year. If there is large interannual and longer variability in a region where scattered sampling in time has occurred, then one can expect the analysis to reflect this. Because the observations are generally scattered randomly with respect to time, except for a few limited areas (*i.e.*, in time series stations such as Hawaii Ocean Time Series, HOTS, Bermuda Atlantic Time Series, BATS; CARIACO), the results cannot, in a strict sense, be considered representative of the long-term climatological average.

We present smoothed analyses of statistical means, based (in certain areas) on relatively few observations. We believe, however, that useful baseline information about the oceans can be gained through our procedures and that the large-scale features are representative of the real ocean. For example, if a hypothetical global synoptic set of ocean data (temperature, salinity, dissolved oxygen, nutrients) existed and one were to smooth these data to the same degree as we have smoothed the climatological statistical means, the large-scale ocean features would be similar to our results. Some differences would certainly occur because of interannual-to-decadal-scale natural and man induced climate variability.

The number of nutrient observations diminish in number with increasing depth. In the upper ocean, the all-data annual mean distributions are reasonable for representing large-scale features, but for the seasonal and monthly periods, the database is inadequate in some regions. With respect to the deep ocean, in some areas the distribution of observations may be adequate for some diagnostic computations but largely inadequate for other purposes. If an isolated deep basin or some region of the deep ocean has only one observation, then no horizontal gradient computations are possible. However, useful information is provided by the observation in the computation of other quantities (*i.e.*, basin-scale inventory content of a nutrient variable).

We note that in portions of the World Ocean such as the Arctic, northern marginal seas, and the Southern Ocean, nutrient data temporal and spatial sampling is noticeably infrequent and seasonally-biased to boreal and austral summer when water sampling from research ships is nominally easier. Furthermore, our statistical flagging of standard level data assumes that the data within each 5-degree box are approximately normally distributed. This assumption fails in certain regions of the ocean. Therefore, we are currently investigating alternative methods for quality control flagging. These include alternative statistics that do not require Gaussian distributions, and leveraging machine learning to better cluster the data before applying statistical checks.

## 1.3. DATA PROCESSING PROCEDURES

### 1.3.1. Vertical interpolation to standard levels

Vertical interpolation of observed depth level data to standard depth levels followed procedures in Joint Panel on Oceanographic Tables and Standards Editorial Panel (JPOTS, 1991). These procedures are in part based on the work of Reiniger and Ross (1968). Four observed depth level values surrounding the standard depth level value were used, two values from above the standard level and two values from below the standard level. The pair of values furthest from the standard level is termed "exterior" points and the pair of values closest to the standard level are termed "interior" points. Paired parabolas were generated via Lagrangian interpolation. A reference curve was fitted to the four data points and used to define unacceptable interpolations caused by "overshooting" in the interpolation. When there were too few data points above or below the standard level to apply the Reiniger and Ross technique, we used a three-point Lagrangian interpolation. If three points were not available (either two above and one below or vice-versa), we used linear interpolation. In the event that an observation occurred exactly at the depth of a standard level, then a direct substitution was made. Table 1.2 provides the range of acceptable distances for which observed level data could be used for interpolation to a standard level.

### 1.3.2. Methods of analysis

#### 1.3.2.1. Overview

An objective analysis scheme of the type described by Barnes (1964) was used to produce the fields shown in this atlas. This scheme had its origins in the work of Cressman (1959). In *World Ocean Atlas 1994* (WOA94), the Barnes (1973) scheme was used. This required only one "correction" to the first-guess field at each grid point in comparison to the successive correction method of Cressman (1959) and Barnes (1964). This was to minimize computing time used in the processing. Barnes (1994) recommends a return to a multi-pass analysis when computing time is not an issue. Based on our own experience we agree with this assessment. The single pass analysis, used in WOA94, caused an artificial front in the Southeastern Pacific Ocean in a data sparse area (Anne Marie Treguier, personal communication). The analysis scheme used in generating of the WOA98, WOA01, WOA05, WOA13, WOA18, and WOA23 analyses uses a three-pass "correction" which does not result in the creation of this artificial front.

Inputs to the analysis scheme were one-degree square means of data values at standard levels (for time period and variable being analyzed), and a first-guess value for each square. For instance, one-degree square means for our annual analysis were computed using all available data regardless of date of observation. For July, we used all historical July data regardless of year of observation.

Analysis was the same for all standard depth levels. Each one-degree latitude-longitude square mean value was defined as being representative of its square. The 360x180 grid points are located at the intersection of half-degree lines of latitude and longitude. An influence radius was then specified. At those grid points where there was an observed mean value, the difference between the mean and the first-guess field was computed. Next, a correction to the first-guess value at all grid points was computed as a distance-weighted mean of all grid location difference values that lie within the area around the grid location defined by the influence radius. Mathematically, the correction factor derived by Barnes (1964) is given by the expression:

$$C_{i,j} = \frac{\sum_{s=1}^{n} W_s Q_s}{\sum_{s=1}^{n} W_s} \qquad (1)$$

in which:

($i,j$) - coordinates of a grid location in the east-west and north-south directions respectively;

$C_{i,j}$ - the correction factor at grid location coordinates ($i,j$);

$n$ - the number of observations that fall within the area around the point $i,j$ defined by the influence radius;

$Q_s$ - the difference between the observed mean and the first-guess at the $S^{th}$ point in the influence area;

$W_s = e^{-\frac{Er^2}{R^2}}$ (for $r \leq R$; $W_s = 0$ for $r > R$);

$r$ - distance of the observation from the grid location;

$R$ - influence radius;

$E = 4$.

The derivation of the weight function, $W_s$, will be presented in the following section. At each grid location we computed an analyzed value $G_{i,j}$ as the sum of the first-guess, $F_{i,j}$ , and the correction $C_{i,j}$. The expression for this is

$$G_{i,j} = F_{i,j} + C_{i,j} \qquad (2)$$

If there were no data points within the area defined by the influence radius, then the correction was zero, the first-guess field was left unchanged, and the analyzed value was simply the first-guess value. This correction procedure was applied at all grid points to produce an analyzed field. The resulting field was first smoothed with a median filter (Tukey, 1974; Rabiner *et al.,* 1975) and then smoothed with a five-point smoother of the type described by Shuman (1957) (hereafter referred to as five-point Shuman smoother). The choice of first-guess fields is important and we discuss our procedures in section 3.2.5.

The analysis scheme is set up so that the influence radius, and the number of five-point smoothing passes can be varied with each iteration. The strategy used is to begin the analysis with a large influence radius and decrease it with each iteration. This technique allows us to analyze progressively smaller-scale phenomena with each iteration.

The analysis scheme is based on the work of several researchers analyzing meteorological data. Bergthorsson and Doos (1955) computed corrections to a first-guess field using various techniques: one assumed that the difference between a first-guess value and an analyzed value at a grid location was the same as the difference between an observation and a first-guess value at a nearby observing station. All the observed differences in an area surrounding the grid location were then averaged and added to the grid location first-guess value to produce an analyzed value. Cressman (1959) applied a distance-related weight function to each observation used in the correction in order to give more weight to observations that occur closest to the grid location. In addition, Cressman introduced the method of performing several iterations of the analysis scheme using the analysis produced in each iteration as the first-guess field for the next iteration. He also suggested starting the analysis with a relatively large influence radius and decreasing it with successive iterations so as to analyze smaller scale phenomena with each pass.

Sasaki (1960) introduced a weight function that was specifically related to the density of observations, and Barnes (1964, 1973) extended the work of Sasaki. The weight

function of Barnes (1964) has been used here. The objective analysis scheme we used is in common use by the mesoscale meteorological community. Several studies of objective analysis techniques have been made. Achtemeier (1987) examined the "concept of varying influence radii for a successive corrections objective analysis scheme." Seaman (1983) compared the "objective analysis accuracies of statistical interpolation and successive correction schemes." Smith and Leslie (1984) performed an "error determination of a successive correction type objective analysis scheme." Smith *et al.* (1986) made "a comparison of errors in objectively analyzed fields for uniform and non-uniform station distribution."

### 1.3.2.2. Derivation of Barnes (1964) weight function

The principle upon which the Barnes (1964) weight function is derived is that "the two-dimensional distribution of an atmospheric variable can be represented by the summation of an infinite number of independent harmonic waves, that is, by a Fourier integral representation". If *f(x,y)* is the variable, then in polar coordinates *(r,θ)*, a smoothed or filtered function *g(x,y)* can be defined:

$$g(x,y)=\frac{1}{2\pi}\int_0^{2\pi}\int_0^{\infty}\eta f(x+r\cos\theta, y+r\sin\theta)\, d(\frac{r^2}{4K})d\theta \tag{3}$$

in which $r$ is the radial distance from a grid location whose coordinates are *(x,y)*. The weight function is defined as

$$\eta = e^{-\frac{r^2}{4K}} \tag{4}$$

which resembles the Gaussian distribution. The shape of the weight function is determined by the value of $K$, which relates to the distribution of data. The determination of $K$ follows. The weight function has the property that

$$\frac{1}{2\pi}\int_0^{2\pi}\int_0^{\infty}\eta d\left(\frac{r^2}{4K}\right)d\theta = 1 \tag{5}$$

This property is desirable because in the continuous case (3) the application of the weight function to the distribution *f(x,y)* will not change the mean of the distribution. However, in the discrete case (1), we only sum the contributions to within the distance $R$. This introduces an error in the evaluation of the filtered function, because the condition given by (5) does not apply. The error can be pre-determined and set to a reasonably small value in the following manner. If one carries out the integration in (5) with respect to $\theta$, the remaining integral can be rewritten as

$$\int_0^{R}\eta d\left(\frac{r^2}{4K}\right)+\int_R^{\infty}\eta d\left(\frac{r^2}{4K}\right)=1 \tag{6}$$

Defining the second integral as $\varepsilon$ yields

$$\int_0^{R} e^{-\frac{r^2}{4K}} d\left(\frac{r^2}{4K}\right)=1-\varepsilon \tag{7}$$

Integrating (7), we obtain

$$\varepsilon = e^{-\frac{R^2}{4K}} \tag{7a}$$

Taking the natural logarithm of both sides of (7a) leads to an expression for $K$,

$$K = R^2 / 4E \tag{7b}$$

where $E \equiv -\ln \varepsilon$

Rewriting (4) using (7b) leads to the form of weight function used in the evaluation of (1). Thus, choice of $E$ and the specification of $R$

determine the shape of the weight function. Levitus (1982) chose $E$=4 which corresponds to a value of $\varepsilon$ of approximately 0.02. This choice implies with respect to (7) the representation of more than 98 percent of the influence of any data around the grid location in the area defined by the influence radius $R$. This analysis (WOA23) and previous analyses (WOA94, WOA98, WOA01, WOA05, WOA13, WOA18) used $E$=4.

Barnes (1964) proposed using this scheme in an iterative fashion similar to Cressman (1959). Levitus (1982) used a four-iteration scheme with a variable influence radius for each pass. WOA94 used a one-iteration scheme. WOA98, WOA01, WOA05, WOA09, WOA13, WOA18, and WOA23 employed a three-iteration scheme with a variable influence radius.

#### 1.3.2.3. Derivation of Barnes (1964) response function

It is desirable to know the response of a data set to the interpolation procedure applied to it. Following Barnes (1964) and reducing to one-dimensional case we let

$$f(x) = A\sin(\alpha x) \tag{8}$$

in which $\alpha = 2\pi/\lambda$ with $\lambda$ being the wavelength of a particular Fourier component, and substitute this function into equation (3) along with the expression for $\eta$ in equation (4). Then

$$g(x) = D\left[A\sin(\alpha x)\right] = Df(x) \tag{9}$$

in which $D$ is the response function for one application of the analysis and defined as

$$D = e^{-\left(\frac{\alpha R}{4}\right)^2} = e^{-\left(\frac{\pi R}{2\lambda}\right)^2}$$

The phase of each Fourier component is not changed by the interpolation procedure. The results of an analysis pass are used as the first-guess for the next analysis pass in an iterative fashion. The relationship between the filtered function $g(x)$ and the response function after $N$ iterations as derived by Barnes (1964) is

$$g_N(x) = f(x)D\sum_{n=1}^{N}(1-D)^{n-1} \tag{10}$$

Equation (10) differs trivially from that given by Barnes. The difference is due to our first-guess field being defined as a zonal average, annual mean, seasonal mean, or monthly mean, whereas Barnes used the first application of the analysis as a first-guess. Barnes (1964) also showed that applying the analysis scheme in an iterative fashion will result in convergence of the analyzed field to the observed data field. However, it is not desirable to approach the observed data too closely, because at least seven or eight grid points are needed to represent a Fourier component.

The response function given in (10) is useful in two ways: it is informative to know what Fourier components make up the analyses, and the computer programs used in generating the analyses can be checked for correctness by comparison with (10).

#### 1.3.2.4. Choice of response function

The distribution of nutrient observations at different depths and for the different averaging periods, are not regular or uniform in space and time. At one extreme, regions exist in which every one-degree square contains data and no interpolation to standard depth levels needs to be performed. At the other extreme are regions in which few if any data of known science quality exist. Thus, with variable data spacing the average separation distance between grid points containing data is a function of geographical position and averaging period. However, if we computed and used a different average separation distance for each variable at each depth and each averaging period, we would

be generating analyses in which the wavelengths of observed phenomena might differ from one depth level to another and from one season to another. In WOA94, a fixed influence radius of 555 kilometers was used to allow uniformity in the analysis of all variables. For the present WOA23 analyses (as well as for the WOA18, WOA13, WOA09, WOA98, and WOA01), a three-pass analysis, based on Barnes (1964), with influence radii of 892, 669 and 446 km was used for the 1° analysis.

Inspection of (1) shows that the difference between the analyzed field and the first-guess field values at any grid location is proportional to the sum of the weighted differences between the observed mean and first-guess at all grid points containing data within the influence area.

The reason for using the five-point Shuman smoother and the median smoother is that our data are not evenly distributed in space. As the analysis moves from regions containing data to regions devoid of data, small-scale discontinuities may develop. The five-point Shuman and median smoothers are used to eliminate these discontinuities. The five-point Shuman smoother does not affect the phase of the Fourier components that comprise an analyzed field.

The response function for the analyses presented in the WOA23 series is given in Table 1.3 and shown in Figure 1.1. For comparison purposes, the response function used by Levitus (1982), WOA94, and other WOA atlases are also presented. The response function represents the smoothing inherent in the objective analysis described above plus the effects of one application of the five-point Shuman smoother and one application of a five-point median smoother. The effect of varying the amount of smoothing in North Atlantic sea surface temperature (SST) fields has been quantified by Levitus (1982) for a particular case. In a region of strong SST gradient such as the Gulf Stream, the effect of smoothing can easily be responsible for differences between analyses exceeding 1.0°C.

To avoid the problem of the influence region extending across large coastal land boundaries or sills to adjacent basins, the objective analysis routine employs basin "identifiers" to preclude the use of data from adjacent basins. Table 1.4 lists these basins and the depth at which no exchange of information between basins is allowed during the objective analysis of data, *i.e.,* "depths of mutual exclusion." Some regions are nearly, but not completely, isolated topographically. Because some of these nearly isolated basins have water mass properties that are different from surrounding basins, we have chosen to treat these as isolated basins as well. Not all such basins have been identified because of the complicated structure of the sea floor. In Table 1.4, a region marked with an (*) can interact with adjacent basins except for special areas such as the Isthmus of Panama.

#### 1.3.2.5. First-guess field determination

There are gaps in the data coverage and, in some parts of the world ocean, there exist adjacent basins whose water mass properties are individually nearly homogeneous but have distinct basin-to-basin differences. Spurious features can be created when an influence area extends over two basins of this nature (basins are listed in Table 1.4). Our choice of first-guess field attempts to minimize the creation of such features. To maximize data coverage and best represent global variability, we attempted to create a set of "time-indeterminant" climatologies as a first-guess for decadal composite climatologies. This was not possible in the case of nutrients. The annual analysis was then used as the first-guess for each seasonal analysis and each seasonal analysis was used as a first-guess for the appropriate monthly analysis if computed.

We then reanalyzed the nutrient data using the newly produced analyses as first-guess fields described as follows and as shown in Figure 1.2. A new annual mean was computed as the mean of the twelve-monthly analyses for the upper 800 m, and the mean of the four seasons below 800 m depth. This new annual mean was used as the first-guess field for new seasonal analyses. These new seasonal analyses in turn were used to produce new monthly analyses. This procedure generally produces slightly smoother means.

These time-indeterminant monthly mean objectively analyzed temperature fields were used as the first-guess fields for each "decadal" monthly climatology. Likewise, time-indeterminant seasonal and annual climatologies were used as first-guess fields for the seasonal and annual decadal climatologies.

We recognize that fairly large data sparse regions exist particularly in the South Pacific and Polar regions, in some cases to such an extent that a seasonal or monthly analysis in these regions is not meaningful. Geographic distribution of observations for the "all-data" annual periods (see appendices) is excellent for the upper layers of the ocean. By using an "all-data" annual mean, first-guess field regions where data exist for only one season or month will show no contribution to the annual cycle. By contrast, if we used a zonal average for each season or month, then, in those latitudes where gaps exist, the first-guess field would be heavily biased by the few data points that exist. If these were anomalous data in some way, an entire basin-wide belt might be affected.

One advantage of producing "global" fields for a particular compositing period (even though some regions are data void) is that such analyses can be modified by investigators for use in modeling studies.

### 1.3.3. Choice of objective analysis procedures

Optimum interpolation (Gandin, 1963) has been used by some investigators to objectively analyze oceanographic data. We recognize the power of this technique but have not used it to produce analyzed fields. As described by Gandin (1963), optimum interpolation is used to analyze synoptic data using statistics based on historical data. In particular, second-order statistics such as correlation functions are used to estimate the distribution of first order parameters such as means. We attempt to map most fields in this atlas based on relatively sparse data sets. By necessity we must composite all data regardless of year of observation, to have enough data to produce a global, hemispheric, or regional analysis for a particular month, season, or even yearly. Because of the paucity of data, we prefer not to use an analysis scheme that is based on second order statistics. In addition, as Gandin has noted, there are two limiting cases associated with optimum interpolation. The first is when a data distribution is dense. In this case, the choice of interpolation scheme makes little difference. The second case is when data are sparse. In this case, an analysis scheme based on second order statistics is of questionable value. For additional information on objective analysis procedures see for example Thiebaux and Pedder (1987) and Daley (1991).

### 1.3.4. Choice of spatial grid

The analyses that comprise WOA23 have been computed using the ETOPO2 (Earth Topography 2 arc minute) land-sea topography to define ocean depths at each grid location (ETOPO2, 2006). From the ETOPO2 land mask, a quarter-degree land mask was created based on ocean bottom depth and land criteria. If sixteen or more 2-minute square values out of a possible forty-nine in a one-quarter-degree box were

defined as land, then the quarter-degree grid box was defined to be land. If no more than two of the 2-minute squares had the same depth value in a quarter-degree box, then the average value of the 2-minute ocean depths in that box was defined to be the depth of the quarter-degree grid box. If ten or more 2-minute squares out of the forty-nine had a common bottom depth, then the depth of the quarter-degree box was set to the most common depth value. The same method was used to go from a quarter-degree to a one-degree resolution. In the one-degree resolution case, at least four points out of a possible sixteen (in a one-degree square) had to be land in order for the one-degree square to remain land and three out of sixteen had to have the same depth for the ocean depth to be set. These criteria yielded a mask that was then modified by:

1. Connecting the Isthmus of Panama;
2. Maintaining an opening in the Straits of Gibraltar and in the English Channel;
3. Connecting the Kamchatka Peninsula and the Baja Peninsula to their respective continents.

The one-degree land mask was created from the quarter-degree mask instead of directly from ETOPO2 in order to maintain consistency between the quarter-degree and one-degree masks.

## 1.4. RESULTS

The on-line figures for this atlas include several types of maps representing annual, seasonal, and monthly spatial distribution of analyzed data and data statistics as a function of selected standard depth levels for dissolved inorganic nutrients over one-degree latitude-longitude grid:

a) Objectively analyzed climatology fields. Grid boxes for which there were less than three values available in the objective analysis defined by the influence radius are denoted by a white "+" symbol.

b) Statistical mean fields. Grid boxes for which there were less than three values available in the objective analysis defined by the influence radius are denoted by a white "+" symbol.

c) Data distribution fields for the number of observations in each grid box used in the objective analysis binned into 1 to 2, 3-5, 6-10, 11-30, 31-50 and greater than 51 observations.

d) Standard deviation fields are binned into several ranges depending on the depth level. The maximum value of the standard deviation is shown on the map.

e) Standard error of the mean fields binned into several ranges depending on the depth level.

f) Differences between observed and analyzed fields are binned into several ranges depending on the depth level.

g) Difference between seasonal/monthly temperature fields and the annual mean field.

h) The number of mean values within the radius of influence for each grid box was also calculated. This is not represented as stand-alone maps, but the results are used on a) and b) maps (see above) to mark the grid boxes with less than three mean values within the radius of influence.

The maps are arranged by composite time periods (annual, seasonal, month). Table 1.5 describes all available maps and data fields. We note that the complete set of all climatological maps (in color), objectively analyzed fields, and associated statistical fields at all standard depth levels shown in Table 1.2, as well as the complete set of data fields and documentation, are all available on-line. The complete set of data fields and

documentation are available on-line as well.

All of the figures use consistent symbols and notations for displaying information. Continents are displayed as light-gray areas. Coastal and open ocean areas shallower than the standard depth level being displayed are shown as solid gray areas. The objectively analyzed fields include the nominal contour interval used. In addition, these maps may include in some cases additional contour lines displayed as dashed black lines. All of the maps were computer drafted using PyGMT (Uieda and Wessel, 2017), a Python wrapper for the Generic Mapping Tools, GMT (Wessel and Smith, 1998).

We describe next the computation of annual, seasonal, and monthly fields (section 1.4.1) and available objective and statistical fields (section 1.4.2).

### 1.4.1. Computation of annual, seasonal, and monthly composite fields

After completion of all of our analyses we operationally define a final annual analysis as the average of our twelve monthly mean nutrient fields in the upper 800 m of the ocean (Figure 1.2). Our final seasonal analysis is defined as the average of monthly analyses in each season in the upper 800 m of the ocean (Winter=January-March, Spring=April-June, Summer=July-September, and Fall= October-December).

### 1.4.2. Available statistical fields

Table 1.5 lists all objective and statistical fields calculated as part of WOA23. Climatologies of oceanographic variables and associated statistics described in this document, as well as global figures of the same can be obtained online.

The sample standard deviation in a grid box was computed using:

$$s = \sqrt{\frac{\sum_{n=1}^{N}(x_n - \bar{x})^2}{N-1}} \qquad (11)$$

in which $x_n$= the $n^{th}$ data value in the grid box, $\bar{x}$=mean of all data values in the grid box, and $N$= total number of data values in the grid box. The standard error of the mean was computed by dividing the standard deviation by the square root of the number of observations in each grid box.

In addition to statistical fields, the land/ocean bottom mask and basin definition mask are available on-line. A user could take the standard depth level data from WOD23 with flags and these masks, and recreate the WOA23 fields following the procedures outlined in this document. Explanations and data formats for the data files are found under documentation on the WOA23 webpage.

### 1.4.3. Obtaining WOA23 fields on-line

The objectively analyzed and statistical data fields can be obtained online in different digital formats at the WOA23 webpage. WOA23 data are compliant with the Findable, Accessible, Interoperable, and Reusable data principles (FAIR; Wilkinson *et al.*, 2016). The WOA23 fields can be obtained in ASCII format (WOA native and comma separated value [CSV]) and Climate and Forecast (CF) compliant Network Common Data Format (NetCDF) through our WOA23 webpage.

For users interested in specific geographic areas, the World Ocean Atlas Select (WOAselect) selection tool can be used to designate a subset geographic area, depth, and oceanographic variable to view, and optionally download, climatological means or related statistics in shapefile format which is compatible with GIS software such as ESRI ArcMap. WOA23 includes a digital collection of "png" images of the objective

and statistical fields. In addition, WOA23 can be obtained in Ocean Data View (ODV, Schlitzer, 2023). format. WOA23 will be available through data portals, and other online locations as well including the IODE website. WOA98, WOA01, WOA05, WOA09, and WOA13 are presently served through the IRI/LDEO Climate Data Library with access to statistical and objectively analyzed fields in a variety of digital formats.

### 1.4.4 Global mean nutrient content and objective analysis uncertainty error

The objectively analyzed field enable estimation of regional to basin scale nutrient estimates. Table 1.6a shows the depth averaged (0-5500 m depth) annual mean nutrient content for different ocean basins. The global mean nutrient content values are approximately 1.76 ± 0.58, 24.6 ± 9.4, and 65. 7 ± 41.2 μmol·kg$^{-1}$ for phosphate, nitrate, and silicate, respectively. Nutrient content is generally higher in the Pacific than in other basins (Figures 2.7 in Chapter 2; Figure 3.6 in Chapter 3; and Figure 4.7 in Chapter 4). Section 1.4.5 compares WOA23 to other gridded data products.

The global mean content inventories for phosphate, nitrate, and silicate are 3.1, 42.2, and 122.4 Pmol (1 Pmol= $10^{15}$ mol), respectively (Table 1.6b). In all cases, the Pacific basin has the greatest nutrient content inventory. If scaled to the volume in the Pacific, then the nutrient content inventory in the Atlantic and Indian basins would be about 2.1 and 2.5 times higher, respectively.

A rough measure of the uncertainty or precision of the climatological objectively analyzed fields can be obtained by quantifying their deviation from the statistical nutrient mean fields at all grids and depths. WOA23 includes fields of the deviation of the statistical mean from the climatological mean at each 1° square at each standard depth. The deviations also reflect the combined effects of data coverage, depth interpolation, and smoothing by the response function (Table 1.3, Figure 1.2).

Table 1.9 shows the depth averaged mean and standard deviation of the differences in different ocean basins. The global mean differences for all nutrients is close to zero which suggests that the objective analyses fields represent well the mean of the observations at basin-scales. We note that the mean differences are slightly negative. This indicates that the climatological fields on average overestimate the statistical mean by a small value (Table 1.9). For context, the mean difference deviation from the climatological annual mean content (Table 1.6) are phosphate 0.2%; nitrate 0.1%; and silicate 0.1%. These deviations are comparable to the measurement precision of nutrient measurements using classical Continuous Flow analysis using an Auto-Analyzer which are in the order of 1-3% (Tanhua *et al.*, 2010).

### 1.4.5 WOA23 comparison to other mapped datasets

We compared the WOA23 (this atlas) to the WOA18 differences (WOA23 minus WOA18) as a function of depth and basin to quantify the internal consistency of the nutrient fields (Table 1.7). The WOA23 and WOA18 compare well in all basins. The global ocean depth averaged (±1 standard deviation) difference in nutrient content are smaller than the precision of the measurements, phosphate (0.001 ± 0.005 μmol·kg$^{-1}$), nitrate (0.001 ± 0.023μmol·kg$^{-1}$), and silicate (-0.027 ± 0.117 μmol·kg$^{-1}$) for the 0-5500 m depth layer. For comparison, these mean deviations are less than or comparable to present day precision of CFA nutrient measurements (*i.e.*, GO-SHIP).

For comparison, we also calculated differences in nutrient content as a function of depth between WOA23 and the Global

Ocean Data Analysis Project version 2.2016b (GLODAPv2.2016b, Olsen *et al.*, 2016; Lauvset *et al.* 2022; Key *et al.*, 2015. Mapped Data Product accessed August 2023; thereafter GLODAP for short). The depth averaged (± 1 standard deviation) content differences are relatively small (Table 1.8). The global ocean depth averaged differences (0-5500 m depth) are about 0.00 ± 0.03, -0.16 ± 0.26, and 0.47 ± 0.41 $\mu mol \cdot kg^{-1}$ for phosphate, nitrate, and silicate respectively (Table 1.8).

It would be surprising if there were no nutrient content differences between WOA23 and GLODAP and other mapped nutrient content data product. First, the WOA23 (and WOA18) is based on a much larger number of quality-controlled nutrient observations in all seasons that overall have much larger spatial and temporal data coverage than GLODAP. Most of the measurements used in GLODAP were collected during Austral and Boreal warm months. Thus, GLODAP has a warm seasonal bias when compared to WOA23. We note that most of the nutrient measurements used in GLODAP were also used in WOA23 and available in WOD23. Second, WOA23 and GLODAP use a number of different quality control tests metrics. Third, WOA23 and GLODAP use different gap-filling mapping methods. WOA23 objective analysis is described in section 1.3. The GLODAP mapped product uses the Data-Interpolating Variational Analysis software (DIVA) on a uniform 1°x1° grid for 33 standard depth surfaces. GLODAP's 33 depth levels are a subset of the WOA23 102 depth levels.

## 1.5. SUMMARY

In the preceding sections we have described the WOA23 objective analysis process used for the quality controlled nutrient data available in WOD23. The WOA23 gridded fields were computed using a similar process as for other WOA23 climatologies (*i.e.*, temperature, salinity, dissolved oxygen, Apparent Oxygen Utilization, percent oxygen saturation). This provides an internally consistent set of analyzed gridded fields of known science quality. Chapters II-IV describe additional features of the analysis for phosphate, nitrate, and silicate.

One advantage of the analysis techniques used in this atlas is that we know the amount of smoothing by objective analyses as given by the response function in Table 1.3 and Figure 1.1. We believe this to be an important function for constructing and describing a climatology of any parameter. Particularly when computing anomalies from a standard climatology, it is important that the field be smoothed to the same extent as the climatology, to prevent generation of spurious anomalies simply through differences in smoothing. A second reason is that purely diagnostic computations require a minimum of seven or eight grid points to represent any Fourier component. Higher order derivatives might require more data smoothing.

We have created objectively analyzed fields and data sets of known science quality. We emphasize that some quality control procedures used are subjective. For those users who wish to make their own choices, all the data used in our analyses are available both at standard depth levels as well as observed depth levels. WOA23 can be reproduced using the WOD23 data. The results presented in this atlas may show some features that are suspect and may be due to non-representative data that were not flagged by the quality control techniques used. Although we have attempted to assess as many of these features as possible by flagging the data which generate these features, some obviously could remain. Some may eventually turn out not to be artifacts but rather to represent real features, not yet

capable of being described in a meaningful way due to lack of data. The views, findings, and any errors in this document are those of the authors.

## 1.6. FUTURE WORK

Our analyses will be updated periodically when justified by additional coastal and open-ocean nutrient observations. As more nutrient data are received at NCEI and WDS-Oceanography, we will also be able to extend the seasonal and monthly nutrient analysis to deeper levels and increase the representativeness of the data of each time period and depth.

Merging and blending nutrient data collected by manual, CFA, and automated nutrient sensors will likely help improve the results and help provide much additional observational baseline constraints on sub-seasonal to decadal-scale variability. For example, recent advances in chemical sensors in Biogeochemical Argo (BGC Argo) profiling floats are enabling additional measurements of nitrate (Johnson *et al.*, 2017a, b). We plan to add sensor-based nitrate data in future WOA data product versions. Each ocean observing system collecting nutrient data adds additional data coverage and may have different data uncertainties and calibrations that must be reconciled before combining into an internally consistent climatology.

We are encouraged by the potential acquisition of additional high-quality oceanographic observations through regional and global projects with large international collaboration such as the Global Ocean Observing System (GOOS) 2030 Strategy and the United Nations Decade of Ocean Science for Sustainable Development (2021-2030). GOOS includes a global array of ocean observations including the ARGO array. It is sponsored by the Intergovernmental Oceanographic Commission of UNESCO, the World Meteorological Organization (WMO), the United Nations Environment Programme (UNEP), and the International Science Council (ISC). Expansion of GOOS spatial and temporal coverage and addition of measured Essential Ocean Variables (EOV) will enable the creation of more representative regional to global climatologies that span sub-seasonal to decadal time scales.

One country cannot afford the observational system needed to monitor the entire ocean domain; and thus, sharing, access and reuse of observations is essential for formulating informed science-based societal-relevant strategies for sustainable ocean use (*i.e.*, blue economy) and to respond to regional and global environmental challenges. The development of increasing representative research-quality ocean climatologies such as WOA23 nutrients serve as reliable science-based baseline from which to estimate low frequency and persistence of ocean variability at spatial and temporal scales of interest (*i.e.*, global ocean heat content, acidification, deoxygenation, eutrophication, nutrient content).

The oceanographic observational data shared and available in WOD23 were collected at great public cost and collected by many scientists, institutions, programs, and countries over many years. The historical instrumental record data are of irreplaceable scientific value as the data our only observational means to assess ocean variability and impacts such as global ocean deoxygenation. WOA23 is openly shared to the global ocean community as a research-quality climatology.

We welcome ocean community comments that would improve the usefulness and quality of WOA23. While we have done extensive efforts to quality control the data, ocean researchers and data users could help

us to identify additional questionable data, new data versions, duplicate data, additional metadata.

A critical gap is the absence of ocean community adopted QC metrics and methods. While the QC process generally addresses the data product fit-for-purpose requirement, it would be useful to identify and document primary level data QC for each variable that the ocean community could adopt for internal consistency. For example, a data range check for some data users could mean the climatological mean content range, a data range that helps identify anomalously low and high data values in different geographic regions and depths, or to identify unrealistic values.

In the acknowledgement section of this atlas, we emphasize our deep and sincere gratitude to all of the worldwide researchers, technicians, data managers, projects, institutions, data centers, IOC IODE, WDS, and others who have collected and openly shared and continue to share oceanographic data to national, regional, global data centers, and the WDS-Oceanography. Documenting ocean climate variability and impacts relies on open access to global measurements. In the WOD23 metadata we acknowledge the investigators and data providers of every single dataset that is included. In all cases, the data in the WOD provides links to the NOAA NCEI long-term data archive where the original data provided are preserved exactly as received and where the provenance and attribution of the data are fully described including DOI's if the information is made available. The WOD aims to merge of the available oceanographic profile data in a uniform, FAIR-compliant, and analysis-ready dataset that can be reliably used by the global ocean science community.

The WOA23 series includes several volumes for different variables and parameters (Table 1.12). The WOA23 is a NOAA NCEI Ocean Climate Laboratory Team effort by many individuals. The views, findings, and any errors in this document are those of the authors and do not reflect any position of the U.S. Government, DOC, or NOAA.

## 1.7 REFERENCES

Achtemeier, G.L. (1987). On the concept of varying influence radii for a successive corrections objective analysis. *Mon. Wea. Rev*., 11, 1761-1771. https://doi.org/10.1175/1520-0493(1987)115<1760:OTCOVI>2.0.CO;2

Bakun, A. (1990). Global climate change and intensification of coastal ocean upwelling. *Science*, 247(4939). https://www.jstor.org/stable/2873492

Barnes, S.L. (1964). A technique for maximizing details in numerical weather map analysis. *J. App. Meteor*., 3, 396-409. https://doi.org/10.1175/1520-0450(1964)003<0396:ATFMDI>2.0.CO;2

Barnes, S.L. (1973). Mesoscale objective map analysis using weighted time series observations. NOAA Technical Memorandum ERL NSSL-62, 60 pp. [PDF]

Barnes, S.L. (1994). Applications of the Barnes Objective Analysis Scheme, Part III: Tuning for Minimum Error. *J. Atmosph. and Oceanic Tech*., 11, 1459-1479. https://doi.org/10.1175/1520-0426(1994)011%3C1459:AOTBOA%3E2.0.CO;2

Bergthorsson, P. and B. Doos (1955). Numerical Weather map analysis. Tellus, 7, 329-340. [PDF]

Boyer, T.P., O.K. Baranova, C. Coleman, H.E. Garcia, A. Grodsky, R.A. Locarnini, A.V. Mishonov, C.R. Paver, J.R. Reagan, D. Seidov, I.V. Smolyar, K.W. Weathers, M.M. Zweng (2019). World Ocean Database 2018. A. Mishonov, Tech. Ed. *NOAA Atlas NESDIS 87*. [PDF]

Capone, D. G., *et al.* (2005). Nitrogen fixation by Trichodesmium spp.: An important source of new nitrogen to the tropical and subtropical North Atlantic Ocean. *Global Biogeochemical Cycles*, 11(2). https://doi.org/10.1029/2004GB002331

Codispoti, L. A., and Christensen, J. P. (1985). Nitrification, denitrification, and nitrous oxide cycling in the eastern tropical South Pacific Ocean. *Marine Chemistry*, 16(3), 277-300. https://doi.org/10.1016/0304-4203(85)90051-9

Cressman, G.P. (1959). An operational objective analysis scheme. *Mon. Wea. Rev.*, 87, 329-340.

Daley, R. (1991). *Atmospheric Data Analysis.* Cambridge University Press, Cambridge, 457 pp.

DeVries, T., and F. Primeau, (2011). Dynamically and observationally constrained estimates of water mass distributions and ages in the global ocean. Journal of Physical Oceanography, 41(12), 2381 2401. https://doi.org/10.1175/JPO-D-10-05011.1

Duce, R. A., *et al.* (2008). Impacts of atmospheric anthropogenic nitrogen on the open ocean. *Science*, 320(5878), 893-897. https://doi.org/10.1126/science.1150369

Duhamel, S., Diaz, J.M., Adams, J.C. *et al.* (2021) Phosphorus as an integral component of global marine biogeochemistry. *Nat. Geosci*. 14, 359–368. https://doi.org/10.1038/s41561-021-00755-8

Falkowski, P. G., *et al.* (1998). The global carbon cycle: A test of our knowledge of Earth as a system. *Science*, 290(5490), 291-296. https://doi.org/10.1126/science.290.5490.291

Gandin, L.S. (1963). Objective Analysis of Meteorological fields. *Gidromet Izdat*, Leningrad (translation by Israel program for Scientific Translations), Jerusalem, 1966, 242 pp.

Garcia, H. E., K. Weathers, C. R. Paver, I. Smolyar, T. P. Boyer, R. A. Locarnini, M. M. Zweng, A. V. Mishonov, O. K. Baranova, D. Seidov, and J. R. Reagan, 2018. World Ocean Atlas 2018, Volume 4: Dissolved Inorganic Nutrients (phosphate, nitrate and nitrate + nitrite, silicate). A. Mishonov Technical Ed.; *NOAA Atlas NESDIS* 84, 35pp. [PDF]

Garcia H.E., C. Bouchard, S.L. Cross, C.R. Paver, T.P. Boyer, J.R. Reagan, R.A. Locarnini, A.V. Mishonov, O.K. Baranova, D. Seidov, Z. Wang, and D. Dukhovskoy (2024a). World Ocean Atlas 2023, Volume 4: Dissolved Inorganic Nutrients (Phosphate, Nitrate, Silicate). A. Mishonov Technical Editor. *NOAA Atlas NESDIS* 92, 79pp. https://doi.org/10.25923/39qw-7j08

Garcia, H. E., T. P. Boyer, R. A. Locarnini, J.R. Reagan, A.V. Mishonov, O.K. Baranova, C.R. Paver (2024b). World Ocean Database 2023: User's Manual. A.V. Mishonov, Tech. Ed., *NOAA Atlas NESDIS 98*, pp 107. https://doi.org/10.25923/j8gq-ee82 (*in preparation*)

Garcia H. E., Z. Wang, C. Bouchard, S.L. Cross, C.R. Paver, J.R. Reagan, T.P. Boyer, R.A. Locarnini, A.V. Mishonov, O.K. Baranova, D. Seidov, and D. Dukhovskoy (2024c). World Ocean Atlas 2023, Volume 3: Dissolved Oxygen, Apparent Oxygen Utilization, Dissolved Oxygen Saturation, and 30 year Climate Normal. A. Mishonov Technical Editor. *NOAA Atlas NESDIS* 91, 98 pp. https://doi.org/10.25923/rb67-ns53

Howarth, R. W., *et al.* (1996). Regional nitrogen budgets and riverine N and P fluxes for the drainages to the North Atlantic Ocean: Natural and human influences. *Biogeochemistry*, 35(1), 75-139. https://doi.org/10.1007/BF0217982

Jiang, L.-Q. *et al.* (2022). Best Practice Data Standards for Discrete Chemical Oceanographic Observations. Front. Mar. Sci. 8, 705638, https://doi.org/10.3389/fmars.2021.705638

JPOTS (Joint Panel on Oceanographic Tables and Standards) Editorial Panel (1991). Processing of Oceanographic Station Data. *UNESCO*, Paris, 138 pp. [PDF]

Johnson, K.S., J.N. Plant, L.D. Talley, and J.L. Sarmiento (2017a). Annual nitrate drawdown observed by SOCCOM profiling floats and the relationship to annual net community production. *J. Geophys. Res. Oceans,* 122, https://doi.org/10.1002/2017JC012839

Johnson, K.S., J.N. Plant, L.J. Coletti, H.W. Jannasch, C.M. Sakamoto, S.C. Riser, D.D. Swift, N.L. Williams, E. Boss, N. Haëntjens, L.D. Talley, J.L Sarmiento (2017b). Biogeochemical sensor performance in the SOCCOM profiling float array. *J. Geophys. Res. Oceans*, 122, https://doi.org/10.1002/2017JC012838

Key, R. *et al.* 2015. Global Ocean Data Analysis Project, Version 2 (GLODAPv2), ORNL/CDIAC-162, NDP-P093. Carbon Dioxide Information Analysis Center, Oak Ridge National Laboratory, US Dept of Energy, Oak Ridge, TN, doi:10.3334/CDIAC/OTG.NDP093_GLODAPv2 [PDF]

Laruelle G. G., Roubeix V., Sferratore A., Brodherr B., Ciuffa D., Conley D. J., *et al.* (2009). Anthropogenic perturbations of the silicon cycle at the global scale: key role of the land-ocean transition. *Global Biogeochem. Cycles,* (23) 1–17. https://doi.org/10.1029/2008GB003267

Lauvset, S. K., N. Lange, T. Tanhua, T., *et al.* (2022). GLODAPv2.2022: the latest version of the global interior ocean biogeochemical data product, *Earth Syst. Sci. Data,* 14, 5543–5572, https://doi.org/10.5194/essd-14-5543-2022

Levitus, S. (1982). Climatological Atlas of the World Ocean. *NOAA Professional Paper No. 13*, U.S. Gov. Printing Office, 173 pp.

Levitus, S. and T.P. Boyer (1994a). World Ocean Atlas 1994. Vol. 2: Oxygen. *NOAA Atlas NESDIS 2*, U.S. Gov. Printing Office, Washington, D.C., 186 pp. [PDF]

Levitus, S. and T.P. Boyer (1994b). World Ocean Atlas 1994. Vol. 4: Temperature. *NOAA Atlas NESDIS 4*, U.S. Gov. Printing Office, Washington, D.C., 117 pp. [PDF]

Levitus, S., S. Sato, C. Maillard, N. Mikhailov, P. Caldwell, and H. Dooley (2005). Building Ocean Profile-Plankton Databases for Climate and Ecosystem Research. *NOAA Technical Report NESDIS 117*, U.S. Gov. Printing Office, Washington, D.C., 29 pp. [PDF]

Locarnini, R.A., A.V. Mishonov, O.K. Baranova, J.R. Reagan, T.P. Boyer, D. Seidov, Z. Wang, H.E. Garcia, C. Bouchard, S.L. Cross, C.R. Paver, and D. Dukhovskoy (2024). World Ocean Atlas 2023, Volume 1: Temperature. A. Mishonov Tech. Ed. *NOAA Atlas NESDIS* 89, 51 pp, https://doi.org/10.25923/54bh-1613

Mishonov, A.V., T.P. Boyer, O.K. Baranova, C.N. Bouchard, S.L. Cross, H.E. Garcia, R.A. Locarnini, C.R. Paver, J.R. Reagan, Z. Wang, D. Seidov, A.I. Grodsky, J. Beauchamp (2024). World Ocean Database 2023. C. Bouchard, Tech. Ed. *NOAA Atlas NESDIS 97*, https://doi.org/10.25923/z885-h264 (in preparation).

Olsen, A., R. M. Key, S. van Heuven, S. K. Lauvset, A. Velo, X. Lin, C. Schirnick, A. Kozyr, T. Tanhua, M. Hoppema, S. Jutterström, R. Steinfeldt, E. Jeansson, M. Ishii, F. F. Pérez and T. Suzuki (2016). The Global Ocean Data Analysis Project version 2 (GLODAPv2) - an internally consistent data product for the world ocean, *Earth System Science Data*, 8, 297-323, https://doi.org/10.5194/essd-8-297-2016

Palastanga, V., Slomp, C. P., and Heinze, C. (2011). Long-term controls on ocean phosphorus and oxygen in a global biogeochemical model. *Global Biogeochemical Cycles*, 25(3) https://doi.org/10.1038/s41561-021-00755-8

Rabiner, L.R., M.R. Sambur, and C.E. Schmidt (1975). Applications of a non-linear smoothing algorithm to speech processing, *IEEE Trans. on Acoustics, Speech and Signal Processing*, 23, 552-557. [PDF]

Reagan, J.R., D. Seidov, Z. Wang, D. Dukhovskoy, T.P. Boyer, R.A. Locarnini, O.K. Baranova, A.V. Mishonov, H.E. Garcia, C. Bouchard, S.L. Cross, and C.R. Paver. (2024). World Ocean Atlas 2023, Volume 2: Salinity. A. Mishonov, Tech. Ed., *NOAA Atlas NESDIS* 90, 51pp. https://doi.org/10.25923/70qt-9574

Reiniger, R.F. and C.F. Ross (1968). A method of interpolation with application to oceanographic data. *Deep-Sea Res*., 9, 185-193.

Ruttenberg, K. C. in Treatise on Geochemistry 2nd edn (eds Holland, H. D. and Turekian, K. K.) 499–558 (Elsevier, 2014).

Sasaki, Y. (1960). An objective analysis for determining initial conditions for the primitive equations. Ref. 60-1 6T, Atmospheric Research Laboratory, *Univ. of Oklahoma Research Institute*, Norman, 23 pp.

Seaman, R.S. (1983). Objective Analysis accuracies of statistical interpolation and successive correction schemes. *Australian Meteor. Mag.*, 31, 225-240.

Shuman, F.G. (1957). Numerical methods in weather prediction: II. Smoothing and filtering. *Mon. Wea. Rev.*, 85, 357-361. https://doi.org/10.1175/1520-0493(1957)085%3C0357:NMIWPI%3E2.0.CO;2

Schlitzer, R., Ocean Data View odv.awi.de, (2023).

Smith, D.R. and F. Leslie (1984). Error determination of a successive correction type objective analysis scheme. *J Atm. and Oceanic Tech*., 1, 121-130. https://doi.org/10.1175/1520-0426(1984)001<0120:EDOASC>2.0.CO;2

Smith, D.R., M.E. Pumphrey, and J.T. Snow (1986). A comparison of errors in objectively analyzed fields for uniform and nonuniform station distribution, *J. Atm. Oceanic Tech*., 3, 84-97. https://doi.org/10.1175/1520-0426(1986)003<0084:ACOEIO>2.0.CO;2

Sverdrup, H.U., M.W. Johnson, and R.H. Fleming (1942). The Oceans: Their physics, chemistry, and general biology. *Prentice Hall*, 1060 pp.

Tanhua, T., van Heuven, S., Key, R. M., Velo, A., Olsen, A., and Schirnick, C. (2010). Quality control procedures and methods of the CARINA database. *Earth Syst. Sci. Data* (2), 35–49. https://doi.org/10.5194/essd-2-35-2010

Thiebaux, H.J. and M.A. Pedder (1987). Spatial Objective Analysis: with applications in atmospheric science. *Academic Press*, 299 pp.

Tréguer, P.J. and C. De La Rocha (2013). The World Ocean Silica Cycle. *Annu. Rev. Mar. Sci.* (5): 477-50. https://doi.org/10.1146/annurev-marine-121211-172346

Tréguer, P.J, J.N. Sutton, M. Brzezinski, M.A. Charette, T. Devries, S. Dutkiewicz, C. Ehlert, J. Hawkings, A. Leynaert, S.M. Liu, N. L. Monferrer, M. López-Acosta, M. Maldonado, S. Rahman, L. Ran, and O. Rouxel (2021). Reviews and syntheses: The biogeochemical cycle of silicon in the modern ocean. *Biogeosciences* (18), 1269–1289, https://doi.org/10.5194/bg-18-1269-2021

Tsandev, I., and Slomp, C. P. (2009). Modeling phosphorus cycling and carbon burial during Cretaceous Oceanic Anoxic Events. *Earth and Planetary Science Letters*, 286(1-2), 71-79. https://doi.org/10.1016/j.epsl.2009.06.016

Tukey, J.W. (1974). Nonlinear (nonsuperposable) methods for smoothing data, in "Cong. Rec.", 1974 *EASCON*, 673 pp.

Tyrrell, T. (1999). The relative influences of nitrogen and phosphorus on oceanic primary production. *Nature* 400, 525–531, https://doi.org/10.1038/22941

Uieda L. and P. Wessel (2017). PyGMT, a Python wrapper for the Generic Mapping Tools (GMT), https://www.pygmt.org

Ward, B. B. (2019). Nitrification in marine systems. In *Nitrogen Cycling in Microbial Ecology* (pp. 203-231). Springer.

Wessel, P., and W.H.F. Smith. (1998). New, improved version of Generic Mapping Tools released, *EOS Trans*. Amer. Geophys. U., 79, 579. https://doi.org/10.1029/98EO00426

Wilkinson, M., Dumontier, M., Aalbersberg, I. *et al.* (2016). The FAIR Guiding Principles for scientific data management and stewardship. *Sci Data* (3), 160018, https://doi.org/10.1038/sdata.2016.18

## 1.8 CHAPTER 1 TABLES

**Table 1.1** Descriptions of climatologies and depths for each nutrient variable in the WOA23.
The climatologies have been calculated based on bottle data (OSD) for the time period January 1, 1965 to December 31, 2022 from WOD23. The standard depth levels are shown in Table 1.2.

| Oceanographic variable | Depths for annual climatology | Depths for seasonal climatology | Depths for monthly climatology |
|---|---|---|---|
| phosphate, nitrate, and silicate | 0-5500 m (102 levels) | 0-800 m (43 levels) | 0-800 m (43 levels) |

**Table 1.2.** Acceptable distances (m) for defining interior (A) and exterior (B) values used in the Reiniger-Ross scheme for interpolating observed level data to standard levels.

| Standard Level # | Standard Depths (m) | A | B | Standard Level # | Standard Depths (m) | A | B |
|---|---|---|---|---|---|---|---|
| 1 | 0 | 50 | 200 | 52 | 1250 | 200 | 400 |
| 2 | 5 | 50 | 200 | 53 | 1300 | 200 | 1000 |
| 3 | 10 | 50 | 200 | 54 | 1350 | 200 | 1000 |
| 4 | 15 | 50 | 200 | 55 | 1400 | 200 | 1000 |
| 5 | 20 | 50 | 200 | 56 | 1450 | 200 | 1000 |
| 6 | 25 | 50 | 200 | 57 | 1500 | 200 | 1000 |
| 7 | 30 | 50 | 200 | 58 | 1550 | 200 | 1000 |
| 8 | 35 | 50 | 200 | 59 | 1600 | 200 | 1000 |
| 9 | 40 | 50 | 200 | 60 | 1650 | 200 | 1000 |
| 10 | 45 | 50 | 200 | 61 | 1700 | 200 | 1000 |
| 11 | 50 | 50 | 200 | 62 | 1750 | 200 | 1000 |
| 12 | 55 | 50 | 200 | 63 | 1800 | 200 | 1000 |
| 13 | 60 | 50 | 200 | 64 | 1850 | 200 | 1000 |
| 14 | 65 | 50 | 200 | 65 | 1900 | 200 | 1000 |
| 15 | 70 | 50 | 200 | 66 | 1950 | 200 | 1000 |
| 16 | 75 | 50 | 200 | 67 | 2000 | 1000 | 1000 |
| 17 | 80 | 50 | 200 | 68 | 2100 | 1000 | 1000 |
| 18 | 85 | 50 | 200 | 69 | 2200 | 1000 | 1000 |
| 19 | 90 | 50 | 200 | 70 | 2300 | 1000 | 1000 |
| 20 | 95 | 50 | 200 | 71 | 2400 | 1000 | 1000 |
| 21 | 100 | 50 | 200 | 72 | 2500 | 1000 | 1000 |
| 22 | 125 | 50 | 200 | 73 | 2600 | 1000 | 1000 |
| 23 | 150 | 50 | 200 | 74 | 2700 | 1000 | 1000 |
| 24 | 175 | 50 | 200 | 75 | 2800 | 1000 | 1000 |
| 25 | 200 | 50 | 200 | 76 | 2900 | 1000 | 1000 |
| 26 | 225 | 50 | 200 | 77 | 3000 | 1000 | 1000 |
| 27 | 250 | 100 | 200 | 78 | 3100 | 1000 | 1000 |
| 28 | 275 | 100 | 200 | 79 | 3200 | 1000 | 1000 |
| 29 | 300 | 100 | 200 | 80 | 3300 | 1000 | 1000 |

| Standard Level # | Standard Depths (m) | A | B | Standard Level # | Standard Depths (m) | A | B |
|---|---|---|---|---|---|---|---|
| 30 | 325 | 100 | 200 | 81 | 3400 | 1000 | 1000 |
| 31 | 350 | 100 | 200 | 82 | 3500 | 1000 | 1000 |
| 32 | 375 | 100 | 200 | 83 | 3600 | 1000 | 1000 |
| 33 | 400 | 100 | 200 | 84 | 3700 | 1000 | 1000 |
| 34 | 425 | 100 | 200 | 85 | 3800 | 1000 | 1000 |
| 35 | 450 | 100 | 200 | 86 | 3900 | 1000 | 1000 |
| 36 | 475 | 100 | 200 | 87 | 4000 | 1000 | 1000 |
| 37 | 500 | 100 | 400 | 88 | 4100 | 1000 | 1000 |
| 38 | 550 | 100 | 400 | 89 | 4200 | 1000 | 1000 |
| 39 | 600 | 100 | 400 | 90 | 4300 | 1000 | 1000 |
| 40 | 650 | 100 | 400 | 91 | 4400 | 1000 | 1000 |
| 41 | 700 | 100 | 400 | 92 | 4500 | 1000 | 1000 |
| 42 | 750 | 100 | 400 | 93 | 4600 | 1000 | 1000 |
| 43 | 800 | 100 | 400 | 94 | 4700 | 1000 | 1000 |
| 44 | 850 | 100 | 400 | 95 | 4800 | 1000 | 1000 |
| 45 | 900 | 200 | 400 | 96 | 4900 | 1000 | 1000 |
| 46 | 950 | 200 | 400 | 97 | 5000 | 1000 | 1000 |
| 47 | 1000 | 200 | 400 | 98 | 5100 | 1000 | 1000 |
| 48 | 1050 | 200 | 400 | 99 | 5200 | 1000 | 1000 |
| 49 | 1100 | 200 | 400 | 100 | 5300 | 1000 | 1000 |
| 50 | 1150 | 200 | 400 | 101 | 5400 | 1000 | 1000 |
| 51 | 1200 | 200 | 400 | 102 | 5500 | 1000 | 1000 |

**Table 1.3.** Response function of the objective analysis scheme as a function of wavelength for the WOA18 and earlier analyses.
**Notes:** Response function is normalized to 1.0.

| Wavelength[1] | Levitus (1982) | WOA94 | WOA98, 01, 05, 09, 13, 18 |
|---|---|---|---|
| 360ΔX | 1.000 | 0.999 | 1.000 |
| 180ΔX | 1.000 | 0.997 | 0.999 |
| 120ΔX | 1.000 | 0.994 | 0.999 |
| 90ΔX | 1.000 | 0.989 | 0.998 |
| 72ΔX | 1.000 | 0.983 | 0.997 |
| 60ΔX | 1.000 | 0.976 | 0.995 |
| 45ΔX | 1.000 | 0.957 | 0.992 |
| 40ΔX | 0.999 | 0.946 | 0.990 |
| 36ΔX | 0.999 | 0.934 | 0.987 |
| 30ΔX | 0.996 | 0.907 | 0.981 |
| 24ΔX | 0.983 | 0.857 | 0.969 |
| 20ΔX | 0.955 | 0.801 | 0.952 |
| 18ΔX | 0.923 | 0.759 | 0.937 |
| 15ΔX | 0.828 | 0.671 | 0.898 |
| 12ΔX | 0.626 | 0.532 | 0.813 |
| 10ΔX | 0.417 | 0.397 | 0.698 |
| 9ΔX | 0.299 | 0.315 | 0.611 |
| 8ΔX | 0.186 | 0.226 | 0.500 |
| 6ΔX | $3.75 \times 10^{-2}$ | 0.059 | 0.229 |
| 5ΔX | $1.34 \times 10^{-2}$ | 0.019 | 0.105 |
| 4ΔX | $1.32 \times 10^{-3}$ | $2.23 \times 10^{-3}$ | $2.75 \times 10^{-2}$ |
| 3ΔX | $2.51 \times 10^{-3}$ | $1.90 \times 10^{-4}$ | $5.41 \times 10^{-3}$ |
| 2ΔX | $5.61 \times 10^{-7}$ | $5.30 \times 10^{-7}$ | $1.36 \times 10^{-6}$ |

[1]For ΔX = 111 km, the meridional separation at the Equator.

**Table 1.4.** Basins defined for objective analysis and the shallowest standard depth level for which each ocean basin is defined.

| # | Basin[1] | Standard Depth Level | # | Basin[1] | Standard Depth Level |
|---|---|---|---|---|---|
| 1 | Atlantic Ocean | 1* | 31 | West European Basin | 82 |
| 2 | Pacific Ocean | 1* | 32 | Southeast Indian Basin | 82 |
| 3 | Indian Ocean | 1* | 33 | Coral Sea | 82 |
| 4 | Mediterranean Sea | 1* | 34 | East Indian Basin | 82 |
| 5 | Baltic Sea | 1 | 35 | Central Indian Basin | 82 |
| 6 | Black Sea | 1 | 36 | Southwest Atlantic Basin | 82 |
| 7 | Red Sea | 1 | 37 | Southeast Atlantic Basin | 82 |
| 8 | Persian Gulf | 1 | 38 | Southeast Pacific Basin | 82 |
| 9 | Hudson Bay | 1 | 39 | Guatemala Basin | 82 |
| 10 | Southern Ocean | 1* | 40 | East Caroline Basin | 87 |
| 11 | Arctic Ocean | 1 | 41 | Marianas Basin | 87 |
| 12 | Sea of Japan | 1 | 42 | Philippine Sea | 87 |
| 13 | Kara Sea | 22 | 43 | Arabian Sea | 87 |
| 14 | Sulu Sea | 25 | 44 | Chile Basin | 87 |
| 15 | Baffin Bay | 37 | 45 | Somali Basin | 87 |
| 16 | East Mediterranean | 41 | 46 | Mascarene Basin | 87 |
| 17 | West Mediterranean | 47 | 47 | Crozet Basin | 87 |
| 18 | Sea of Okhotsk | 47 | 48 | Guinea Basin | 87 |
| 19 | Banda Sea | 55 | 49 | Brazil Basin | 92 |
| 20 | Caribbean Sea | 55 | 50 | Argentine Basin | 92 |
| 21 | Andaman Basin | 62 | 51 | Tasman Sea | 87 |
| 22 | North Caribbean | 67 | 52 | Atlantic Indian Basin | 92 |
| 23 | Gulf of Mexico | 67 | 53 | Caspian Sea | 1 |
| 24 | Beaufort Sea | 77 | 54 | Sulu Sea II | 37 |
| 25 | South China Sea | 77 | 55 | Venezuela Basin | 37 |
| 26 | Barents Sea | 77 | 56 | Bay of Bengal | 1* |
| 27 | Celebes Sea | 62 | 57 | Java Sea | 16 |
| 28 | Aleutian Basin | 77 | 58 | East Indian Atlantic Basin | 97 |
| 29 | Fiji Basin | 82 | 59 | Chiloe | 1 |
| 30 | North American Basin | 82 | 60 | Bransfield Strait | 37 |

[1]Basins marked with a "*" can interact with adjacent basins in the objective analysis.

**Table 1.5.** Statistical fields calculated as part of the WOA23 nutrients covering the time period 1965 and 2022.
**Notes:** ("√" denotes field was calculated and is publicly available online at NCEI).

| Statistical field | One-degree Field Calculated | Five-degree Statistics calculated |
|---|---|---|
| Objectively analyzed climatology - Annual | √ | |
| Objectively analyzed climatology - Seasonal | √ | |
| Objectively analyzed climatology - Monthly | √ | |
| Statistical mean[1] | √ | √ |
| Number of observations | √ | √ |
| Seasonal (monthly) climatology minus annual climatology | √ | |
| Standard deviation from statistical mean[1] | √ | √ |
| Standard error of the statistical mean | √ | √ |
| Statistical mean minus objectively analyzed climatology[1] | √ | |
| Number of mean values within radius of influence | √ | |

[1]Statistical fields are only available when the objectively analyzed fields are available for one-degree fields.

**Table 1.6a.** WOA23 annual mean and standard deviation phosphate, nitrate, and silicate content for different ocean basins between the surface and 5500 m depth (102 levels).
**Notes:** Figures 2.7 (Chapter 2), Figure 3.6 (Chapter 3), and Figure 4.7 (Chapter 4) show the global annual mean nutrient content as a function of depth and basin.

| | **Mean ± standard deviation content (µmol·kg$^{-1}$)** | | |
|---|---|---|---|
| **Ocean Basin** | **Phosphate** | **Nitrate** | **Silicate** |
| Global | 1.76 ± 0.58 | 24.59 ± 9.35 | 65.67 ± 41.15 |
| Atlantic | 1.47 ± 0.43 | 21.37 ± 6.94 | 42.98 ± 21.95 |
| Pacific | 2.01 ± 0.74 | 27.91 ± 11.45 | 82.30 ± 57.73 |
| Indian | 1.86 ± 0.58 | 26.14 ± 8.86 | 71.93 ± 44.47 |
| Arctic | 0.92 ± 0.10 | 11.42 ± 3.98 | 9.85 ± 2.12 |

**Table 1.6b.** WOA23 mean content inventory (Pmol) in different ocean basins for phosphate, nitrate, and silicate in the 0-5500 m depth layer.

**Notes:** Basin volumes are approximate based on 1x1-degree mean depths.

| **Ocean Basin** (0-5500 m) | **Nutrient mean content inventory (Pmol)** | | | **Ocean Basin Volume (x $10^{15}$ $m^3$)** |
|---|---|---|---|---|
| | **Phosphate** | **Nitrate** | **Silicate** | |
| Global | 3.06 | 42.24 | 122.39 | 1355.4 |
| Atlantic | 0.57 | 8.11 | 15.34 | 332.3 |
| Pacific | 1.82 | 24.82 | 79.83 | 712.0 |
| Indian | 0.64 | 9.00 | 26.79 | 287.1 |
| Arctic | 0.02 | 0.25 | 0.21 | 18.7 |

**Table 1.7** Difference of the WOA23 (This atlas) minus the WOA18 (Garcia *et al.*, 2019) objectively analyzed annual mean and standard deviation phosphate, nitrate, and silicate content for different ocean basins between the surface and up to 5500 m depth.

| | **WOA23 minus WOA18 mean ± standard deviation content (µmol·$kg^{-1}$)** | | |
|---|---|---|---|
| **Basin** | **Phosphate** | **Nitrate** | **Silicate** |
| Global | 0.00 ± 0.01 | 0.00 ± 0.02 | -0.03 ± 0.12 |
| Atlantic | 0.00 ± 0.00 | -0.02 ± 0.04 | 0.01 ± 0.03 |
| Pacific | -0.00 ± 0.01 | -0.04 ± 0.04 | -0.03 ± 0.13 |
| Indian | 0.01 ± 0.01 | 0.14 ± 0.09 | 0.11 ± 0.14 |
| Arctic | –0.01 ± 0.02 | 0.00 ± 0.01 | -0.37 ± 0.48 |

**Table 1.8.** Depth averaged difference and standard deviation of WOA23 (This atlas) minus GLODAPv2.2016b annual mean phosphate, nitrate, and silicate content for different ocean basins between the surface and up to 5500 m depth.

| | **WOA23 minus GLODAPv2.2016b mean ± standard deviation content difference (µmol·kg$^{-1}$)** | | |
|---|---|---|---|
| **Basin** | **Phosphate** | **Nitrate** | **Silicate** |
| Global | -0.00 ± 0.03 | -0.16 ± 0.26 | 0.47 ± 0.26 |
| Atlantic | 0.01 ± 0.03 | -0.11 ± 0.30 | -0.27 ± 0.48 |
| Pacific | -0.01 ± 0.03 | -0.16 ± 0.36 | 0.83 ± 0.49 |
| Indian | -0.01 ± 0.02 | -0.12 ± 0.15 | 0.40 ± 0.54 |
| Arctic | –0.02 ± 0.06 | -0.41 ± 0.54 | 0.57 ± 1.04 |

**Table 1.9** Uncertainty estimates of the objectively analyzed climatological fields.
**Notes:** These are calculated as the depth-averaged difference and standard deviation of the annual statistical mean values of the measurements and the objectively analyzed climatological fields at all grids and depths for phosphate, nitrate, and silicate.

| | **Mean and standard deviation of the statistical annual mean content of the observations minus the objectively analyzed climatological mean content (µmol·kg$^{-1}$)** | | |
|---|---|---|---|
| **Basin** | **Phosphate** | **Nitrate** | **Silicate** |
| Global | -0.004 ± 0.010 | -0.036 ± 0.158 | -0.067 ± 0.203 |
| Atlantic | -0.004 ± 0.010 | -0.043 ± 0.164 | -0.038 ± 0.193 |
| Pacific | -0.005 ± 0.012 | -0.069 ± 0.168 | -0.084 ± 0.249 |
| Indian | -0.002 ± 0.006 | -0.118 ± 0.154 | -0.019 ± 0.669 |
| Arctic | –0.006 ± 0.019 | 0.075 ± 0.479 | -0.021 ± 0.396 |

**Table 1.10** Depth-dependent variables present in WOD23.

| Variable (nominal abbreviations) | WOD standard unit or scale (nominal abbreviation) | Dataset(s) where variable(s) is/are stored |
|---|---|---|
| Temperature | Degrees Celsius (°C) | OSD, CTD, MBT, XBT, SUR, APB, MRB, PFL, UOR, DRB, GLD |
| Salinity | Dimensionless | OSD, CTD, SUR, MRB, PFL, UOR, DRB, GLD |
| Oxygen | Micro-mole/kilogram ($\mu mol \cdot kg^{-1}$) | OSD, CTD, PFL, UOR, DRB |
| Phosphate | Micro-mole/kilogram ($\mu mol \cdot kg^{-1}$) | OSD |
| Silicate | Micro-mole/kilogram ($\mu mol \cdot kg^{-1}$) | OSD |
| Nitrate and Nitrate + Nitrite | Micro-mole/kilogram ($\mu mol \cdot kg^{-1}$) | OSD, PFL |
| pH | Dimensionless | OSD, SUR |
| Chlorophyll | Micro-gram per liter ($\mu g \cdot l^{-1}$) | OSD, CTD, SUR, UOR, DRB |
| Alkalinity | Milli-mole liter$^{-1}$ (mmol $l^{-1}$) | OSD, SUR |
| Partial pressure of carbon dioxide | Micro-atmosphere (µatm) | OSD, SUR |
| Dissolved Inorganic carbon | Milli-mole liter$^{-1}$ (mmol $l^{-1}$) | OSD |
| Transmissivity (Beam Attenuation Coefficient) | Per meter ($m^{-1}$) | CTD |
| Pressure | Decibar | OSD, CTD, UOR, GLD, PFL, DRB |
| Air temperature | Degree Celsius (°C) | SUR |
| $xCO_2$atmosphere | Parts per million (ppm) | SUR |
| Air pressure | Millibar (mbar) | SUR |
| Latitude | Degrees | SUR, APB, UOR |
| Longitude | Degrees | SUR, APB, UOR |
| Julian year-day[1] | Day | SUR, APB, UOR |
| Tritium [$^3H$] | Tritium Unit (TU) | OSD |
| Helium [He] | Nano-mole/kilogram ($nmol \cdot kg^{-1}$) | OSD |
| Delta Helium-3 [$\Delta^3He$] | Percent (%) | OSD |
| Delta Carbon-14 [$\Delta^{14}C$] | Per mille (‰) | OSD |
| Delta Carbon-13 [$\Delta^{13}C$] | Per mille (‰) | OSD |
| Argon | Nano-mole/kilogram ($nmol \cdot kg^{-1}$) | OSD |
| Neon | Nano-mole/kilogram ($nmol \cdot kg^{-1}$) | OSD |
| Chlorofluorocarbon 11 (CFC 11) | Pico-mole/kilogram ($pmol \cdot kg^{-1}$) | OSD |
| Chlorofluorocarbon 12 (CFC 12) | Pico-mole/kilogram ($pmol \cdot kg^{-1}$) | OSD |
| Chlorofluorocarbon 113 (CFC113) | Pico-mole/kilogram ($pmol \cdot kg^{-1}$) | OSD |
| Delta Oxygen-18 [$\Delta^{18}O$] | Per mille (‰) | OSD |

[1] Julian year-day is the decimal day for the year in which the observations were made

**Table 1.11.** Datasets in the WOD23.

| DATASETS | DATASETS INCLUDES |
|---|---|
| OSD | Ocean Station Data, Low-resolution CTD/XCTD, Plankton data |
| CTD | High-resolution Conductivity-Temperature-Depth / XCTD data |
| MBT | Mechanical / Digital / Micro Bathythermograph data |
| XBT | Expendable Bathythermograph data |
| SUR | Surface-only data |
| APB | Autonomous Pinniped data |
| MRB | Moored buoy data |
| PFL | Profiling float data |
| DRB | Drifting buoy data |
| UOR | Undulating Oceanographic Recorder data |
| GLD | Glider data |

**Table 1.12.** WOA23 data product volumes

| World Ocean Atlas 2023 Products | Digital Object Identifier (DOI) |
|---|---|
| Volume 1: Temperature | https://doi.org/10.25923/54bh-1613 |
| Volume 2: Salinity | https://doi.org/10.25923/70qt-9574 |
| Volume 3: Dissolved Oxygen, Apparent Oxygen Utilization, Dissolved Oxygen Saturation, and 30-year Climate Normal | https://doi.org/10.25923/rb67-ns53 |
| Volume 4: Dissolved Inorganic Nutrients (phosphate, nitrate and silicate) | https://doi.org/10.25923/39qw-7j08 |
| Volume 5: Density | https://doi.org/10.25923/mcn4-d695 |
| Volume 6: Conductivity | https://doi.org/10.25923/wz4d-6x65 |
| Volume 7: Mixed Layer Depth | https://doi.org/10.25923/4adh-kq71 |
| Volume 8: Bottom Temperature | https://doi.org/10.25923/s47b-gm86 |

## 1.9 CHAPTER 1 FIGURES

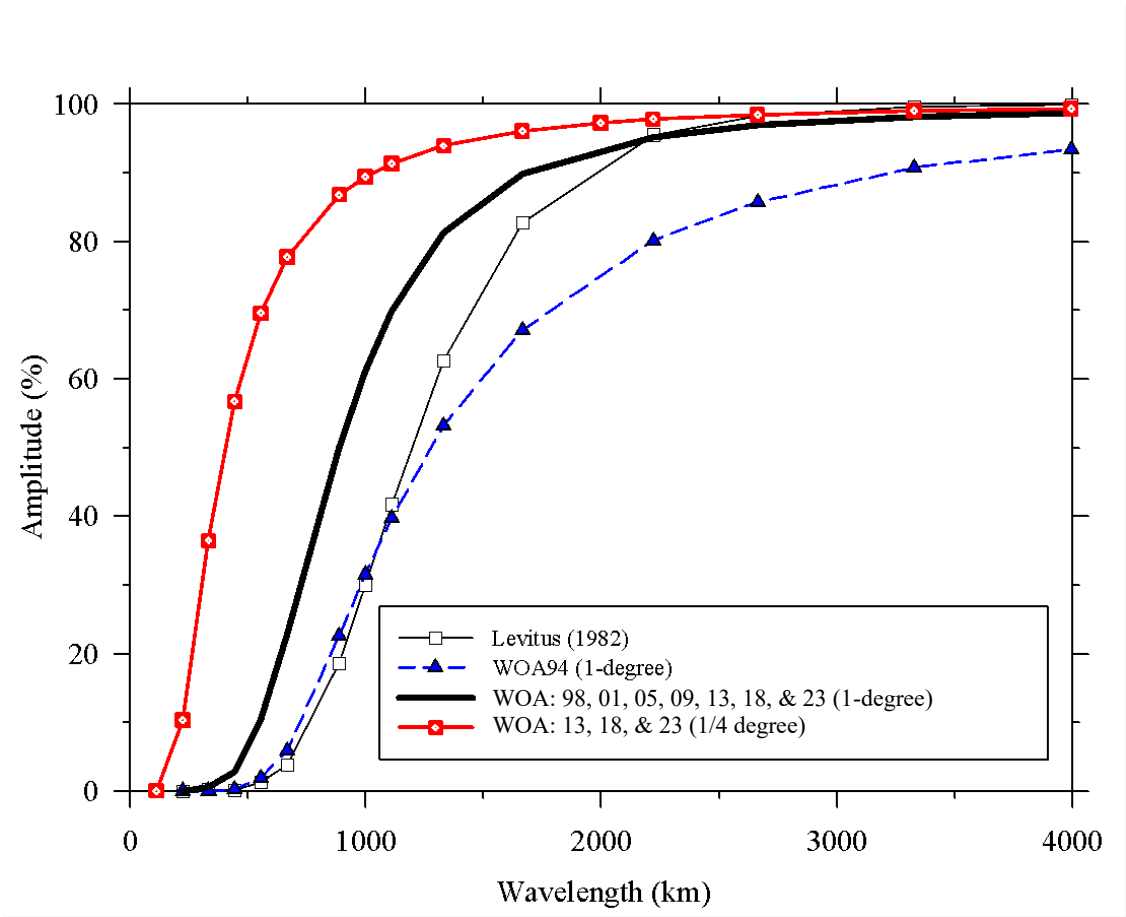


**Figure 1.1** Response function of the WOA23, WOA18, WOA13, WOA05, WOA01, WOA98, WOA94, and Levitus (1982) objective analysis schemes.

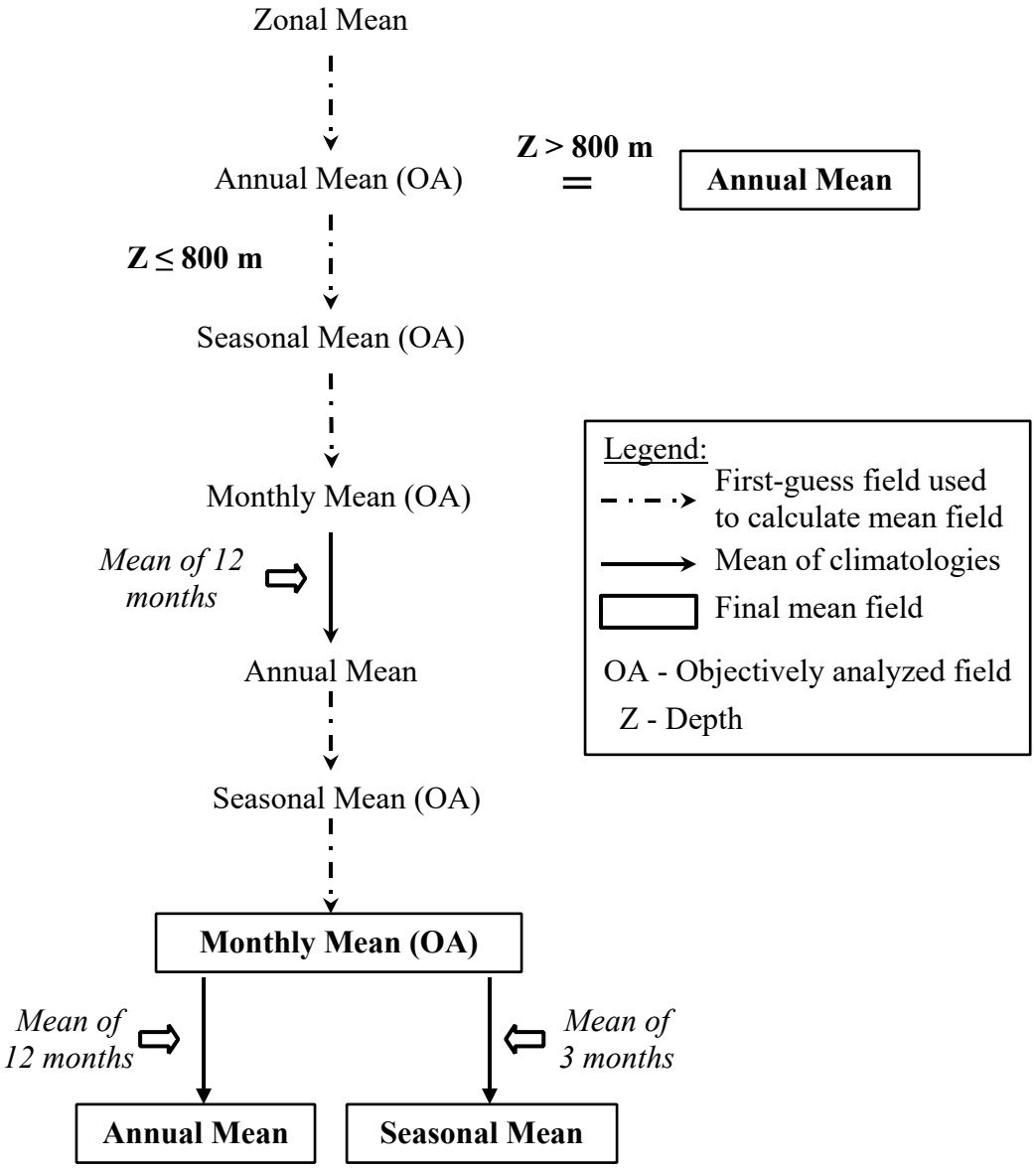


**Figure 1.2.** Scheme used in computing annual, seasonal, and monthly objectively analyzed mean content for phosphate, nitrate, and silicate.

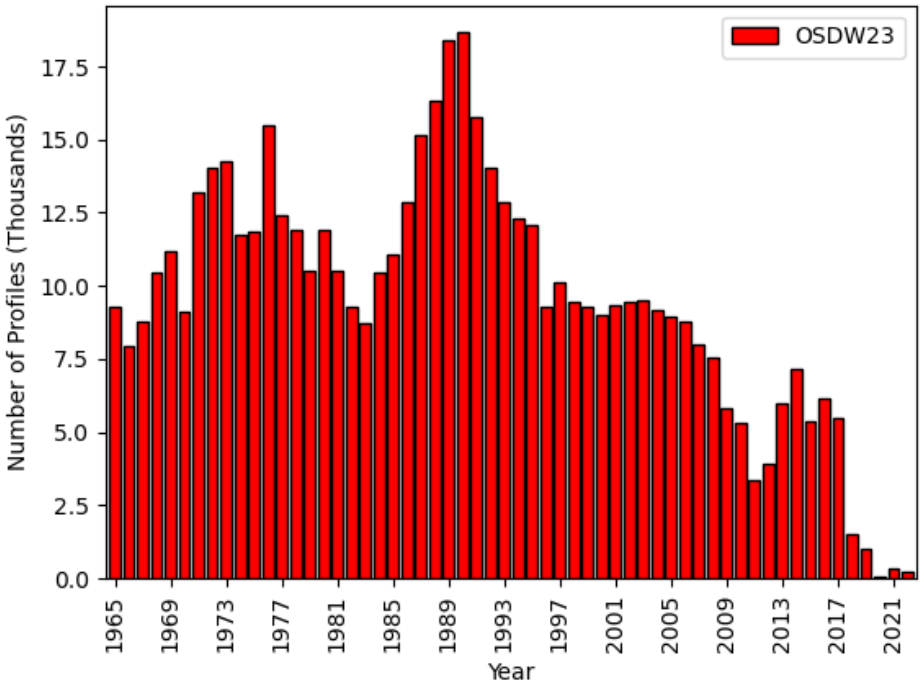


**Figure 1.3a.** Number of phosphate profiles per year in WOD23 used in WOA23.

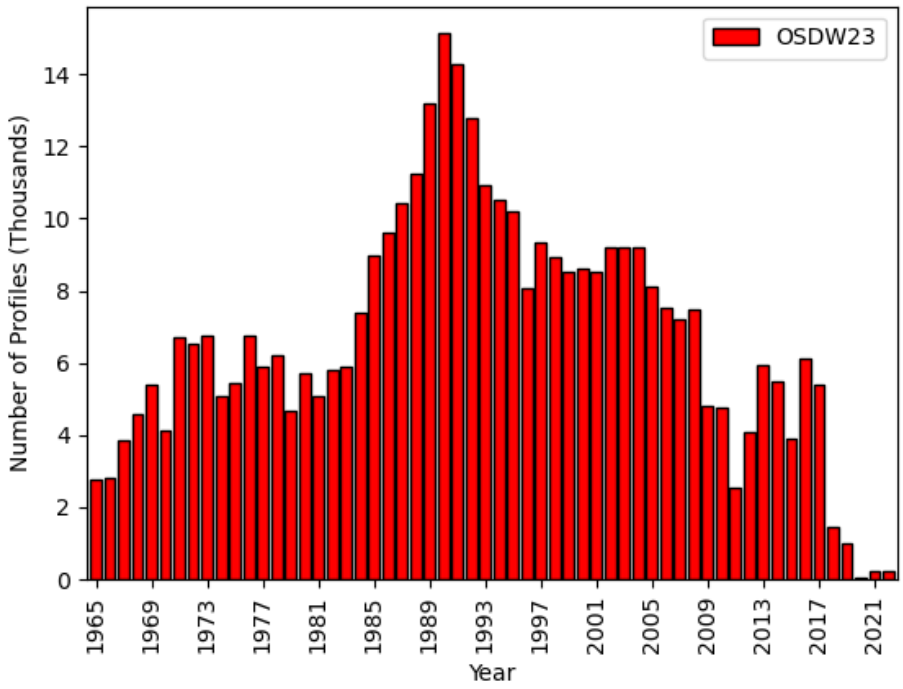


**Figure 1.3b.** Number of nitrate profiles per year in WOD23 used in WOA23.

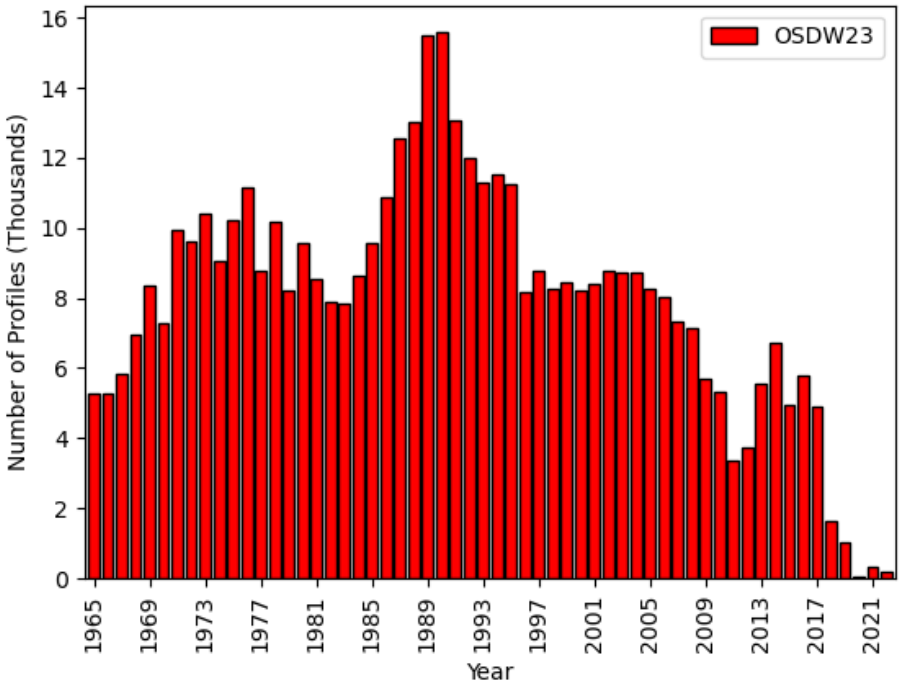


**Figure 1.3c.** Number of silicate profiles per year in WOD23 used in WOA23.

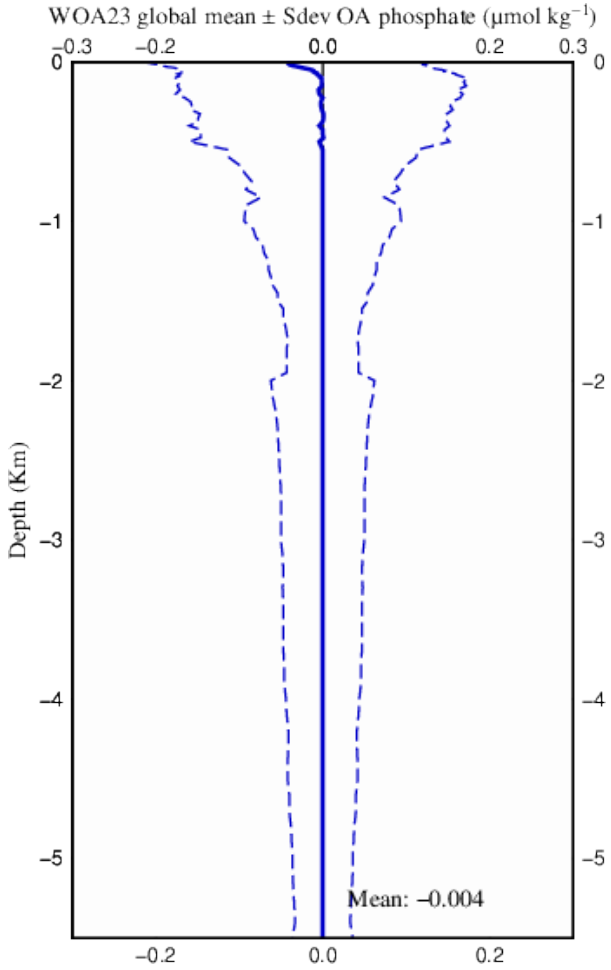


**Figure 1.4a.** Global mean and standard deviation difference between the climatological statistical annual mean minus the objectively analyzed climatological mean phosphate content (µmol·kg$^{-1}$) as a function of depth (km).

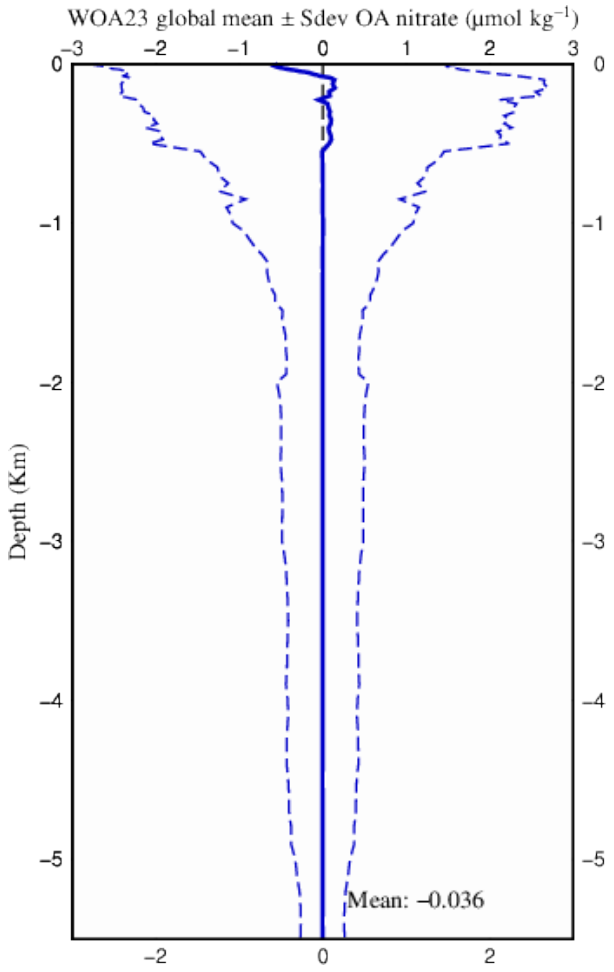


**Figure 1.4b.** Global mean and standard deviation difference between the climatological statistical annual mean minus the objectively analyzed climatological mean nitrate content (µmol·kg$^{-1}$) as a function of depth (km).

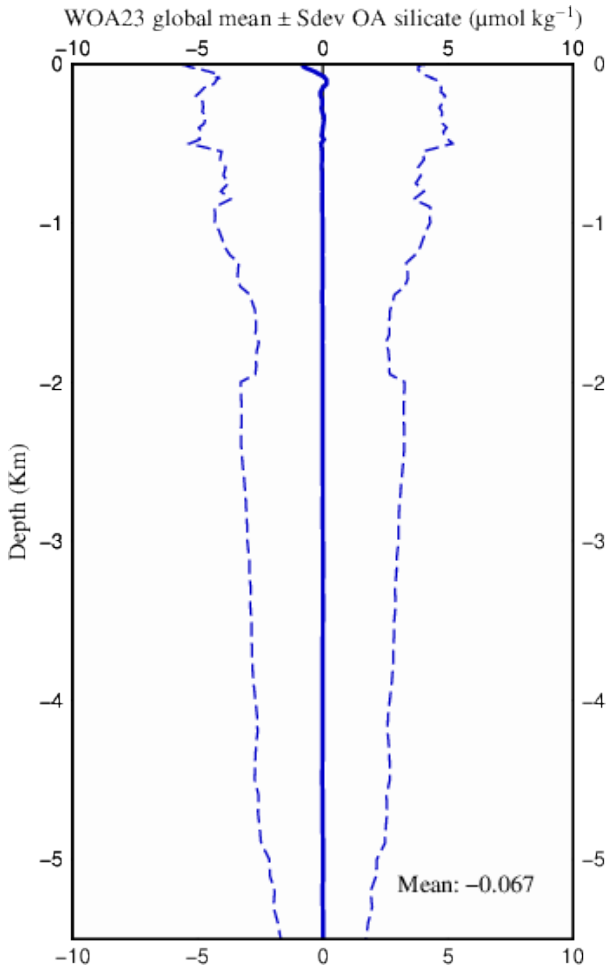


**Figure 1.4c.** Global mean and standard deviation difference between the climatological statistical annual mean minus the objectively analyzed climatological mean silicate content (µmol·kg$^{-1}$) as a function of depth (km).

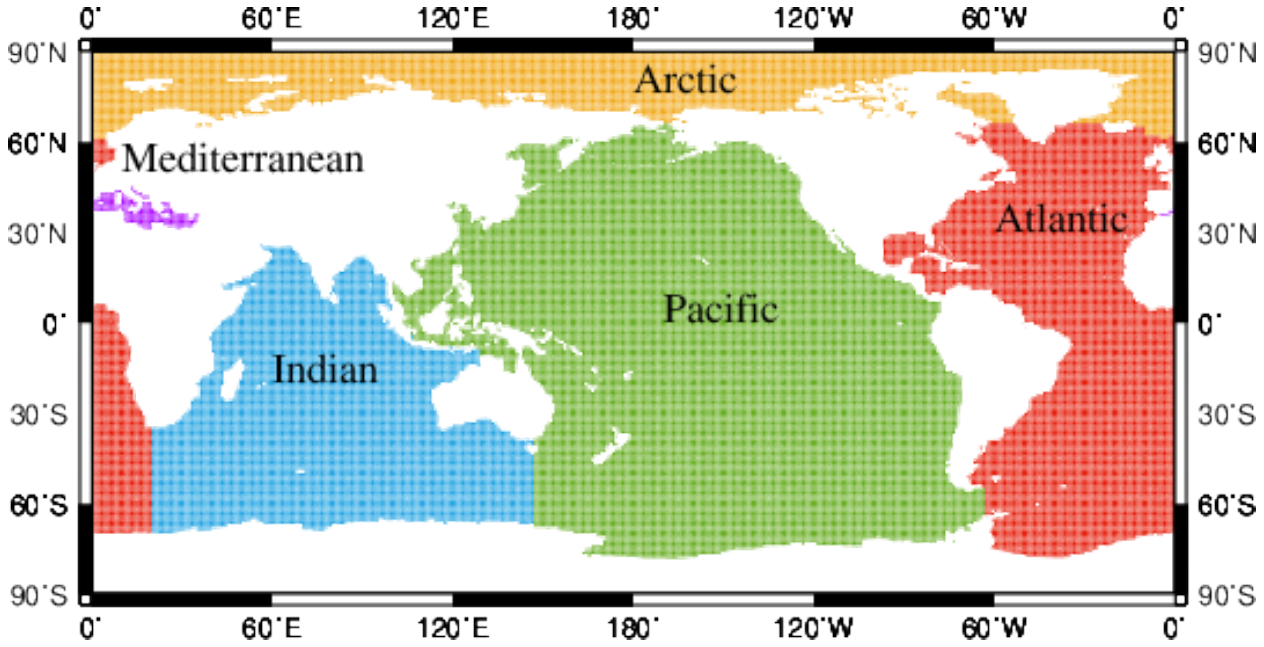


**Figure 1.5a.** Ocean basin geographic definitions.

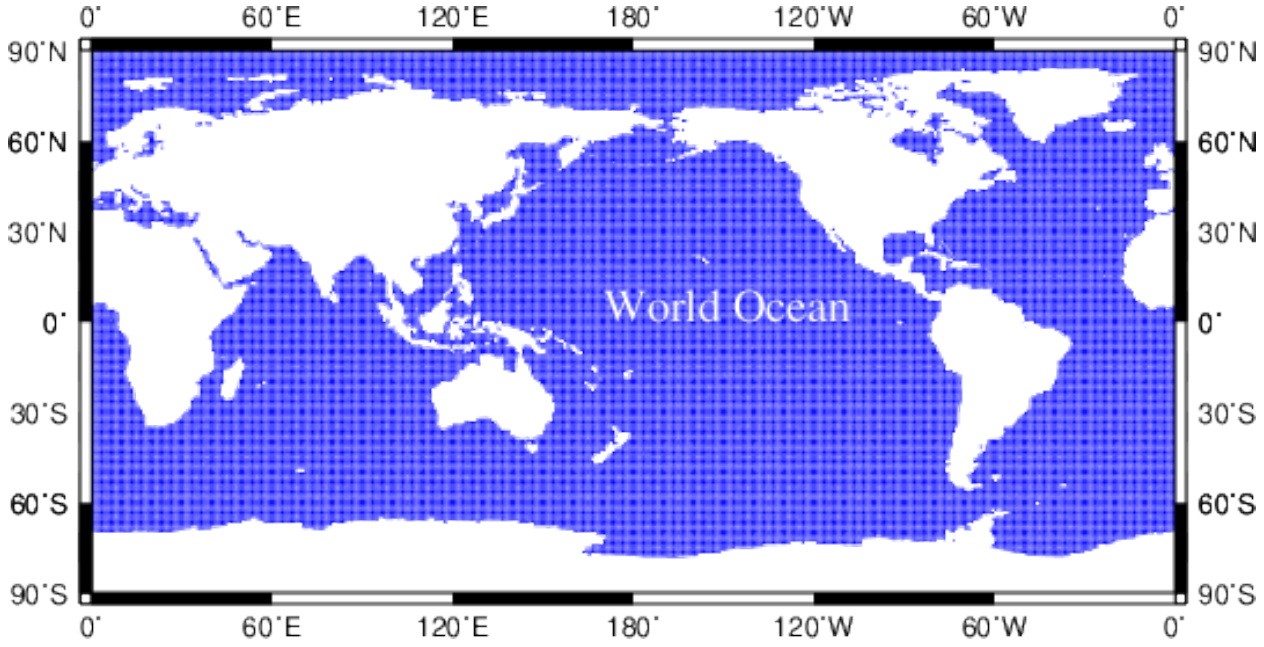


**Figure 1.5b.** World ocean basin geographic definition.

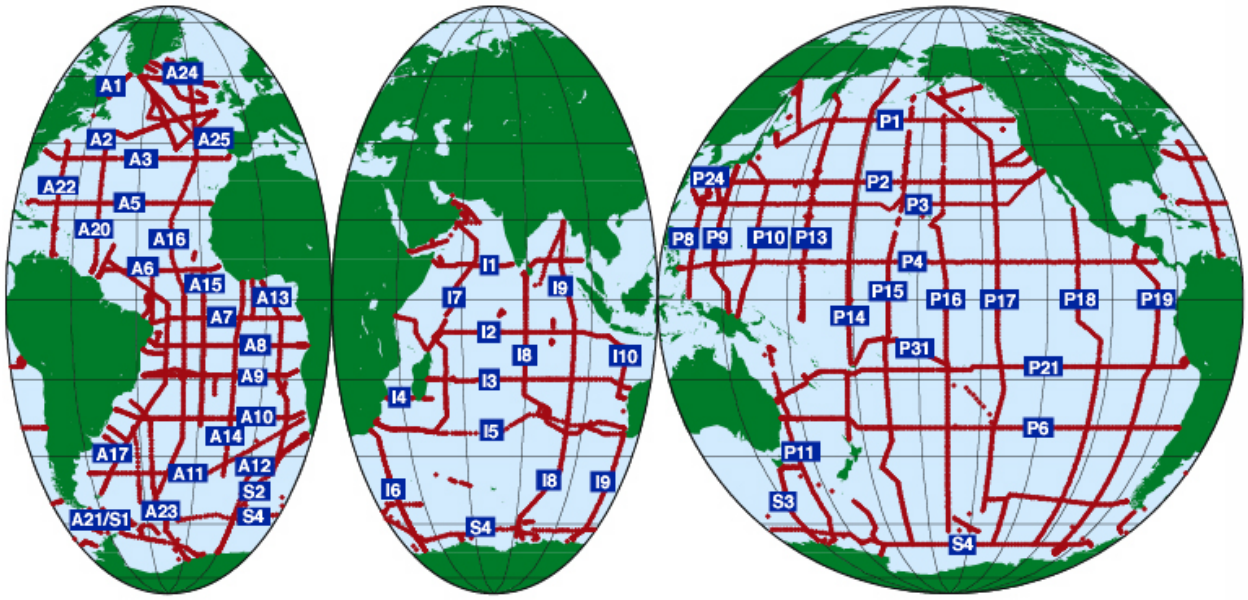


**Figure 1.6.** Stations occupied during the WOCE One-Time Survey.

# Chapter 2: Dissolved Inorganic Phosphate

## Courtney Bouchard

### ABSTRACT

This atlas describes the WOA23 content for dissolved phosphate: the global, all-data (1965-2022) climatological mean fields for the World Ocean at 102 standardized depth levels (0-5500 m), gridded on a one-degree latitude-longitude grid. NOAA's *World Ocean Database, 2023* historical dissolved phosphate data was used to create the climatological maps shown in this chapter. The maps are presented for climatological composite periods (annual, seasonal, and monthly, monthly and seasonal difference fields, and the number of observations). The global ocean content inventory of phosphate is estimated to be 3.06 Pmol. Also provided are estimates of basin-scale uncertainty of the phosphate objectively analyzed fields (-0.004 ± 0.010 μmol·kg$^{-1}$). The aim of the maps is to illustrate large-scale characteristics of the distribution of phosphate. WOA23 phosphate is also compared to other mapped gridded products.

## 2.1. INTRODUCTION

Phosphorus (P) is an essential nutrient found in the macromolecules of organisms, providing a backbone to DNA and RNA as well as a crucial nutrient providing energy to living cells through the ATP molecule. In nature the majority of phosphorus dissolved in the ocean exists predominantly in the form of dissolved reactive phosphate. Phosphorus is also present in the marine environment in a number of inorganic and organic forms that convert between dissolved and particulate forms of matter within the marine P cycle.

Organic and inorganic phosphate compounds are carried into water bodies by precipitation and runoff to rivers, lakes and oceans and taken up by aquatic organisms. Weathering of sedimentary rocks slowly leaches P into the surface water and soils. Volcanic ash, aerosols, and mineral dust can be a significant source of inorganic P from the atmosphere. Inorganic P is taken up by plants and converted to organic P which can then be transferred to other organisms as they eat and excrete waste.

Marine sediment P reserves are primarily formed from the burial of the aquatic organisms that take up this organic P after they have died or excrete waste and sunk into the deeper ocean. Organic P is converted back to its inorganic form by bacterial decomposition and is dissolved and attached to particles. Disturbances to the bottom sediment can reintroduce the inorganic P (predominantly as phosphate) into the water column where it can be taken up by aquatic plants or organisms again.

Phosphate plays a key role in marine photosynthesis and subsequently primary production and is often considered the limiting macronutrient necessary for growth in aquatic systems. Marine microorganisms have adapted for optimal P acquisition and

metabolism for growth and survival. Changes in marine P inventories are hypothesized to affect ocean productivity as it is considered the ultimate limiting nutrient on global scales by geochemists (Tyrell, 1999, Tsandev and Slomp, 2009; Palastanga *et al.*, 2011).

Over recent decades, more research has updated our understanding of the complexities of the marine P cycle from the simple, tectonically slow biogeochemical cycling that was previously understood (Duhamel *et al.*, 2021). For example, revised estimates of ocean residence time for P from ~80 Kyr to 10-20 Kyr (Ruttenberg, 2014). These differing estimates bring forth a demand for updated baseline estimates of the total mean global phosphate content inventory, such that this atlas can provide. This baseline can serve to document phosphate low frequency variability.

This atlas presents annual, seasonal, and monthly profile climatologies and related statistical fields for phosphorus in the form of orthophosphate and phosphate. This Chapter is divided into sections. We begin by describing the data sources and data distribution (Section 2.2). Then we describe the general data processing procedures (Section 2.3), and a summary (Section 2.4).

## 2.2. DATA AND DATA DISTRIBUTION

Data sources and quality control procedures are briefly described below. For further information on the data sources used in WOA23 refer to the *World Ocean Database 2023* (WOD23, Mishonov *et al.,* 2024). The quality control procedures used in preparation of these analyses are described in Chapter 1 of this atlas.

### 2.2.1. Data sources

Historical oceanographic data used in this atlas were obtained from the NCEI World Ocean Database 2023 (WOD23). They include all the OSD (bottle-sample) data from 1965 - 2022, with certain data excluded through automated or subjective quality control measures. Climatological fields are presented on the standard depth levels,

### 2.2.2. Data coverage

A total of 13,687 additional phosphate profiles have been added to the WOD23 database since the previous version of the atlas (WOA18). The WOA23 phosphate data (Fig 2.1) is widespread globally with coverage biased towards nearshore and shelf locations as well as vertically in the water column from the surface to about 1000 m depth. Global coverage is widespread but sparse, with many 1-degree grid cells having one or two observations in total. Areas in the northern and northwest Pacific (East China Sea/Japan/Korea, Bering Sea), the northern North Atlantic (GIN Sea, North Sea, Baltic Sea, Arctic) and the coastal U.S. are relatively well sampled. Areas that are shaded in white have no historical data within the WOD and present an opportunity to describe the regions with the highest data needs for future sampling efforts.

The fields presented here are a function of both observation density (spatial and temporal coverage) and variability in the measured quantity. The representativeness of large-scale features in the upper ocean, where the variability is high, is reasonable in the all-data annual mean distributions. Sampling density drops off somewhat with depth, but a similar overall pattern of geographic distribution is maintained, and there is some coverage to abyssal depths in all major basins. Coverage is seasonal, with highest density in northern spring and summer. The southern hemisphere has seemingly less seasonal variability that might be attributed to limited data coverage primarily in Austral Summer. Globally, there is coverage in all

months, save in the high latitudes in boreal and austral winter.

There are a number of basin-wide sections in all major basins, generally oriented E-W or N-S, and visible on the data density plots as light blue-colored lines (*e.g.* Figure 2.2). These may be repeat sections (*e.g.* HOT and BATS), or single sections that sampled multiple sites in each 1-degree bin. These can be especially important for establishing some sense of the variability in the measurements, in areas that are otherwise sparsely sampled.

While in certain areas we present smoothed climatological analyses of historical phosphate means with few observations, we believe that useful information about the oceans can be gained through our procedures outlined in the introduction. We believe the large-scale features shown in our analyses are reasonable, but for the monthly and seasonal periods the database may be inadequate for some areas.

## 2.3. RESULTS

### 2.3.1. Climatological phosphate content distribution

Figure 2.2 shows the objectively analyzed global distribution of phosphate content at the ocean surface. Highest surface content, >2 μmol·kg$^{-1}$, are found near Antarctica in the Southern Ocean. High content can also be found in the High-Nutrient Low Chlorophyll (HNLC) zones around the subarctic Pacific. The Atlantic Ocean is overall depleted of phosphate (< 0.5 μmol·kg$^{-1}$) and the Pacific is split by higher content (~ 1-1.5 μmol·kg$^{-1}$) in the equatorial region.

Phosphate is typically depleted at or near the surface and increases in content at depth with exceptions. At 200 m depth (Figure 2.3) displays increasing content overall, especially in the northern Pacific and eastern equatorial Pacific. The objectively analyzed global distribution of phosphate at 1000 m depth (Figure. 2.4) displays a mean content around 2 - 3 μmol·kg$^{-1}$. The highest content is in the northern Pacific (< 2.75 μmol·kg$^{-1}$) and the lowest is in the north Atlantic and Arctic. At 3000 m (Figure. 2.5) the Pacific has the highest P content and there is a decrease in content in the Southern Ocean. In the Atlantic lower content is observed further south than at other depth levels.

### 2.3.2 Vertical Distribution

Meridional cross sections of the global mean objectively analyzed phosphate content roughly follow the World Ocean Circulation Experiment (WOCE) transect lines (Figure 2.6) are generally low at the surface, increase at the phosphate maximum (~1000m), then decrease slightly at deeper depths.

The Pacific Ocean basin (Figure 2.6a) has the highest phosphate content in the northern Pacific and Bering Sea around 1200m depth of ~3.5 μmol·kg$^{-1}$. The Indian Ocean basin (Figure 2.6b) has slightly lower phosphate content with a maximum of 2.2-2.6 μmol·kg$^{-1}$ that spans from around 700m to 5500m depth. The Atlantic Ocean basin (Figure 2.6c) generally exhibits the lowest phosphate content of the major basins. The phosphate content has a maximum of about 2.5-3 μmol·kg$^{-1}$ in the Southern Ocean and in the Atlantic Equatorial Intermediate Current (EIC) at about 500m to 1000m depth.

Phosphate and nitrate (Chapter 3 of this atlas) content show linear trends that closely resemble the nitrate/phosphate Redfield ratios (P:N = 1:15). Mean basin wide content (Figure. 2.7) shows that the Arctic and Atlantic have the lowest values in phosphate content throughout the water column, while the Pacific and Indian display higher content than the global mean. This is a trend that is consistent also in the nitrate (Chapter 3) and

silicate (Chapter 4) content distribution. This pattern is also consistent with low $O_2$ values in these regions (Garcia *et al.,* 2024c)

### 2.4 Objective analysis error estimates and comparison to other datasets

Table 1.9 (Chapter 1) provides estimates of the basin-scale nutrient content mean deviation of the statistical minus the objectively analyzed fields. In the case of phosphate, the mean differences are nearly zero. The global mean difference in content is about -0.004 $\mu mol \cdot kg^{-1}$. Figure 1.4a (Chapter 1) shows the global mean content differences as a function of depth. Sections 1.4.1 and 1.4.2 (Chapter 1) describes the mean differences.

We next compared the WOA23 global phosphate annual mean content fields as a function of depth to those in the WOA18 (Garcia *et al.*, 2019). The WOA23 and WOA18 compare well (*i.e.*, internal consistency). The depth averaged (± 1 standard deviation) phosphate content difference (WOA23 minus WOA18) for different ocean basins is small (Table 1.7 Chapter 1). The global mean difference is small, about $0.00 \pm 0.01$ $\mu mol \cdot kg^{-1}$.

We also compared WOA23 to the Global Ocean Data Analysis Project version 2.2016b (GLODAPv2.2016b, Olsen *et al.*, 2016, Lauvset *et al.*, 2022; thereafter GLODAP). The global depth averaged (± 1 standard deviation) phosphate content difference (WOA23 minus GLODAP) is small, about $0.00 \pm 0.03$ $\mu mol \cdot kg^{-1}$ for the 0-5500 m depth layer. Spatial and depth layer differences are expected because WOA23 is based on a larger spatial and temporal data coverage and number of quantifiable quality control metrics than GLODAP.

## 2.4. SUMMARY

In the preceding sections we have described the results of a project to objectively analyze all quality-controlled phosphate data in WOD23 for the years 1965 to 2022. We desire to build a set of climatological analyses that are identical in all respects for all variables in WOA23 including relatively data sparse EOV variables such as phosphate. This provides investigators with an internally consistent set of WOA23 gridded analyses. The WOA23 phosphate fields compare well to the previous version WOA18.

Phosphate has a relatively small open ocean content range. All the WOA23 data used in our analyses are available both at standard depth levels as well as observed depth levels. When provided, WOD23 preserves the data provider quality control flags. Data users can choose what quality flags to use or conduct independent data quality control for fit-for-purpose applications.

The results presented in this atlas show some ocean features that are suspect and may be due to non-representative or questionable data that were not flagged by the quality control techniques used. Although we have attempted to eliminate as many of these features as possible by flagging the data which generate these features, some obviously could remain. Some may eventually turn out not to be artifacts but rather to represent real features, not yet capable of being described in a meaningful way due to lack of data coverage.

## 2.5. REFERENCES

(See Chapter 1, Section 1.7. References)

## 2.6 CHAPTER 2 FIGURES

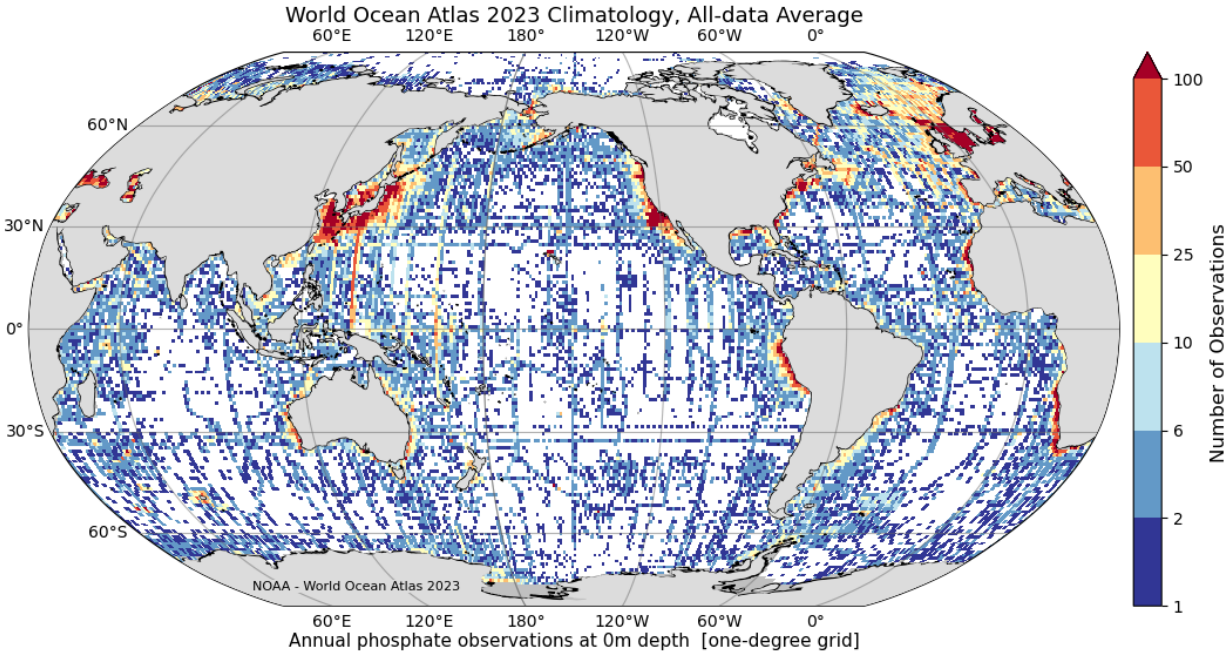


**Figure 2.1** Phosphate data density distribution at the surface, binned by 1-degree squares.
**Notes:** Deeper depths show a similar pattern with lower densities.

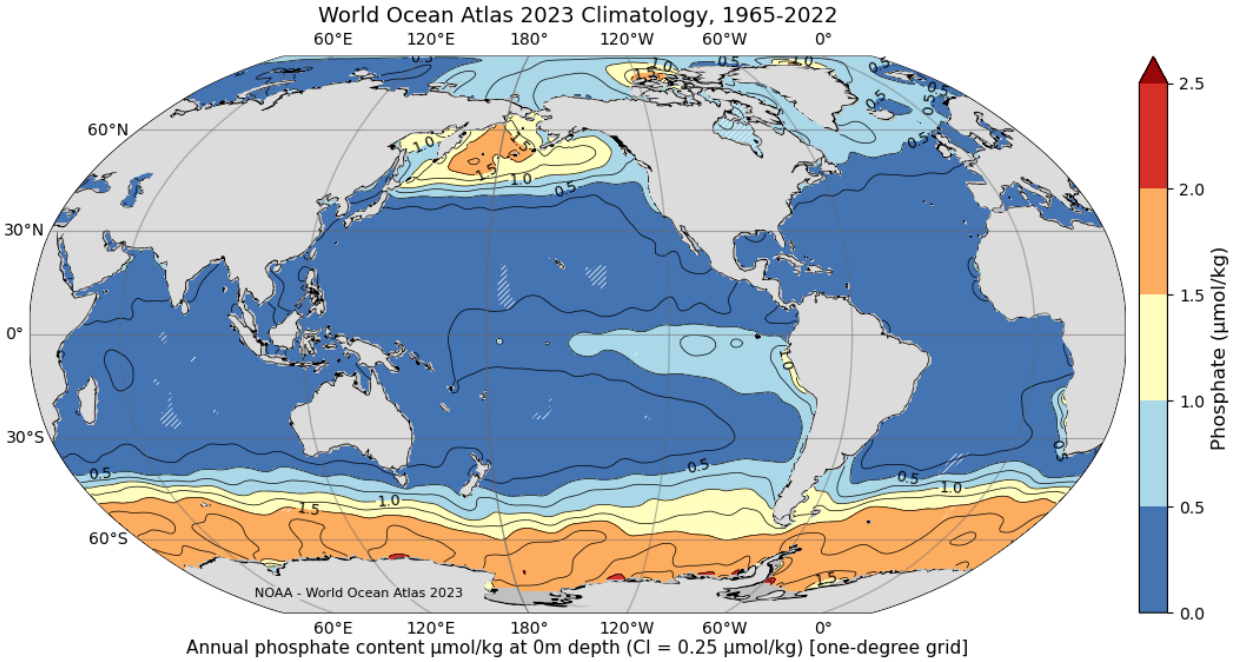


**Figure 2.2.** Objectively analyzed mean phosphate content (µmol·kg$^{-1}$) distribution at the surface ocean.

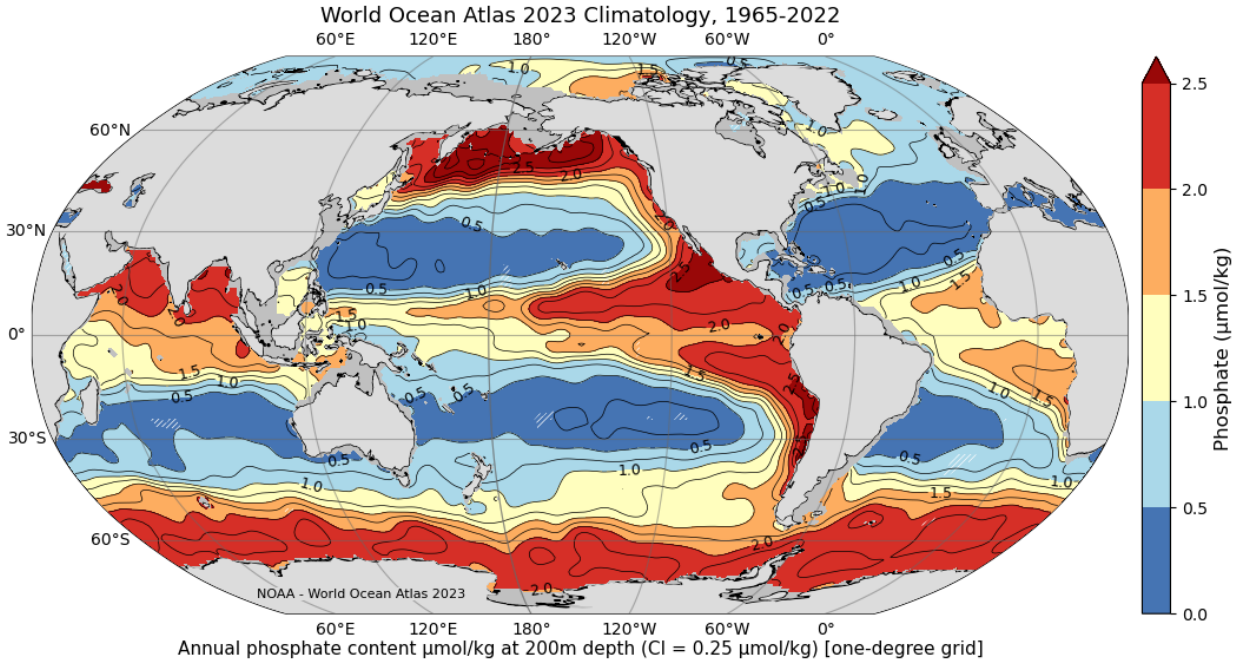


**Figure 2.3.** Climatological mean phosphate content (µmol·kg$^{-1}$) distribution at 200 m depth.

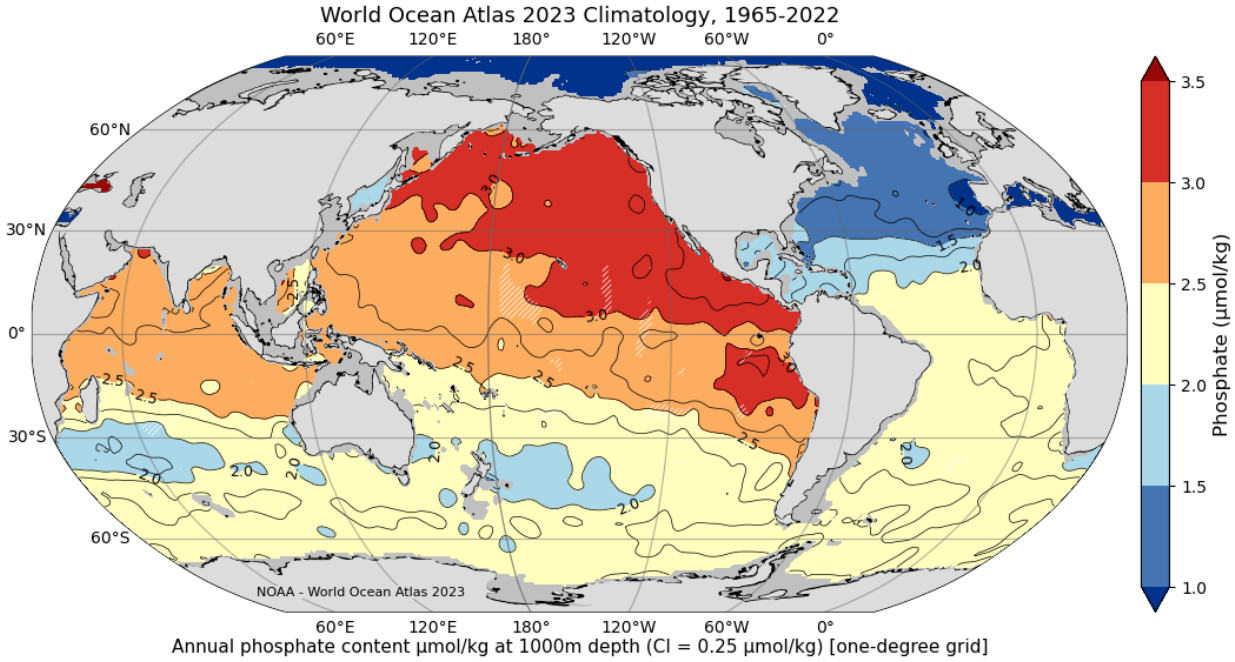


**Figure 2.4.** Climatological mean phosphate content (µmol·kg$^{-1}$) distribution at 1000 m depth.

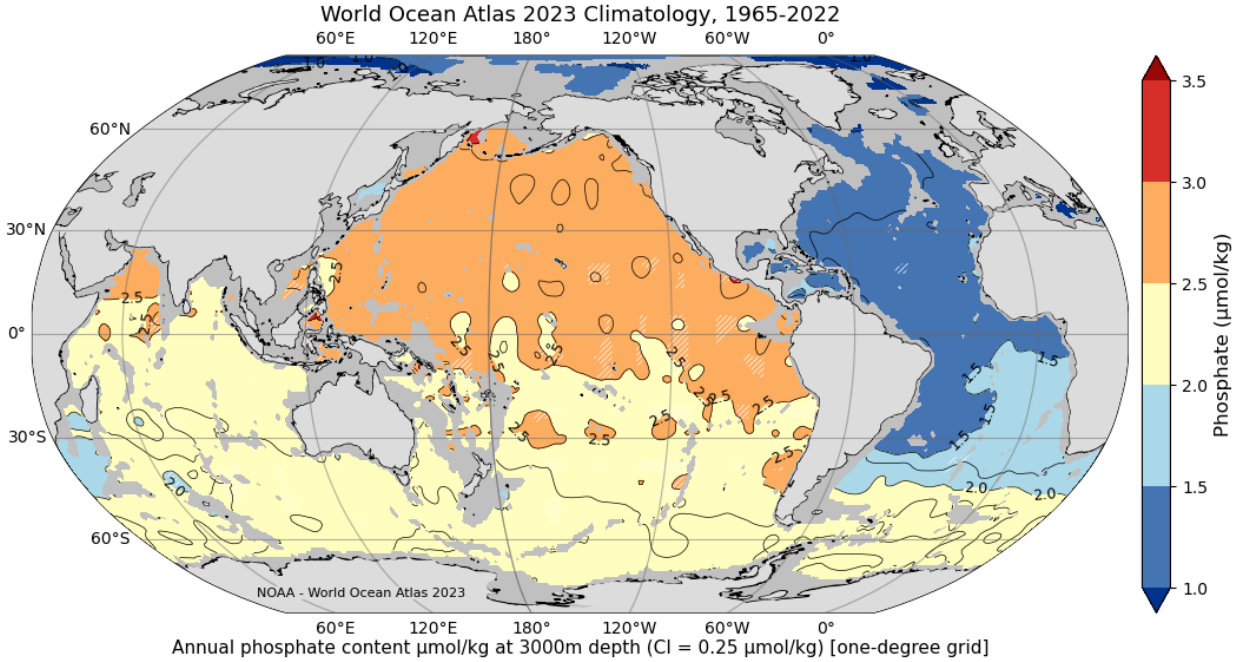


**Figure 2.5.** Climatological mean phosphate content (µmol·kg$^{-1}$) distribution at 3000 m depth.
**Notes:** Note the change in color scale**.**

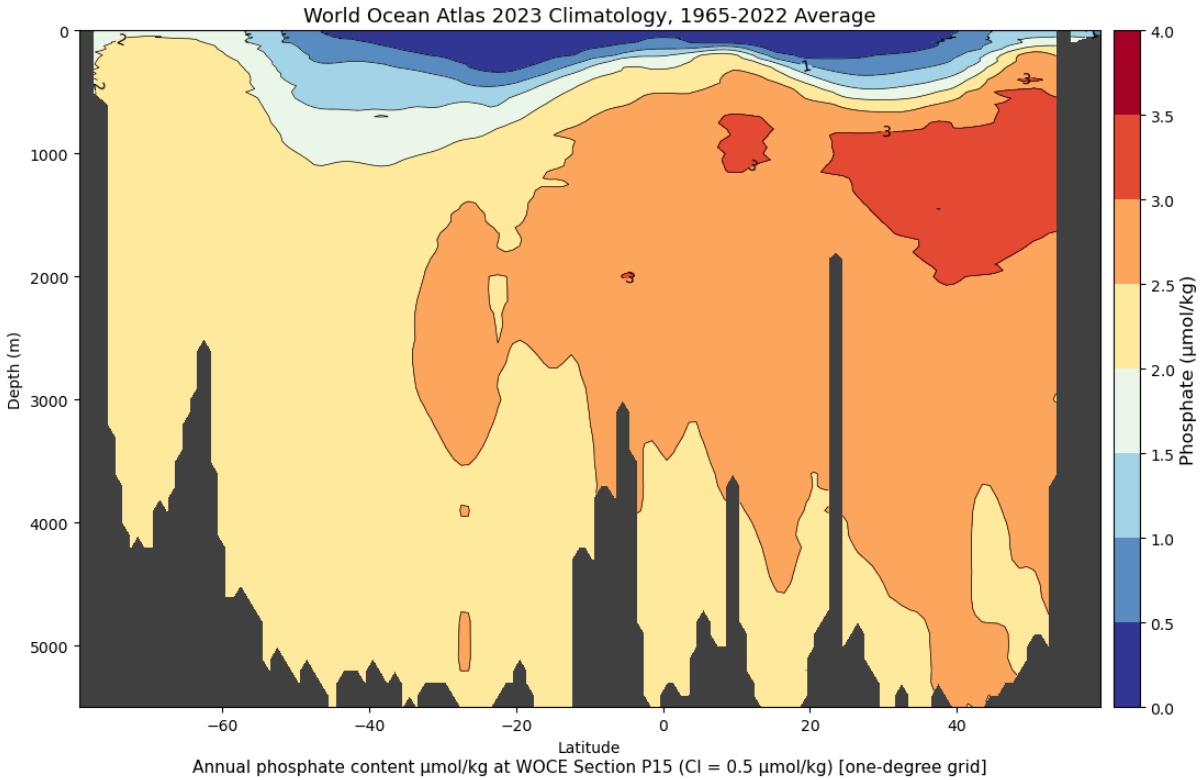


**Figure 2.6a.** Meridional cross sections of climatological mean phosphate content (µmol·kg$^{-1}$) in the Pacific Ocean at 165°W; roughly the WOCE P15 line (See figure 1.6 for WOCE lines).

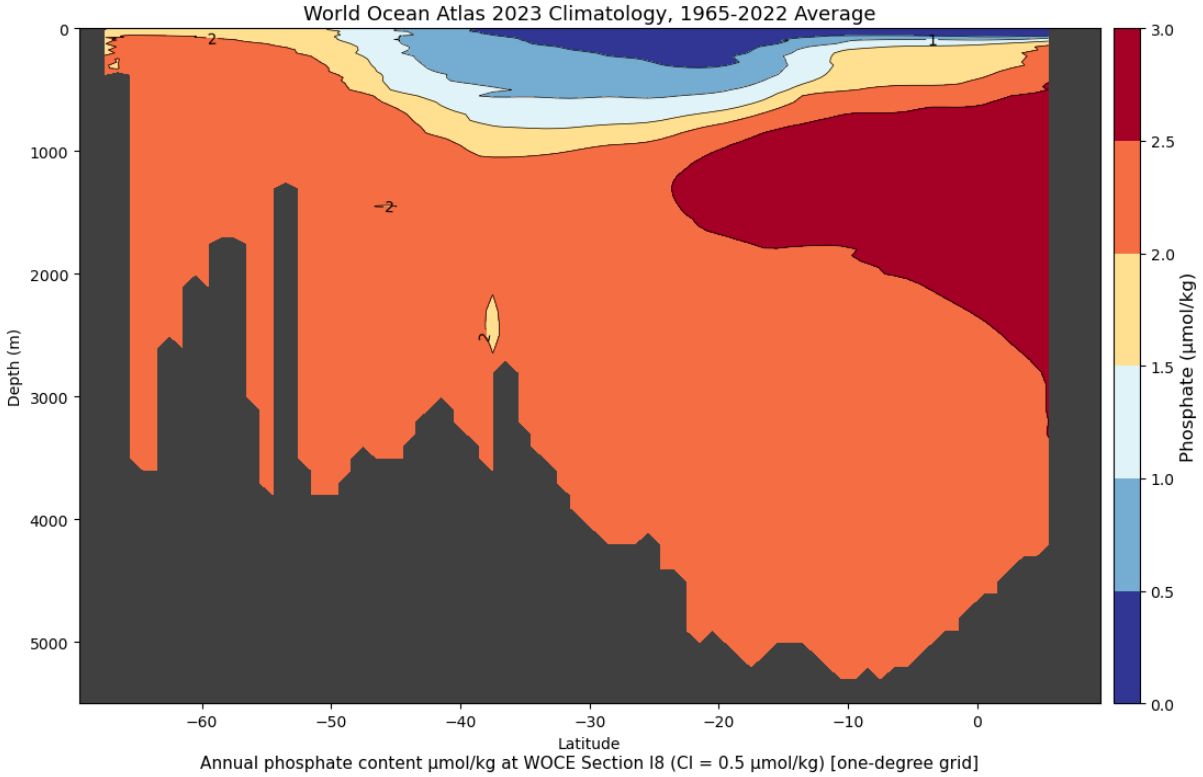


**Figure 2.6b.** Meridional cross sections of climatological mean phosphate content (µmol·kg$^{-1}$) in the Indian Ocean at 80°E; roughly the WOCE I8 line (See figure 1.6 for WOCE lines).

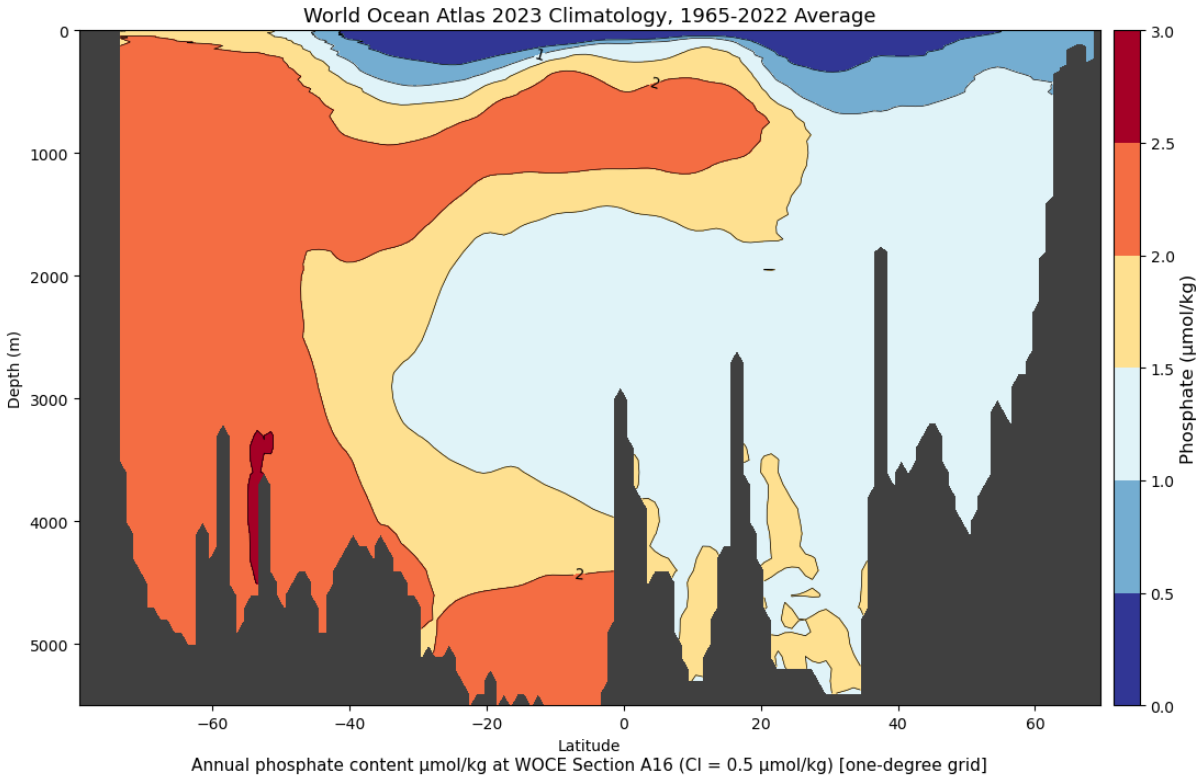


**Figure 2.6c.** Meridional cross sections of climatological mean phosphate content (µmol·kg$^{-1}$) in the Atlantic Ocean at 25°W; roughly the WOCE A16 line (See figure 1.6 for WOCE lines).

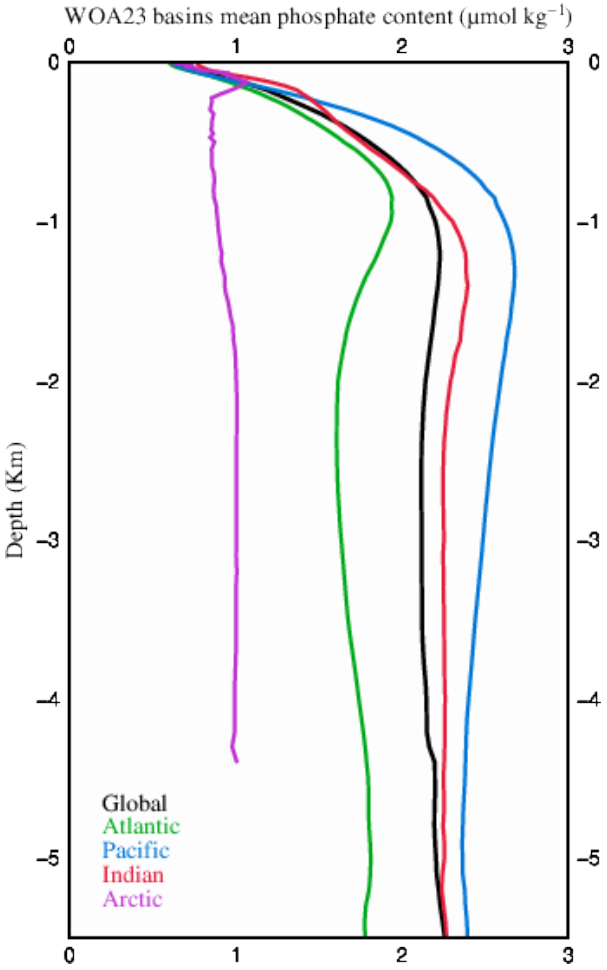


**Figure 2.7.** Annual mean phosphate content (µmol·kg$^{-1}$) as a function of depth (km) for different ocean basins.

**Notes:** Table 1.6 (Chapter 1) shows the mean phosphate content for different oceanic basins. See Figure 1.5 (Chapter 1) for ocean basin definitions.

# Chapter 3: Dissolved Inorganic Nitrate

## Christopher R. Paver

## ABSTRACT

This World Ocean Atlas 2023 (WOA23) atlas consists of a description of data analysis procedures and horizontal maps of climatological distribution fields of nitrate (and nitrate + nitrite) at selected standard depth levels of the World Ocean on a one-degree latitude-longitude grid. The aim of the maps is to illustrate large-scale characteristics of the distribution of nitrate. The oceanographic data fields used to generate these climatological maps were computed by objective analysis of all scientifically quality-controlled historical nitrate data collected on or after 1965 and 2022 in the *World Ocean Database 2023*, including roughly 134,000 additional profiles containing nitrate observations made available since the previous (WOA18) analysis. Maps are presented for climatological composite periods (annual, seasonal, monthly, seasonal and monthly difference fields from the annual mean field, and the number of observations) at 102 standard depths. The global ocean content inventory of nitrate is about 42.2 Pmol. Estimates of the uncertainty of the objective analysis to represent the nitrate statistical mean fields are provided. WOA23 nitrate is also compared to other mapped gridded products.

## 3.1. INTRODUCTION

Dissolved inorganic nitrate ($NO_3^-$) and nitrite ($NO_2^-$) are components of the global nitrogen cycle and play a critical role in marine ecosystems. Nitrate is an essential ocean variable (EOV) nutrient for marine organisms, supporting primary production and influencing ocean biogeochemistry. Its sources include atmospheric deposition, river runoff, nitrification, and upwelling, whereas biological uptake, denitrification, biogeochemical processes that can act as sink or source of nutrients, and sedimentation are sinks.

The global nitrogen cycle, which includes nitrogen fixation, nitrification, and denitrification are important processes with regards to nitrate. Nitrogen fixation is the process by which some microorganisms, such as cyanobacteria and Rhizobium bacteria convert dinitrogen ($N_2$) into ammonium ($NH_4^+$) (Capone *et al*, 2005). In turn, the ammonium produced through nitrogen fixation or released from organic matter is converted to nitrate through two sequential microbial processes called nitrification. First is the process of ammonium oxidation to nitrite and then nitrite oxidation to nitrate. This is an important step in the nitrogen cycle, as it makes the nitrogen readily available for primary production (Ward, 2019). Another important component of the nitrogen cycle is denitrification, wherein bacteria located in oxygen depleted environments reduce nitrate and nitrite back into dinitrogen that is reintroduced to the atmosphere (Codispoti and Christensen, 1985).

Atmospheric sources of nitrogen include the flux of naturally occurring gaseous dinitrogen ($N_2$) and the deposition of nitrogen oxides ($NO_X$) primarily as a result of agricultural and industrial activities (Duce *et al*, 2008). Terrestrial runoff, including nitrogen containing compounds from

agricultural runoff and wastewater discharge, contributes to nitrate input in coastal areas. Rivers act as the major conduit for transporting these compounds from the land to the ocean, mainly accumulating in estuaries and coastal regions (Howarth *et al*, 1996). Deep ocean upwelling is another source of nitrate, wherein cold, nutrient rich waters rise to the surface, supporting primary productivity (Bakun, 1990).

Primary producers, such as phytoplankton act as a sink by assimilating the nitrate to support their growth, which contributes to the marine food web (Falkowski *et al*, 1998). Denitrification is a significant sink for nitrate in oxygen depleted zones. Microbial activity in these regions reduces nitrate to nitrogen gas. Particulate organic matter, including dead phytoplankton and detritus, can sink to the ocean floor. This process, known as sedimentation, sequesters nitrate in the deep ocean, effectively removing it from surface waters (DeVries and Primeau, 2011).

This Chapter presents annual, seasonal, and monthly climatologies and related statistical fields for nitrate and nitrate plus nitrite.

## 3.2. DATA COVERAGE

The World Ocean Database 2023 (WOD23) includes close to 14,000 new nitrate and nitrate + nitrite (from here on referred to as nitrate) profiles since the WOD18 (Boyer *et al*., 2019). This brings the total holdings of nitrate to just over 2.23 million profiles. However, due to the extensive quality control screening conducted during WOD and WOA processing, roughly 340,000 of the 2.23 million profiles (6,123,954 discrete observations) are used to generate the WOA23 nitrate climatologies. The previous climatology, the WOA18 (Garcia *et al*., 2019), incorporated roughly 206,000 profiles.

Figure 3.1 displays the distribution of surface observations. The majority of the observations are in the coastal regions, *e.g.* around Japan and the Korean Peninsula, and are identified by the red shading. While the open ocean is sparsely observed compared to the coastal regions, a majority of the observations are collected along zonal and meridional cruise transects. Some of these transects, however, are repeat observations and detail the variability over time, both seasonally and annually.

Further review of the surface observation density figures displays a seasonal effect in the northern hemisphere, wherein there are fewer observations in the fall and winter months, and more observations in the spring and summer months. The southern hemisphere, on the other hand, seems to display little seasonal variation.

## 3.3. RESULTS

### 3.3.1. Climatological distribution

Figure 3.2 displays the objectively analyzed global distribution of nitrate at the ocean surface. As with the other nutrients in this atlas, the highest nitrate content is found in the Southern Ocean with a maximum of over 25 $\mu mol \cdot kg^{-1}$ near Antarctica and decreasing northward to about 5 $\mu mol \cdot kg^{-1}$ around 40°S. Another area of high content is in the subarctic northern Pacific Ocean with a range of roughly 5-20 $\mu mol \cdot kg^{-1}$. The Greenland, Iceland, and Norwegian Seas (GINS) display a moderately high content between 5-10 $\mu mol \cdot kg^{-1}$. In contrast the temperate and equatorial regions (40°N to 40°S) display content at or lower than 5 $\mu mol \cdot kg^{-1}$.

At 200 m depth, nitrate content displays an overall increase as it approaches the nitrate maximum (Figure 3.3). The Southern Ocean nitrate content continues to rise above 30 $\mu mol \cdot kg^{-1}$, as well as the northern Pacific

Ocean (> 40 μmol·kg$^{-1}$). The equatorial current regions display increased content in the eastern basins, globally.

At 1000 m depth, at or near the nitrate maximum, global nitrate content is generally over 30 μmol·kg$^{-1}$, with exceptions such as in the Arctic Ocean, northern Atlantic Ocean, and Mediterranean Sea (Figure 3.4). The highest content is observed in the Pacific Ocean (> 40 μmol·kg$^{-1}$).

At 3000 m depth, the northeast Pacific Ocean has the highest content around 38 μmol·kg$^{-1}$ and decreases southward to about 30 μmol·kg$^{-1}$ in the Southern Ocean (Figure 3.5). The Indian Ocean also has high nitrate content in the northern part of the basin (34-36 μmol·kg$^{-1}$), decreasing southward. The northwestern Atlantic Ocean displays relatively low content (< 20 μmol·kg$^{-1}$), and increases to the southwest. The Arctic Ocean displays the lowest nitrate content of all the basins (< 20 μmol·kg$^{-1}$).

### 3.3.2. Vertical distribution

Global mean objectively analyzed nitrate content is generally low at the surface (< ~5 μmol·kg$^{-1}$) and increase to a mean content at the nitrate maximum (~1000 m) to about 33 μmol·kg$^{-1}$, and slightly reduce approaching the bottom to about 30 μmol·kg$^{-1}$ (Figure 3.6). Table 1.6 (Chapter 1) illustrates the mean nitrate content for different ocean basins.

The Atlantic Ocean basin generally has the lowest nitrate content with a maximum of about 35 μmol·kg$^{-1}$ in Southern Ocean waters and Antarctic Bottom Water (AABW; Figure 3.7a). Another area of higher nitrate content can be found in the Atlantic Equatorial Intermediate Current (EIC), and North and South Equatorial Undercurrents between 500 and 1000 m depth (around 35 μmol·kg$^{-1}$).

The Indian Ocean basin has slightly higher nitrate content than the Atlantic with a maximum mean in the northern region of around 35 μmol·kg$^{-1}$. This maximum goes from around 750 m depth to the bottom (Figure 3.7b).

The Pacific Ocean basin has the highest nitrate content and inventory (Table 1.6a,b). The global nitrate content (0-5500 m) is about 42.2 Pmol. The northern Pacific and Bering Sea display a maximum mean content of 45 μmol·kg$^{-1}$ in the North Pacific Intermediate Waters (NPIW) around 1200 m depth (Figure 3.7c).

### 3.3.3. Objective analysis uncertainty error estimates and comparison to other datasets

Table 1.9 (Chapter 1) provides estimates of the basin-scale nutrient content mean deviation of the statistical minus the objectively analyzed fields. In the case of nitrate, the mean differences are nearly zero. The global mean difference in content is about -0.04 μmol·kg$^{-1}$. Figure 1.4b (Chapter 1) shows the global mean content differences as a function of depth. Sections 1.4.1 and 1.4.2 (Chapter 1) describes the mean differences.

We compared the WOA23 global nitrate annual mean content fields as a function of depth to those in the WOA18. The WOA23 and WOA18 compare well (*i.e.*, internal consistency). The global depth averaged (±1 standard deviation) nitrate content difference is near zero, about 0.00 ± 0.02 μmol·kg$^{-1}$ for the 0-5500 m depth layer (Table 1.7, Chapter 1).

We also compared WOA23 to the Global Ocean Data Analysis Project version 2.2016b (GLODAPv2.2016b, Olsen *et al.*, 2016, Lauvset *et al.*, 2022; thereafter GLODAP). The depth averaged (± 1 standard deviation) nitrate content difference is small, about -0.23 ± 0.38 μmol·kg$^{-1}$ and -0.16 ± 0.26

for the 0-500 and 0-5500 m depth layers, respectively. WOA23 mean nitrate content as a function of depth is slightly lower than GLODAPv2.2. The average content differences are generally small. Spatial and depth layer differences are expected because WOA23 is based on a much larger spatial and temporal nitrate data coverage, number of observations, as well and quality-control metrics than GLODAPv2.2.

### 3.4 REFERENCES

(See Chapter 1, Section 1.7. References)

## 3.5 CHAPTER 3 FIGURES

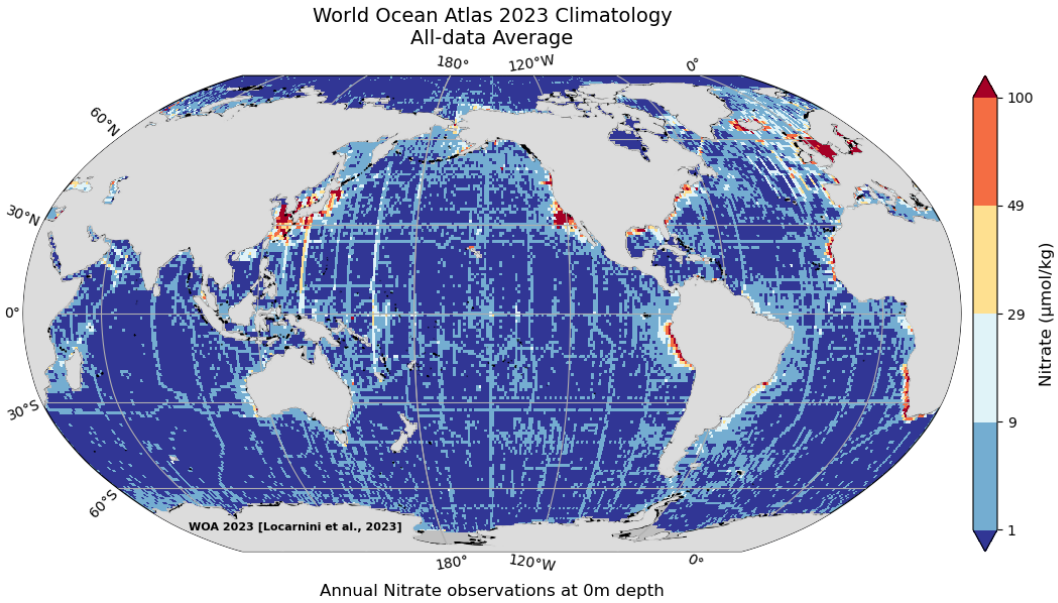


**Figure 3.1.** Global distribution of nitrate observations at 0 m depth.

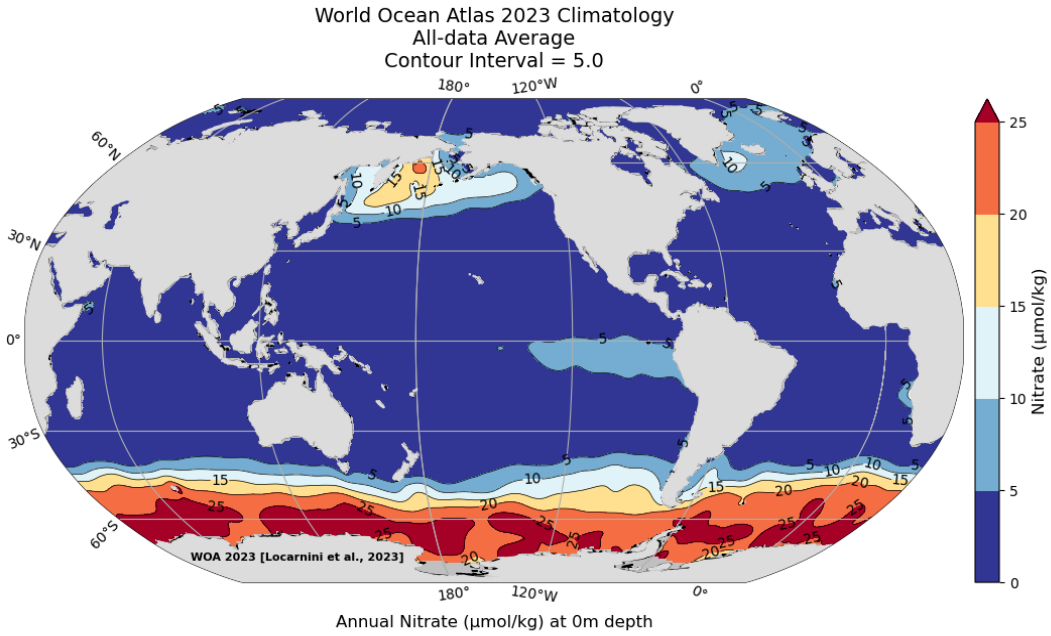

Annual Nitrate (µmol/kg) at 0m depth

**Figure 3.2.** Annual nitrate content (µmol·kg$^{-1}$) objectively analyzed content fields at 0 m depth.

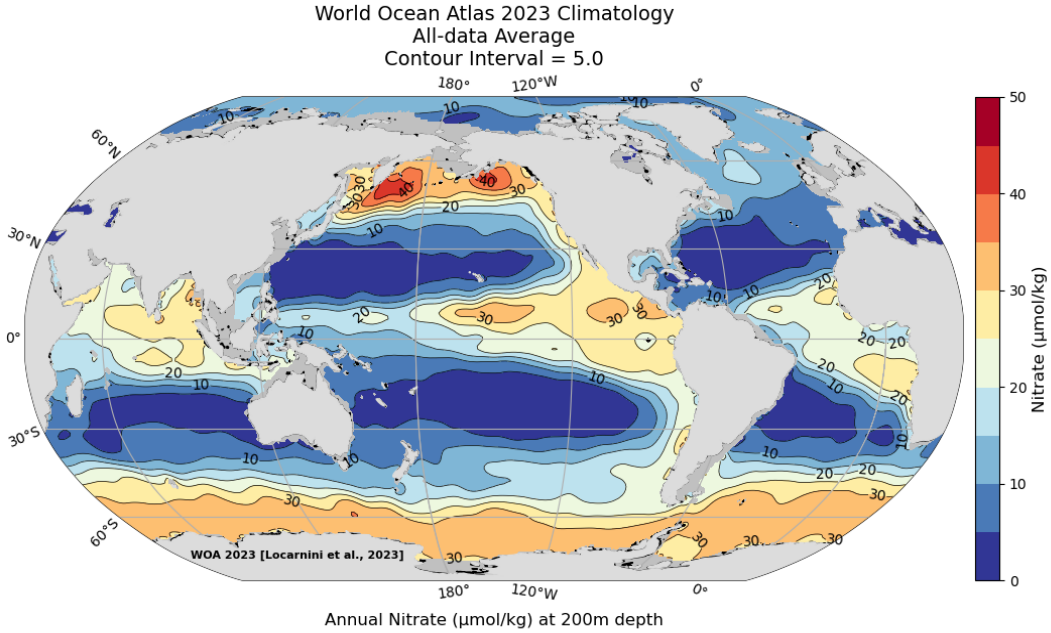

Annual Nitrate (µmol/kg) at 200m depth

**Figure 3.3.** Annual nitrate content (µmol·kg$^{-1}$) objectively analyzed fields at 200 m depth.

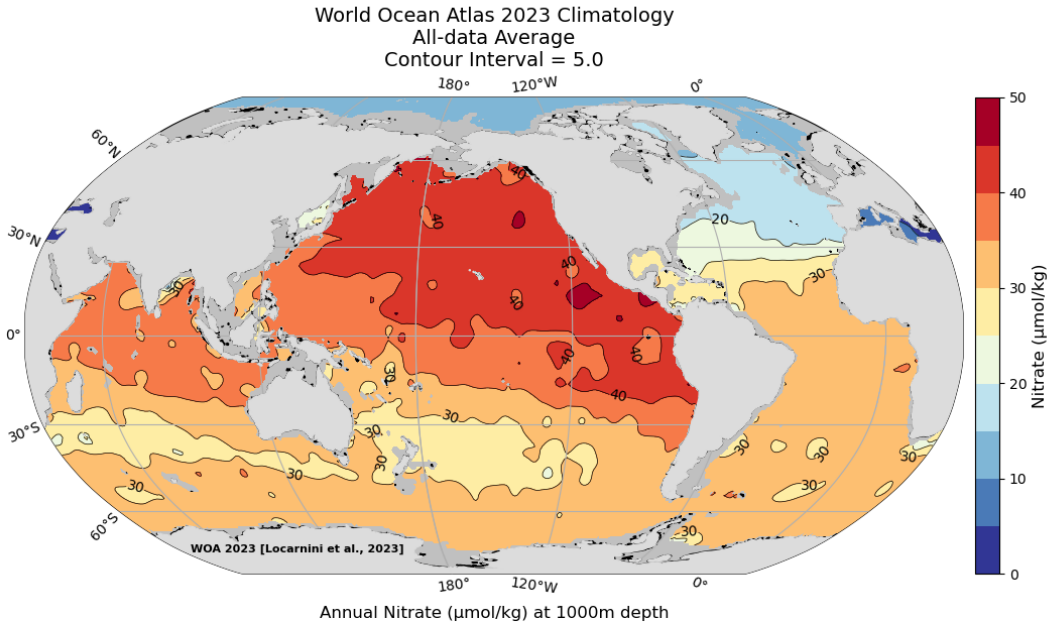


**Figure 3.4.** Annual nitrate content (µmol·kg$^{-1}$) objectively analyzed fields at 1000 m depth.

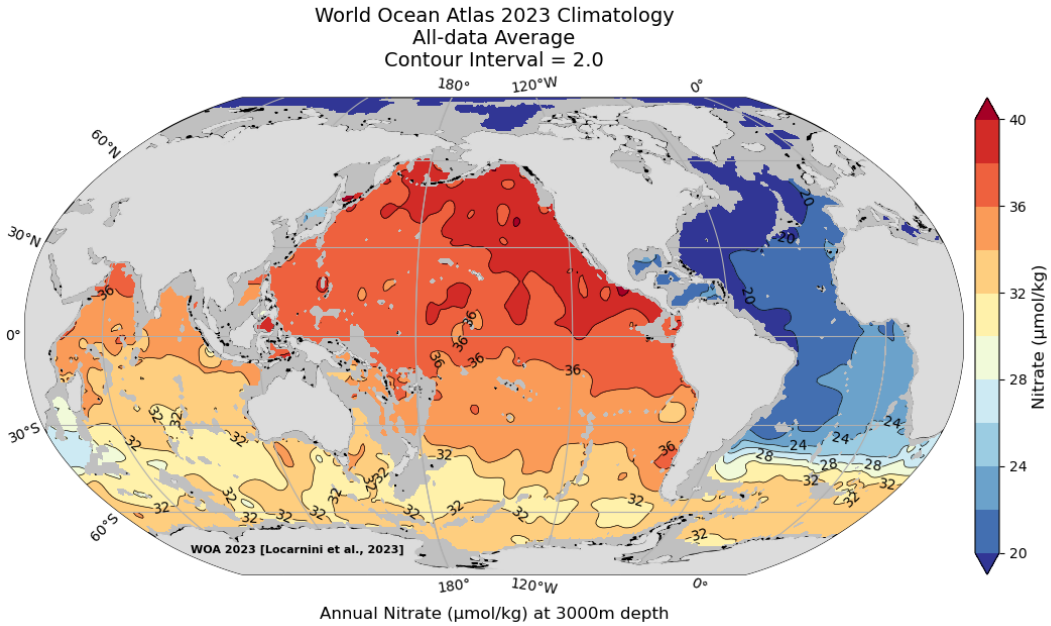


**Figure 3.5.** Annual nitrate content (µmol·kg$^{-1}$) objectively analyzed fields at 3000 m depth.

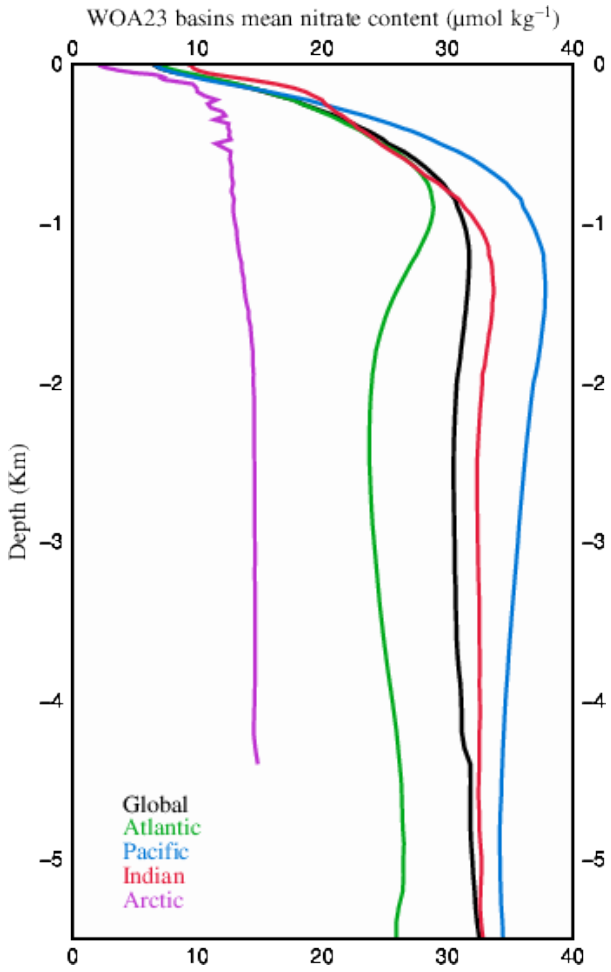


**Figure 3.6.** Annual mean nitrate content ($\mu mol \cdot kg^{-1}$) as a function of depth (km) for different ocean basins.

Note: Table 1.6 (Chapter 1) shows the mean phosphate content for different oceanic basins. See Figure 1.5 (Chapter 1) for ocean basin definitions.

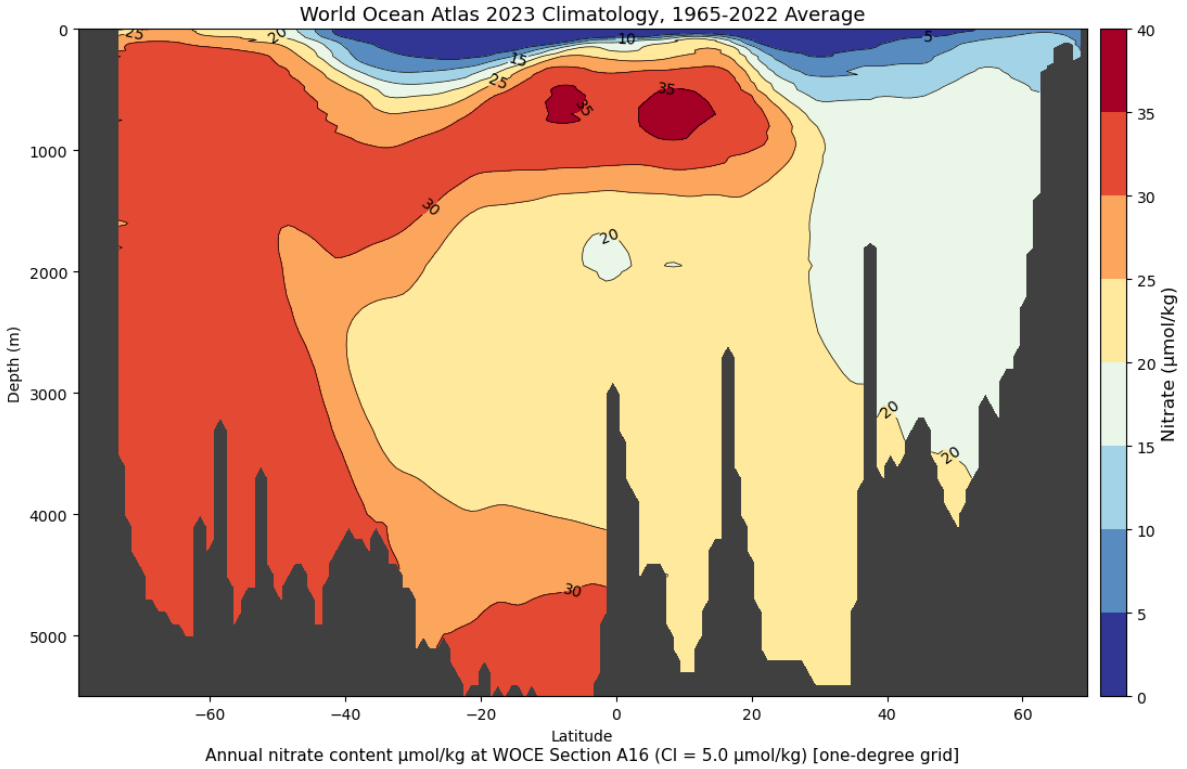


**Figure 3.7a.** Meridional nitrate content (µmol·kg$^{-1}$) section in the Atlantic Ocean at about 25°W; roughly the WOCE A16 line.

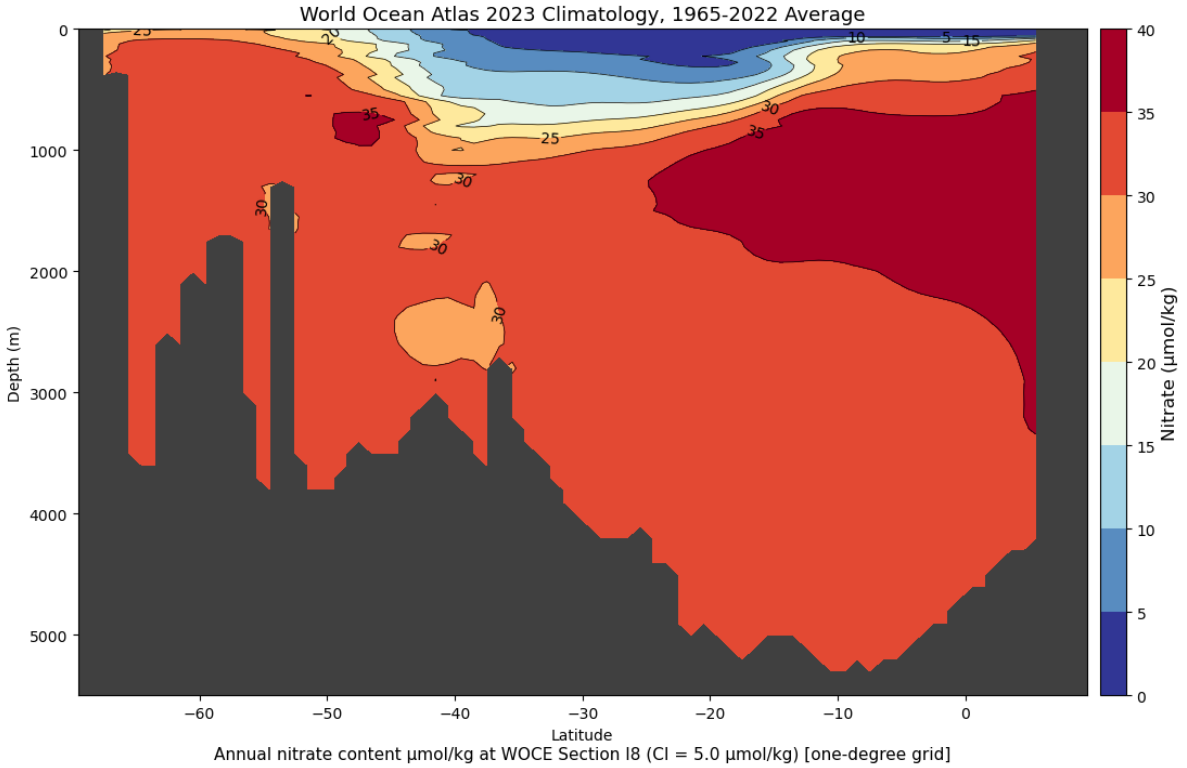


**Figure 3.7b.** Meridional nitrate content (µmol·kg$^{-1}$) section in the Indian Ocean at about 80°E; roughly the WOCE I8 line.

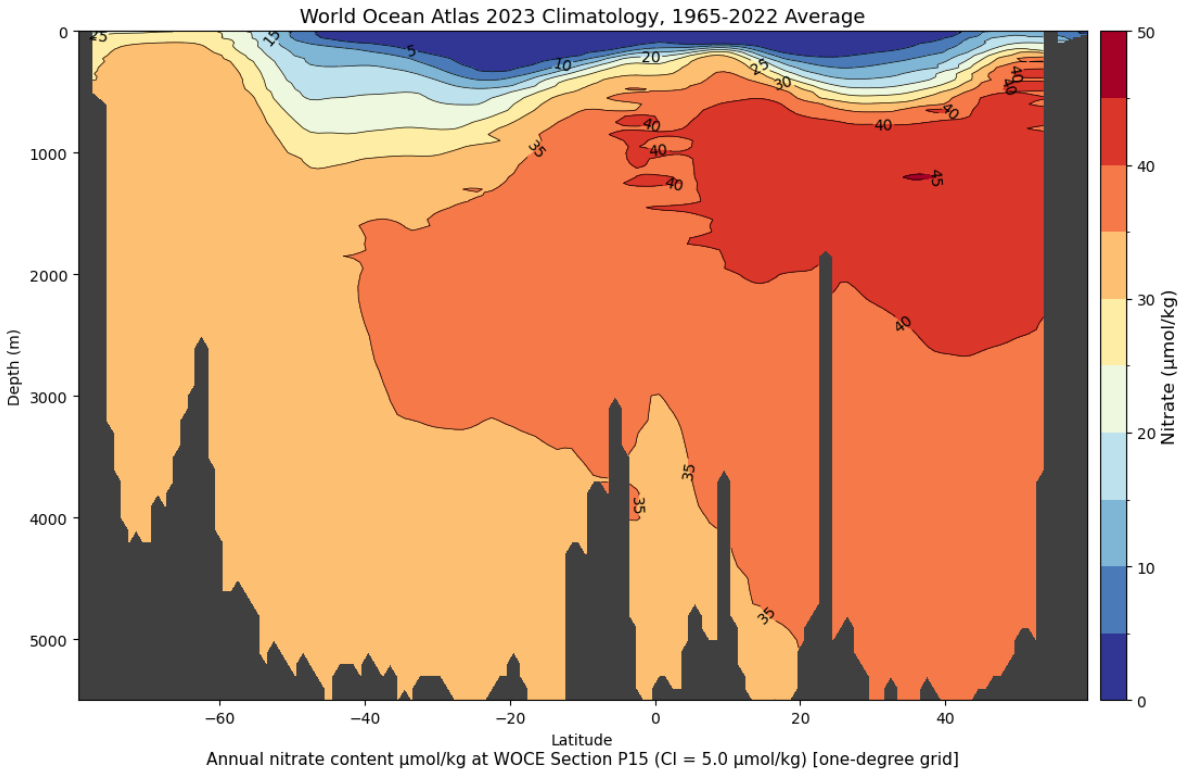


**Figure 3.7c.** Meridional nitrate content (µmol·kg$^{-1}$) section in the Pacific Ocean at about 165°W; roughly the WOCE P15 line.

# Chapter 4: Dissolved Inorganic Silicate


## Scott L. Cross



## ABSTRACT

This chapter describes the WOA23 atlas content for dissolved silicate: a set of global, all-data (1965-2022) climatological mean fields of silicate for the World Ocean at selected standard depth levels, gridded on a one-degree latitude-longitude grid. The aim is to illustrate large-scale, climatological characteristics of the distribution of dissolved silicate. The data fields used to generate these climatological maps were computed by objective analysis of all scientifically quality-controlled historical dissolved silicate data in the *World Ocean Database 2023* that were collected between 1965 and 2022, including almost 14,000 additional measurements of dissolved silicate made available since the previous (2018) WOA analysis. The WOA23 includes maps for climatological composite periods (annual, seasonal, monthly, seasonal and monthly difference fields from the annual mean field, and the number of observations) at 102 standard depths, along with ancillary descriptive fields including data distribution, statistical mean, and the observed (mean) minus objectively analyzed values. The global silicate ocean content inventory is about 122.4 Pmol. Estimates of the uncertainty error or precision of the objective analysis to represent the statistical fields are provided. The WOA23 silicate is compared to other gridded products.


## 4.1. INTRODUCTION

Silicon is the second most abundant chemical element in the Earth's crust, though the vast majority is bound in the form of quartz and other silicate minerals that are largely biologically unreactive. Chemical weathering of crustal materials and dissolution produces dissolved silicate, which is transported to the oceans via rivers. Rivers discharging into the ocean and marginal seas are the main supply of reactive dissolved silicate to the oceans (Tréguer and de la Rocha, 2013; Tréguer *et al.* 2021; Laruelle *et al.*, 2009).

The predominant form of silica dissolved in seawater is silicic acid; often referred to as silicate. For simplicity, we adopt the silicate term here. Unlike phosphate (Chapter 2) and nitrate (Chapter 3), silicate is not used directly to synthesize soft, labile organic tissue; instead, silicate is used by a variety of marine plants and animals (*e.g.* diatoms, radiolaria, silicoflagellates, siliceous sponges) to construct external or internal hard parts. When these organisms die and decompose, they contribute biogenic particulate and dissolved silicate to seawater and the sediments.

Cycling of silicate within the ocean water column is largely dominated by uptake by diatoms within the photic zone, and subsequent release through dissolution of biogenic silica within the water column. According to a synthesis by Tréguer and de la Rocha (2013), somewhat more than half of this recycling occurs within the photic zone, with the remainder being transported to the deep ocean via particle settling. Of the latter, about a quarter is recycled within the deep ocean water column, with the remainder being deposited in sediments. Dissolution during sediment diagenesis recycles a significant portion of the sedimentary

biogenic silica contributing to elevated dissolved silicate in the deep ocean; upwelling and vertical diffusion transport dissolved silicate back to the upper ocean to complete the cycle. These processes of transport, uptake, and recycling control the patterns of dissolved silicate observed in the world oceans.

This atlas Chapter presents annual, seasonal, and monthly climatologies and related statistical fields for dissolved silicate. The Chapter is divided into sections: we begin by describing the data sources and data distribution (Section 4.2), then the results (Section 4.3), and finally, a summary (Section 4.4).

## 4.2. DATA AND DATA DISTRIBUTION

Data sources and quality control procedures are briefly described below. For further information on the data sources used in WOA23 refer to the *World Ocean Database 2023* (WOD23, Mishonov *et al.,* 2023). The quality control procedures used in preparation of these analyses are described in Chapter 1 of this atlas.

### 4.2.1. Data sources

The data used in this objective analysis are taken from the World Ocean Database 2023 (WOD23), and include all OSD (bottle-sample) data from the time range 1965-2022, minus those data excluded through automated or subjective quality control procedures.

### 4.2.2. Data coverage

A total of 13,747 new profiles of dissolved silicate were added to the WOD23 database since the previous version of the Atlas (WOA18), representing an increase of roughly 3%. The additional profiles contribute substantial coverage in the North Atlantic, as well as in the South Atlantic proximal to South America. A plot of the total data density at the ocean surface (Figure 4.1) reveals that global coverage is widespread but sparse, with many 1-degree latitude and longitude grids having one or two observations in total. Spatial coverage is markedly biased towards nearshore and shelf locations. Areas in the northern and northwest Pacific (East China Sea/Japan/Korea, Bering Sea), the northern North Atlantic (Greenland, Iceland and Norwegian Sea, North Sea, Baltic Sea, Arctic) and the coastal U.S. are all relatively well sampled. Sampling density declines with depth, but a similar overall pattern of geographic distribution is maintained, and there is some coverage to abyssal depths in all major basins.

Coverage is somewhat seasonal, with highest density in boreal and austral spring and summer, but there is global coverage in all months, save in the high latitudes particularly in winter.

There are a number of basin-wide cruise track sections in all major basins, generally oriented E-W or N-S, and visible on the data density plots (Figure 4.1). These may be repeat sections or time series (*e.g.* WOCE, HOTS/BATS, GO-SHIP repeat hydrography, etc.), or single hydrographic sections that sampled multiple sites in each 1-degree bin. These can be especially important for establishing a sense of the decadal scale variability of the silicate content distribution, in areas that are otherwise sparsely sampled.

The representativeness of the fields presented here is a function of both observation density and variability in the measured quantity. In the upper ocean, where nutrient variability is high, the all-data annual mean distributions are reasonable for representing large-scale features, but for the shorter (seasonal and monthly) compositing periods, the database is likely inadequate in some regions. In the

deep ocean variability is low, and a few observations may be sufficient to characterize property distributions there.

## 4.3. RESULTS

### 4.3.1. Climatological silicate distribution

Figure 4.2 shows the objectively analyzed global distribution of dissolved silicate at the ocean surface. Highest surface content values, over 70 μmol·kg$^{-1}$, are generally found in the Southern Ocean, circling the Antarctic Continent. High content values are found also in the subarctic Pacific– a classic High Nutrient Low Chlorophyll (HNLC) zone as well as locally in the coastal Arctic. Atlantic surface waters are relatively depleted (generally < 5 μmol·kg$^{-1}$), with highest content in the northern North Atlantic, in some marginal seas (North Sea, Baltic Sea), and fjords.

There is pronounced seasonality in surface ocean silicate, particularly in the northern Pacific, where content generally peaks in winter/spring and is at a minimum in summer/fall.

Silicate generally increases with depth in all oceans (Figures 4.2 - 4.7). At 200 m depth, approximately the bottom of the surface mixed layer, silicate content shows a similar geographic pattern as at the surface, with more pronounced zones of elevated silicate in the equatorial upwelling zones, as well as the northern Indian Ocean and Southern Ocean (Figure 4.3). Seasonality is muted at this depth, and mostly absent in the deeper ocean.

At 1000 m, roughly the base of the main thermocline, silicate content declines from north to south in the North Pacific and Indian Oceans, and increases north to south in the north Atlantic (Figure 4.4). In the southern hemisphere, between about 30 and 50 deg South, there is a pronounced silicate content minimum reaching up to 40 μmol·kg$^{-1}$or less in all ocean basins.

In the deep ocean dissolved silicate is elevated everywhere, though generally higher in the Pacific, Southern, and Indian Oceans than in much of the Atlantic (Figure 4.5). At levels below about 3000 m, the Atlantic (Figure 4.5) is divided meridionally by the mid-ocean ridge system: silicate is generally higher on the eastern side of the basin than on the west. This is true southwards to about 40 degrees south, approaching the Southern Ocean, where silicate content is generally elevated across the basin. Tables 16a, b provides estimates of the mean content and inventory in different ocean basins. The global ocean content inventory of silicate is about 122.4 Pmol.

Meridional sections highlight the similarities and differences between the major basins with respect to subsurface silicate distribution. The Pacific and Indian Oceans (Figures 4.6a and 4.6b) are both characterized by subsurface maxima in the high latitudes of both hemispheres, separated by the aforementioned minimum centered at about 30 deg S, which extends to the bottom in both basins. Highest content in both basins are found at roughly 2500 to 4000 m depth in the northern hemisphere.

Subsurface silicate content is quite different in the Atlantic (Figure 4.6c). In particular, there is no obvious subsurface maximum in the northern hemisphere; content is quite low (< ~15 μmol·kg$^{-1}$) in the north, increasing southwards to a maximum at about 60 deg South that extends throughout the water column. Figure 4.8 shows the mean silicate content as a function of depth for different ocean basins. The Arctic and the Pacific basins have the lowest and highest silicate content values as a function of depth.

### 4.3.2. Objective analysis error estimates and comparison to other datasets

Table 1.9 (Chapter 1) provides estimates of the basin-scale nutrient content mean deviation of the statistical minus the objectively analyzed fields. In the case of silicate (and phosphate and nitrate), the mean basin scale differences are nearly zero. The global mean difference in content is about -0.067 µmol·kg$^{-1}$. Figure 1.4c (Chapter 1) shows the global mean silicate content differences as a function of depth. Sections 1.4.1 and 1.4.2 (Chapter 1) describes the mean differences.

We compared the WOA23 silicate annual mean content as a function of depth to silicate in the WOA18 (Garcia *et al.*, 2019). The WOA23 and WOA18 compare well, indicating high internal consistency between the WOA data products. The global ocean depth-averaged (± 1 standard deviation) silicate content difference is about -0.03 ± 0.12 µmol·kg$^{-1}$for the 0-5500 m depth layer (Chapter 1, Table 1.7). Largest content differences are found in the Arctic basin, where the WOA23 mean silicate content is smaller than in the WOA18 by almost 0.4 µmol·kg$^{-1}$, a decrease of approximately 4 percent. This may be attributed to less data coverage in the WOA18 when compared to the WOA23 in the Arctic.

We also compared the WOA23 to the mapped Global Ocean Data Analysis Project version 2.2016b (GLODAPv2.2016b, Olsen *et al.*, 2016, Lauvset *et al.*, 2022; hereafter GLODAP). WOA23 silicate content is slightly larger than silicate in GLODAP except in the Atlantic Basin (Chapter 1, Table 1.8). The global ocean depth averaged (± 1 standard deviation) silicate content difference is about 0.48 ± 0.41 µmol·kg$^{-1}$ for the 0-5500 m depth layer. In the Atlantic, WOA23 silicate content is slightly lower than GLODAP by about -0.27 ± 0.48 µmol·kg$^{-1}$. The mean silicate content differences are < 1% when compared to the global mean silicate content, about 65.7 ± 41.2 µmol·kg$^{-1}$ (Table 1.6 Chapter 1). As described in Section 1.4.5 (Chapter 1), regional and depth layer differences are expected between WOA23 and GLODAP.

## 4.4. SUMMARY

This new objective analysis of global silicate observations for the 1965-2022 time period adds almost 14,000 profiles to the previous analysis from the WOA18. Surface values for silicate content range from a high around 70 µmol·kg$^{-1}$in the Southern Ocean to around 7 µmol·kg$^{-1}$ in the North Atlantic. Silicate content generally increases with depth; near-bottom values range from ~25 µmol·kg$^{-1}$ in the Arctic to well above 150 µmol·kg$^{-1}$ in the north Pacific and Southern Oceans.

The WOA23 and WOA18 silicate content differences as a function of depth and basin are small reflecting a high degree of internal data quality control and processing. The WOA23 and WOA18 global mean silicate content as a function of depth is small, -0.03 ± 0.16 µmol·kg$^{-1}$ (0-5500 m). When compared to GLODAP, WOA23 silicate mean content values are also generally consistent. The global mean WOA23 silicate content is slightly higher than in the GLODAP by about 0.48 ± 0.41 µmol·kg$^{-1}$ (0-5500 m).

## 4.5. REFERENCES

(See Chapter 1, Section 1.7. References)

## 4.6. CHAPTER 4 FIGURES

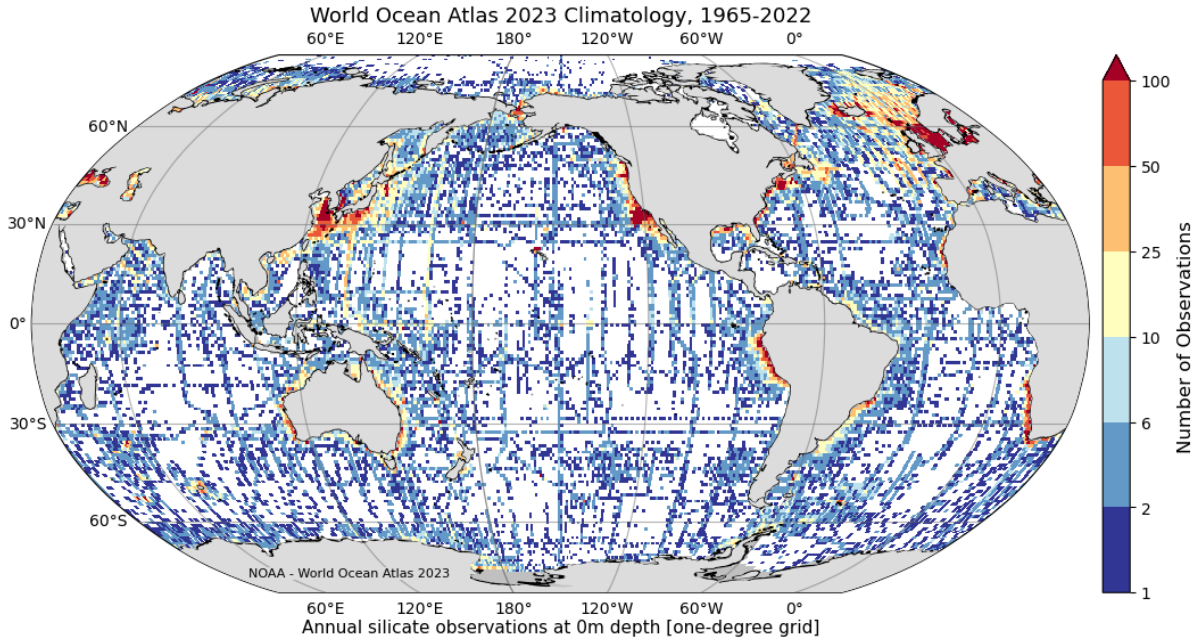


**Figure 4.1.** Number of silicate observations in each 1x1 degree latitude and longitude grid box at the ocean surface. Deeper depths show a similar spatial pattern but lower densities, especially below about 1000 m depth.

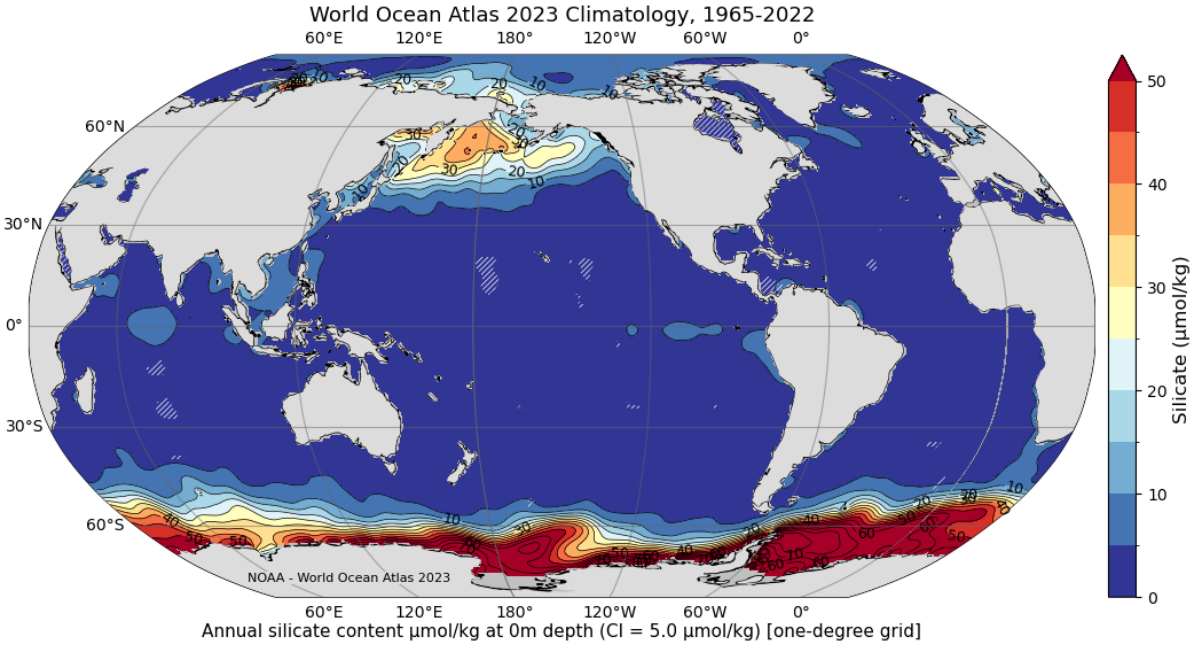


**Figure 4.2.** Climatological mean silicate content ($\mu mol \cdot kg^{-1}$) distribution at the surface. Lighter-shaded (grayed-out) patches indicate regions where there was no data within the radius of influence for the objective analysis.

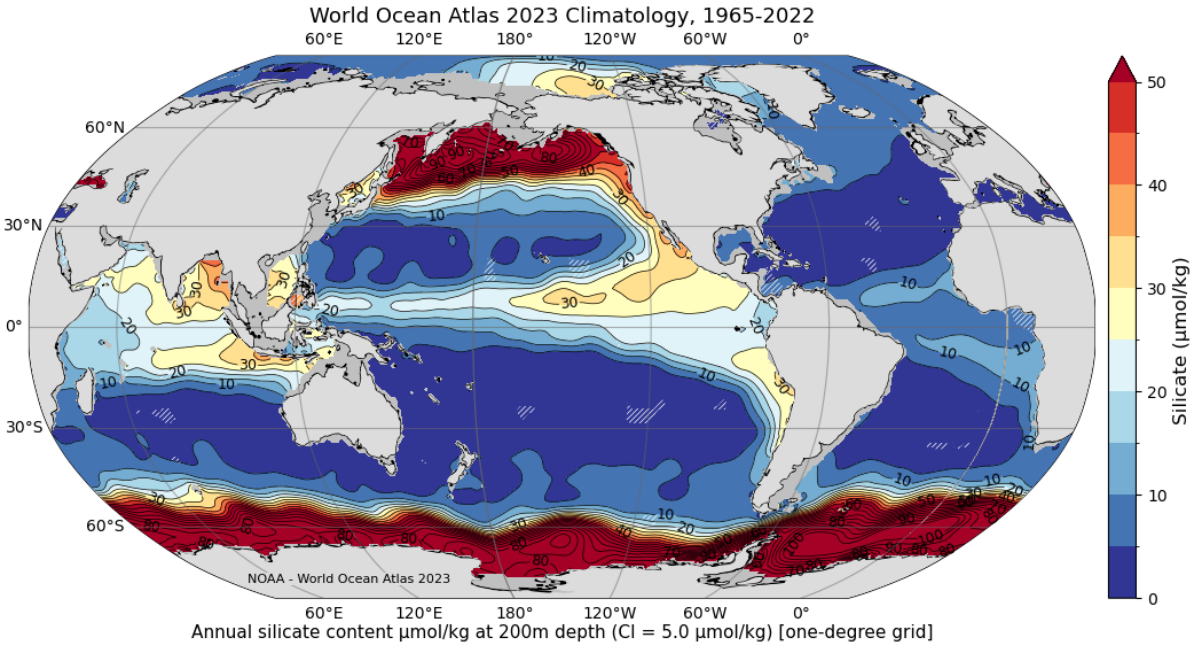


**Figure 4.3.** Climatological mean silicate content (µmol·kg$^{-1}$) distribution at 200 m depth. Lighter-shaded (grayed-out) patches indicate regions where there was no data within the radius of influence for the objective analysis.

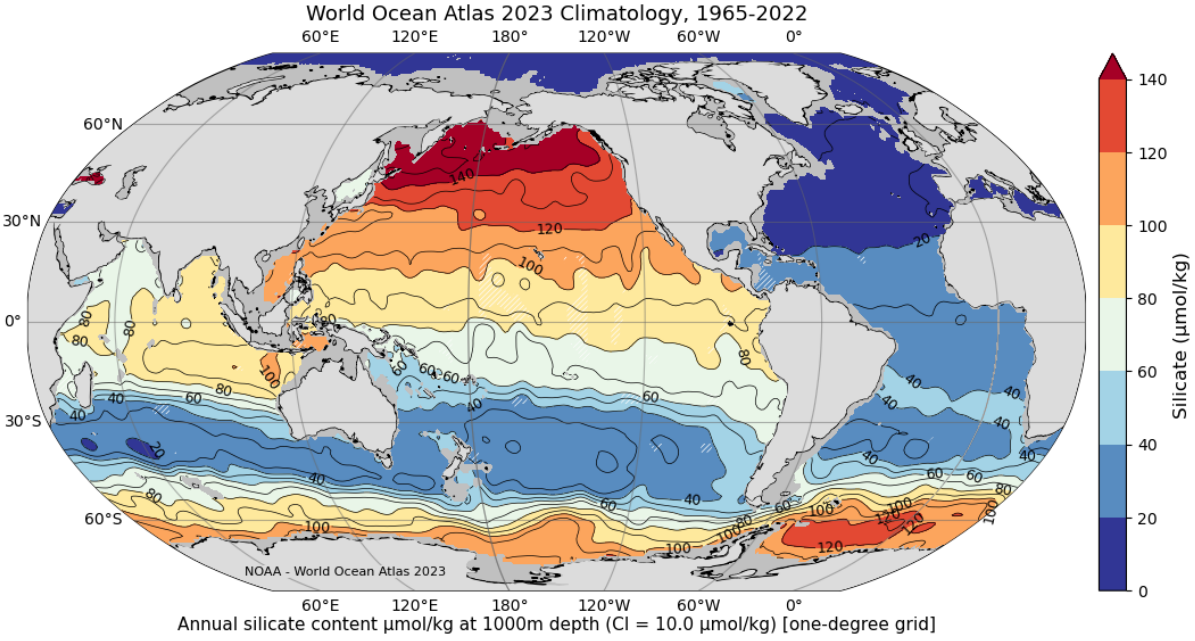


**Figure 4.4.** Climatological mean silicate content (µmol·kg$^{-1}$) distribution at 1000 m depth. Lighter-shaded (grayed-out) patches indicate regions where there was no data within the radius of influence for the objective analysis.

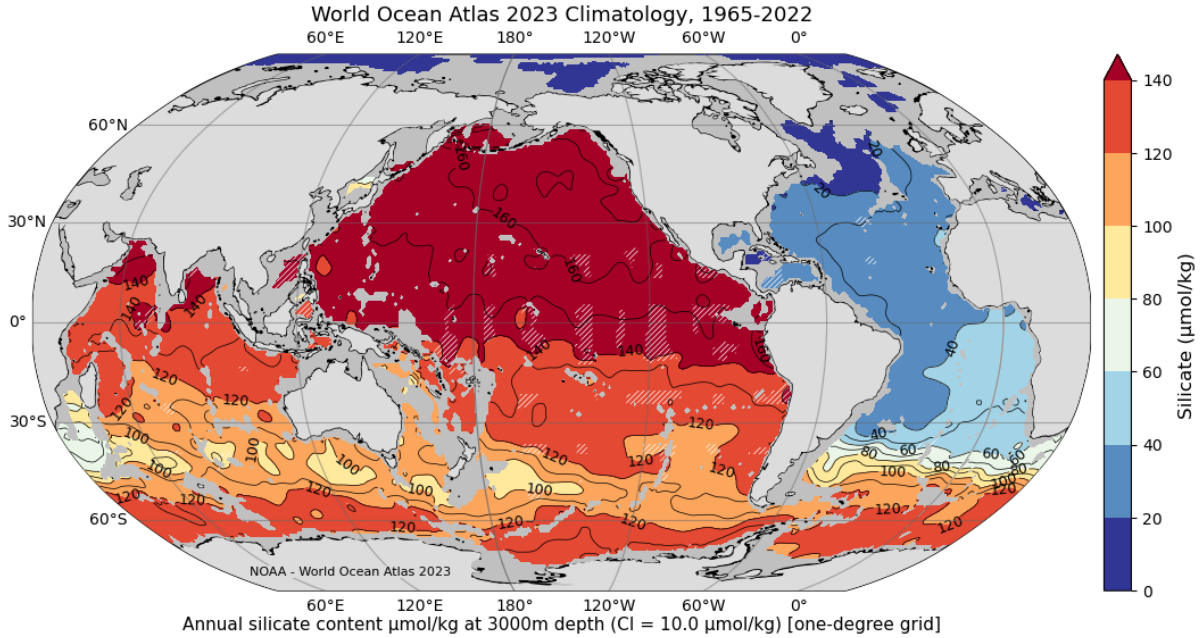


**Figure 4.5.** Climatological mean silicate content (µmol·kg$^{-1}$) distribution at 3000 m depth. Lighter-shaded (grayed-out) patches indicate regions where there was no data within the radius of influence for the objective analysis.

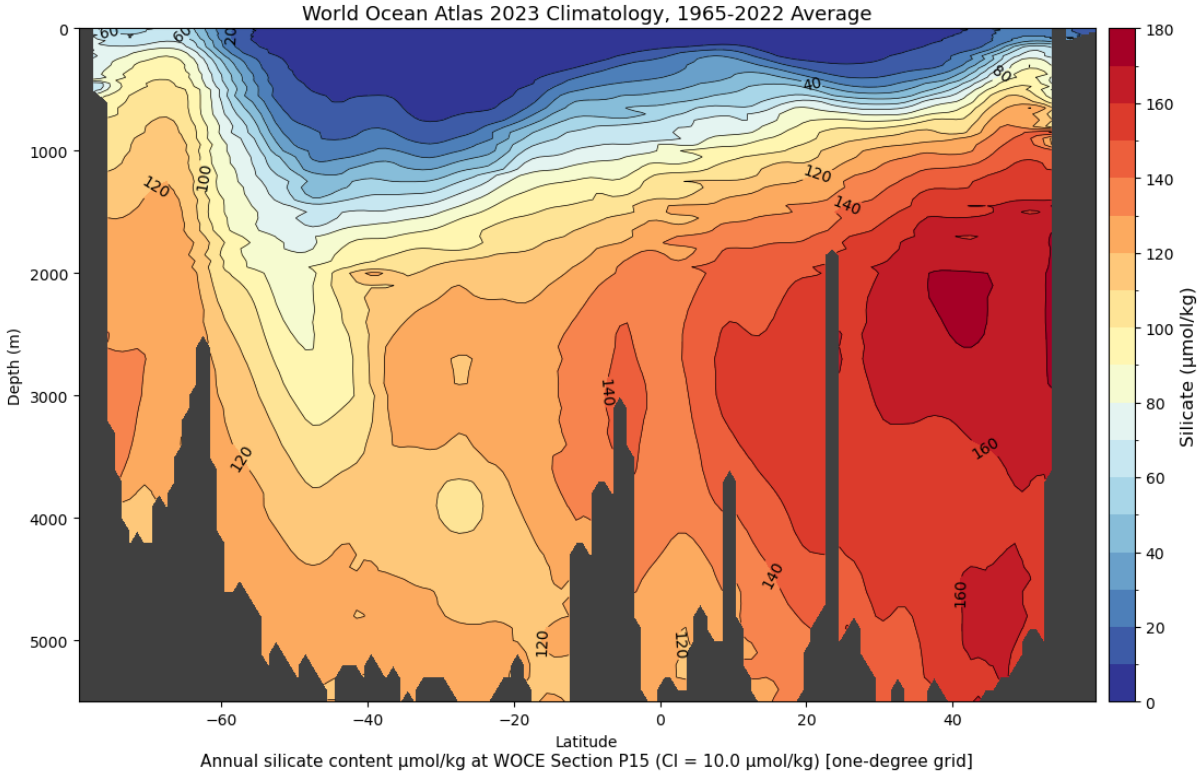


**Figure 4.6a.** Climatological mean silicate content (µmol·kg$^{-1}$) meridional cross section in the Pacific Ocean (near WOCE Line P15).

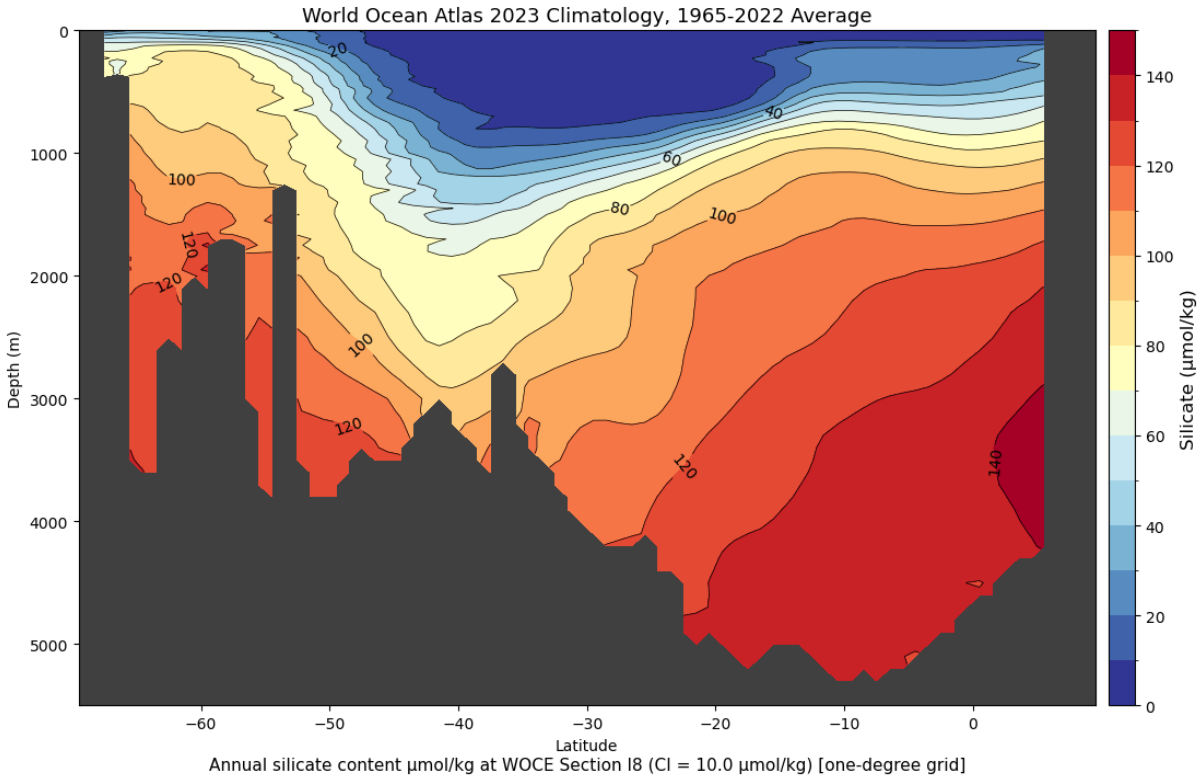


**Figure 4.6b.** Climatological mean silicate content (µmol·kg$^{-1}$) meridional cross section in the Indian Ocean (near WOCE Line I8).

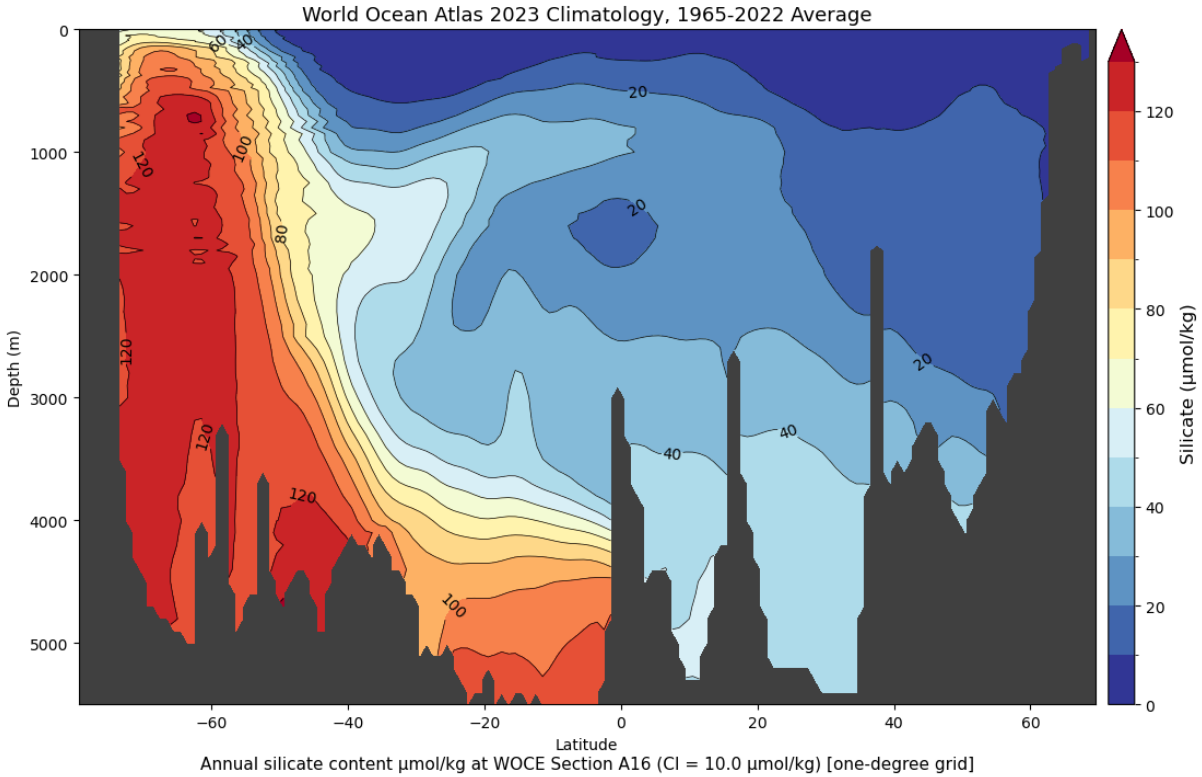


**Figure 4.6c.** Climatological mean silicate content (µmol/kg) meridional cross section in the Atlantic Ocean (near WOCE Line A16).

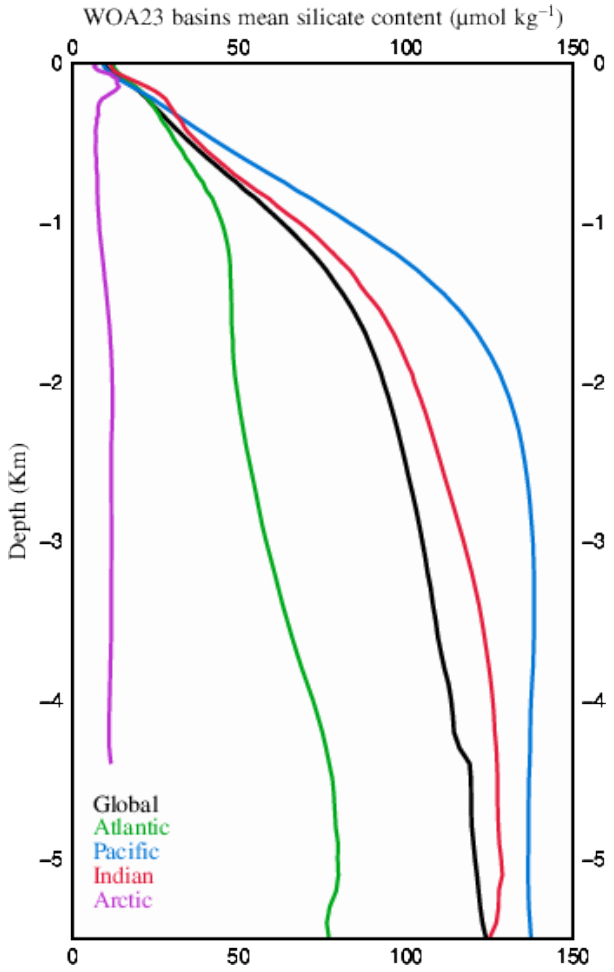


**Figure 4.7.** Annual mean silicate content (µmol·kg$^{-1}$) as a function of depth (km) for different ocean basins.

**Notes:** Table 1.6 (Chapter 1) shows the mean phosphate content for different oceanic basins. See Figure 1.5 (Chapter 1) for ocean basin definitions.